EURO Advanced Tutorials on Operational Research
Series Editors: M. Grazia Speranza · José Fernando Oliveira

Femke Kessels

Traffic Flow Modelling

Introduction to Traffic Flow Theory Through a Genealogy of Models

EXTRAS ONLINE

EURO Advanced Tutorials on Operational Research

More information about this series at http://www.springer.com/series/13840

Femke Kessels

Traffic Flow Modelling

Introduction to Traffic Flow Theory Through a Genealogy of Models

Springer

Femke Kessels
Department of Transport & Planning
Delft University of Technology
Delft, The Netherlands

Logistics, Tourism and Service
Management
German University of Technology
Muscat, Sultanate of Oman

Additional material to this book can be downloaded from http://extras.springer.com.

ISSN 2364-687X ISSN 2364-6888 (electronic)
EURO Advanced Tutorials on Operational Research
ISBN 978-3-319-78694-0 ISBN 978-3-319-78695-7 (eBook)
https://doi.org/10.1007/978-3-319-78695-7

Library of Congress Control Number: 2018938797

This Springer imprint is published by the registered company Springer Nature Switzerland AG
The registered company address is: Gewerbestrasse 11, 6330 Cham, Switzerland

To Emma, Julia and Sofie

Preface

This book shows the history of traffic flow modelling from the perspective of modern day applications. Traffic flow models describe how vehicles travel over roads, at which speeds, what the distance is between them, how long they take to travel over a certain road section, etc. Combining the models with other information supports estimations about current and future traffic states. This allows answering questions about the presence and duration of congestion, travel times and travel time delays, emissions and safety assessment. In turn, the information can be used in a variety of applications including transportation planning and traffic control.

This book shows the historical development of traffic flow theory by means of a genealogical tree of traffic flow models. The tree, included on page 15, shows the main developments in traffic flow modelling. The focus on the history of traffic flow models gives the reader insight into the basics of traffic flow modelling all through to the most advanced models that are currently under development. In addition, the book discusses numerical methods which are applied to create computer simulations based on the traffic flow models.

The history of traffic flow modelling starts in the 1930s. Bruce D. Greenshields presented his findings about the relationship between vehicle speed and the distance between vehicles at the Annual Meeting of the Highway Research Board (United States). Even though he had some predecessors doing similar research, Greenshields is often considered the founder of Traffic Flow Theory. The 1940s were a relatively quiet time for traffic flow theory, but from the mid 1950s many new models were introduced. Most of these new models include dynamics of traffic flow, i.e. they describe how traffic flows change over time, due to for examples changes in inflow of vehicles or traffic lights changing colour. Different types of models were developed and applied for road design. However, research in this area mostly stalled again in the 1980s. Faster and easier to use computers brought a new era of traffic flow research from the mid-1990s, resulting in most of the models that are still applied today. Many of today's applications require efficient numerical methods for fast and accurate predictions. Applications include transportation planning, road design, safety assessment, environmental assessment, traffic management, evacuation planning and route advice.

Previous versions of this work were published as the state-of-the-art chapter in the author's PhD dissertation (2013) and as a review article in the *EURO Journal on Transportation and Logistics* (2015). The book format gives more space to provide more basics, to go more in depth into the most important aspects of traffic flow modelling and simulation, and to include problem sets that will reinforce the newly gained knowledge and insights of the reader. Furthermore, the most recent developments in the field of traffic flow theory have been included.

The book aims at students (MSc and PhD), researchers and practitioners who want to learn more about the background of the models they are applying. No preliminary knowledge about traffic is assumed. Some background in calculus and differential equations is required, but references will be given for those who need to refresh their knowledge. Problem sets are included at the end of each chapter, with answers to selected problems in Chap. 8. Some of the exercises require the reader to perform simulations, for which software is provided online, at the publisher's website (http://extras.springer.com). Some previous experience with Octave (or Matlab) is useful for these exercises.

After reading the book and exploring some of the problems, readers will understand the main concepts in traffic flow modelling and simulation in such a way that they can (1) choose an appropriate model for their research or other application and build a simple but useful simulation tool based on this model; (2) understand a newly published scientific article that builds on traffic flow theory, modelling and simulation presented in this book, review that article and apply the models/methods that are presented; (3) start developing their own models and numerical methods to create new branches of the model tree.

Delft, The Netherlands Femke Kessels
June 2018

Acknowledgements

The seeds of expanding the idea of the genealogical model tree into something to be used in education were planted during my PhD research. When the editors of this series, Grazia Speranza and José Fernando Oliveira, invited me to write a proposal, I was reminded of the encouragements from Serge Hoogendoorn and Robert Bertini and I decided to accept. After my proposal was accepted, also Christian Rauscher from Springer was always quick to respond to any of my questions. Also thanks to the colleagues in Delft who gave valuable feedback on draft versions of (parts of) this book, Serge Hoogendoorn, Hans van Lint, Simeon Calvert and Meng Wang.

When working on this book, I have been writing at many different places, surrounded by even more different people. Many days I found inspiration and motivation from going to the shared office of our Personal Development Network and working in the same room as likeminded other 'expat partners'. Thank you Steven, Eveline, Tina, Chris, Hanna, Emma and Maryam for just being there and the many coffees outside! On other days I went to the German University of Technology in Oman, to be around other academics: it was always worth the long drive and I made good progress among my now colleagues to be. Thank you Heba, Amjaad, Osman, Amaani and all interns for the hospitality! Still, all this time spent outside the house was not enough and I often worked at home, only to be disturbed in case of 'blood or fire', which fortunately never happened. I am forever thankful to Rosa who has been a great help and caretaker for our children during these times. The last bit of progress was made not in Muscat, but in Delft, among colleagues and friends at Delft University of Technology. Also thank you for your hospitality!

Finally, a big thanks to my family, mam, pap, Mia, Giel, Manon and Niels, who have been encouraging me and giving me space to grow during calm and tumultuous times. And of course thanks and hugs to those who helped me keep a balance between all this serious stuff and love, fun, play and adventure: Emma, Julia and Sofie.

Contents

Symbols

Variables

x	Position (m)
t	Time (s)
n	Vehicle number (-)
v	Speed (m/s)
a	Acceleration (m/s^2)
ρ	Density (veh/m)
q	Flow (veh/s)
s	Spacing (m/veh)

Model Parameters

v_{max}	Maximum speed (m/s)
v_{crit}	Critical speed (m/s)
ρ_{crit}	Critical density (veh/m)
ρ_{jam}	Jam density (veh/m)
s_{jam}	Jam spacing (veh/m)
a_{min}	Maximum deceleration (m/s^2)
a_{max}	Maximum acceleration (m/s^2)
T	Minimum time headway (s)
τ	Time delay or reaction time (s)

Numerical Parameters and Indices

Δt	Time step size (s)
Δx	Grid cell size (m)
Δn	Vehicle group size (# of veh's)
ν	CFL number (-)
k	Time step index
n	Vehicle number
j	Grid cell index
i	Vehicle group index

Chapter 1
Introduction to Traffic Flow Modelling

Population growth and economic growth come with an increase in traffic demand and—more often than not—increased levels of congestion and accompanying delays, pollution and decrease in safety. There are several strategies to reduce congestion, keep cities liveable, clean and safe and limit travel time increase. Examples are encouraging people to travel using modes of transport that put less strain on the transportation network, to encourage people to travel at different times or on different routes, to apply traffic management to use roads in a more efficient way or to expand the road network. For all these measures, it is important to know how traffic flow will actually look: where and when will there be congestion, what are the bottlenecks and where is the road capacity already sufficient? Traffic flow models support this assessment by describing and predicting traffic on roads. For example, they model the number of vehicles on the road and their speeds. Using the models, travel times and congestion can be predicted.

To describe and predict traffic appropriately, real world observations are used to build theories, models and discretized models of traffic flow. By doing simulations based on these models the performance of roads or traffic networks can be assessed. In turn, this information is used for traffic management or the (re)design of roads and road networks.

This process is called the traffic flow modelling cycle, which is shown in Fig. 1.1 and is discussed in more detail in the next section. The rest of this chapter discusses some of its elements in more detail and the scope of this book is detailed in the last section.

The reader of this chapter will understand the importance and context of traffic flow modelling, they will have an understanding of the different types of traffic flow data and some important phenomena that can be identified in them. Furthermore, the reader will be able to work with the key variables of traffic flow modelling, which forms in important ingredient of the models that are discussed in the following chapters. Finally, the reader becomes familiar with classifications of traffic flow models and the genealogy of traffic flow modelling, including the four families.

F. Kessels, *Traffic Flow Modelling*, EURO Advanced Tutorials
on Operational Research, https://doi.org/10.1007/978-3-319-78695-7_1

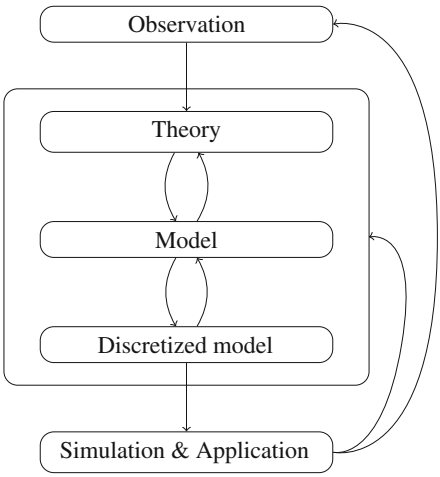

Fig. 1.1 Traffic flow modelling cycle. The genealogical tree focusses on the models. This book discusses the models more in depth, also including theories behind models and discretization methods

1.1 Traffic Flow Modelling Cycle

Traffic flow modelling is a largely inductive process: traffic observations are used to build a theory about the behaviour of individual drivers and vehicles or about traffic flow in general. Subsequently, that theory is used to build a model, discretize it and apply it in simulations. A simple example is the observations by Greenshields (1934) of vehicles passing his camera in the 1930s, see Fig. 1.2. Plotting the distance between the vehicles (spacing) and their change in position in consecutive photographs leads to a theory that spacing and speed are related. Subsequently, this leads to a model with a linear relationship between spacing and speed.

In more general terms, the development and application of traffic flow models is schematized in Fig. 1.1. As a first step, data is collected using, for example, loop detectors, cameras or GPS devices that many vehicles have on-board, such as navigation systems or mobile phones. Alternatively, data is collected using lab experiments for example with a driving simulator. These observations are analyzed and phenomena that characterize traffic flow are recognized.

In the second step, observations are used to build a theoretical framework. The theoretical framework consists of (mainly qualitative) statements and (behavioural) assumptions. For example, it is assumed that drivers perceive short space headways as more dangerous at high velocities than at low velocities. This is assumed to be the reason why at low velocities shorter headways are maintained. Another assumption is that drivers only react to their leaders and not to their followers.

In the third step, the theoretical framework is used to build a traffic flow model. The model consists of a set of equations, sometimes supplemented with a set of (behavioral) rules. For example, the theory about short headways at low velocities and long headways at high velocities is quantified in a fundamental diagram. It expresses the average vehicle velocity as a function of the average headway. Alternatively, a car-following model is developed that describes how a following

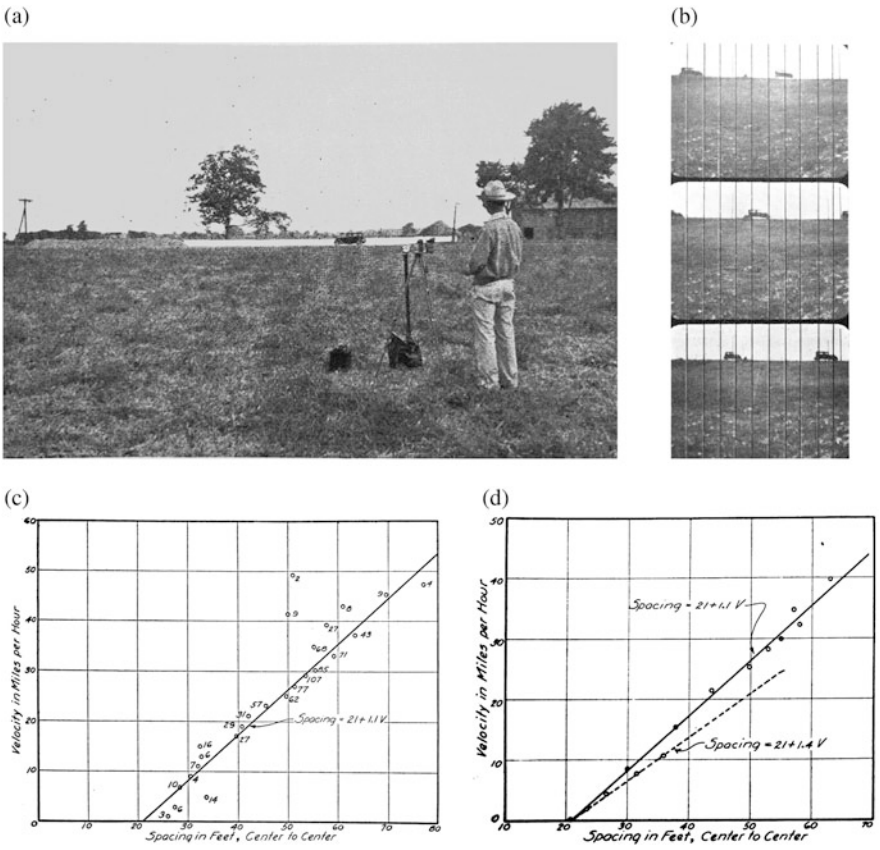

Fig. 1.2 Greenshields making field observations and turning this into a simple traffic flow model. Pictures reproduced with permission from Greenshields (1934). (**a**) Making field observations. (**b**) Resulting photographs. (**c**) Plotting data: speed against spacing. (**d**) Determining a linear relationship between spacing and speed

vehicle reacts to its leader(s), at which distance the leading vehicle is followed, and how the distance depends on the speeds of both leading and following vehicle.

The models can not be used directly in applications using computer simulation. Therefore, discretization is applied in the fourth step. In most simulation tools, time is divided into discrete time steps. Furthermore, depending on the model, also space or other continuous variables are discretized. Numerical methods are applied to approximate the new traffic state each time step. This results in a discrete traffic flow model.

Finally, the discrete traffic flow model is implemented in a computer program, resulting in a simulation tool. By applying this tool, and combining it with input such as data from traffic sensors, traffic state estimation and predictions can be made. Simulation results are compared to observations to calibrate the parameters and to validate the simulation tool.

Traffic flow models have many applications, for different purposes. They include:

- State estimation & short term predictions to inform travellers
- State estimation & short term predictions for traffic management
- Decision support for (semi-)autonomous vehicles
- Long term assessment of development plans, e.g. the (re)design of a transportation network
- Assessment of the impact of traffic on safety and emissions
- Design of evacuation plans

Naturally, different applications, call for different type of models. For example, when the goal is to inform commuters about the expected traffic situation if they'd decide to go home within 30 min, or to decide about activating traffic management measures in the next few minutes, it is most important to have almost instantaneous access to state estimation or prediction. In the more extreme case of decision support for autonomous vehicles, there is an even more urgent need of immediate information about, for example, driving into congestion. On the other end of the spectrum, when redesigning a network, it may be less important to get results quickly. However, in this application, many different scenarios may need to be calculated, for example using different socio-economic scenarios as input. Furthermore, besides computational speed, accuracy also plays a role. For example, when making long term plans, it may not be very interesting to know exactly what time of the day congestion will occur, but when informing travellers about the travel time if they would leave now, it is very important to know exact time and location of congestion.

Because of the difference in applications, different types of models have been developed, each of them more suited for certain applications than for others. Those interested in more detailed discussions of applications are referred to e.g. Treiber and Kesting (2013); Elefteriadou (2013).

1.2 Observations and Phenomena

While this book focusses on the central part of the traffic flow modelling cycle, this section introduces some of the other elements, in order to place the content in context and to support the reader in applying the materials covered in this book.

1.2.1 Observing Traffic

Traffic can be observed in many different ways. Most data comes from 'real world' observations where there is no intervention by researchers. Usually, the main purpose for collecting this data is not research or traffic model development but

traffic management and information. Data is collected to get insights about actual traffic and then manage traffic accordingly or to inform road users. Typically, data collection is done using loop detectors which count the number of passing vehicles, sometimes also including information on their speed or the vehicle length. Other ways to collect data for traffic management and information include the use of camera's and systems to collect trajectory data from GPS or other in-car devices.

Observations are also collected using lab experiments where drivers are instructed to drive on a certain closed off road (network) or with driving simulators. Lab experiments have proven useful for qualitative model development, but are only limited applicable for quantitative observations, for example because safety perception in a driving simulator can be different from when driving on a real road. Driving simulators have seen a rapid development over the last years and the interested reader is referred to Auberlet et al. (2014) for more details. An other interesting data source are camera recordings from helicopters, which are gathered with the special purpose of research.

Summarizing, traffic can be observed from three perspectives, which are illustrated in Fig. 1.3:

- Local (fixed position): a loop detector, camera or other sensor that observes traffic passing at a certain point along the road.
- Instantaneous (fixed in time): a camera or other sensor that captures the traffic on a longer road stretch at a certain time (e.g. a picture taken from a helicopter)
- Trajectory (moving with vehicle): an in-car device or other sensor that collects data about the position of the vehicle over a certain time period.

A fourth perspective combines the first and second: observing traffic over a limited space and time period. For example, this type of observations combines a series of local observations over a few minutes to an hour and over a few hundred meter to a few kilometer. These observations can be obtained using for example camera's placed on a high building or bridge. The perspectives are compared in Table 1.1. How exactly to derive the variables introduced in the table is subject of Sect. 1.3.

Finally, different types of observations are combined to get a more complete image of traffic flow. In many applications, such as traffic state estimation and traffic

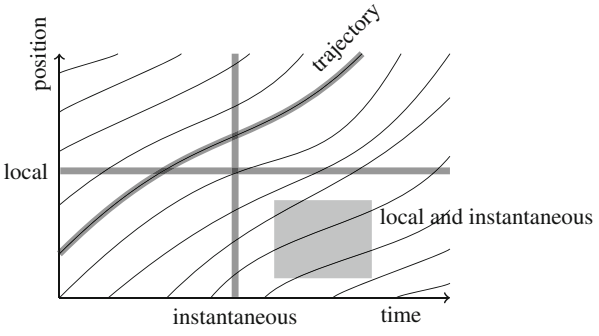

Fig. 1.3 Three ways to observe traffic

Table 1.1 Comparison of different types of traffic data

Type	Principle data	Derived variables
Local	Vehicle counts	Time headways, flows
Instantaneous	Vehicle positions	Space headways, densities
Trajectory	Location, time	Trajectories
Local and instantaneous	Counts at series of positions	Headways, flows, densities

state prediction, data from different types of sensors is fused to give a consistent image of the (current or future) traffic state. The applied techniques, including Kalman filtering, are beyond the scope of this book, the interested reader is referred to van Lint and Djukic (2012); Sun and Work (2017).

1.2.2 Phenomena in Traffic

Special patterns can be observed in traffic flow data, they are usually referred to as phenomena. Traffic flow models are designed to reproduce or predict these patterns. The simplest of those—which we would usually not call 'phenomena'—are low speeds at high densities (i.e. short headways) and long headways (i.e. low densities) at high speeds. Related to this is the observation that flow (or throughput) is highest at an intermediate density level, also known as critical density. If densities are well below the critical value, there are so few vehicles, that the flow (density $\times$ speed) is low, if densities are well above the critical value, the vehicle speed is so low that again the flow is low. Other patterns—or traffic flow phenomena—that can be observed include hysteresis and stop-and-go-waves.

1.2.2.1 Hysteresis and Capacity Drop

In general, hysteresis can be defined as follows. Consider a system where some variable (e.g. speed) changes when an other variable (e.g. space headway) changes. The system shows hysteresis when the change of dependent variable (speed in the example) lags behind the change in the other variable. Observations often show that accelerating takes longer than decelerating: when headways become larger, as is the case when leaving a queue, it takes longer for vehicles to adapt their speed to these new headways then when they enter a queue and slow down. An other example is the capacity drop observed at bottlenecks. Just before congestion sets in, the flow (capacity) through the bottleneck is high. Vehicles don't slow down in the bottleneck. However, slightly later, when the bottleneck has become active and a jam has developed upstream of the bottleneck, the flow (capacity) through the bottleneck is lower, see for example Fig. 1.4.

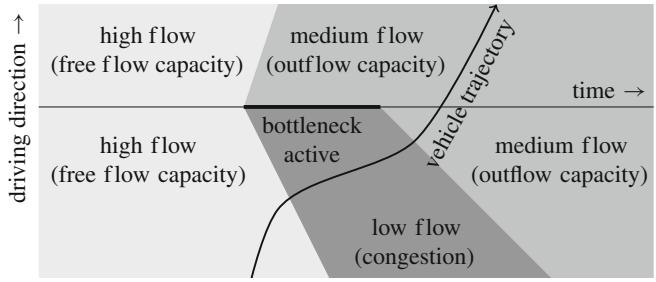

Fig. 1.4 Example of capacity drop: initially (on the left), the bottleneck is inactive and flow is high, at the 'free flow capacity'. When the bottleneck is activated (e.g. through a random event, a slight disturbance), congestion starts developing upstream of the bottleneck and—most importantly—the outflow out of the bottleneck drops to 'outflow capacity'

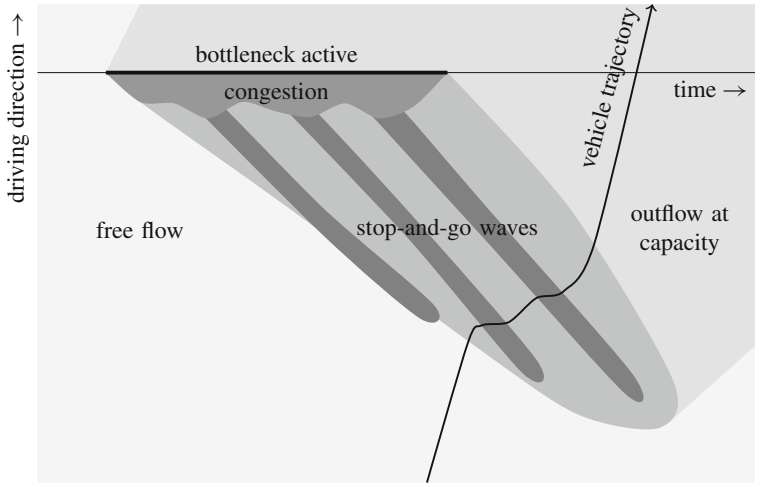

Fig. 1.5 Example of stop-and-go waves: upstream of a bottleneck is congestion. Within the congested area, stop-and-go waves are created: the waves travel upstream, vehicles encounter alternating relatively light congestion (high speed, low density) and heavy congestion (low speed, high density)

1.2.2.2 Stop-and-Go Waves

Stop-and-go-waves (also known as wide moving jams) are sometimes observed by drivers in congestion: alternatingly a driver has to slow down and can speed up again, see Fig. 1.5. This typical pattern can be very persistent, but poses a challenge to modelling. Again, delayed reactions (hysteresis) are proposed as a possible cause for their existence.

1.3 Traffic Flow Models

Traffic flow models have been developed and used since the beginning of the twentieth century. Traffic flow models are part of a long history of mathematical modelling of physical and other systems. Scientists and engineers use mathematical models as simplified representations of real-world systems. They are applied to explain and predict weather or chemical reactions, behaviour of materials or humans, fluid or traffic flow, etc. In this section we present a short overview of the traffic flow modelling efforts up to date.

Since the introduction of the first traffic flow model in the 1930s the number of models has increased. We only focus on the ones that are still most relevant in practical and scientific applications, but we can still identify about 50 different models, many of which have been developed over the last two decades.

To gain some basic insight into traffic flow modelling and the principle variables involved, we shortly discuss the main concepts of agent based and continuum traffic flow modelling. They are discussed in much more detail in the following chapters. Furthermore, we introduce other classifications of models and make a link between traffic flow models and models of other complex systems.

1.3.1 Agent-Based Models and Their Variables

Microscopic (or agent-based) traffic flow models are often considered the most intuitive, as they describe the behaviour of individual vehicles and trace their trajectories through space. They describe the longitudinal and lateral behaviour of individual vehicles, often based on assumptions regarding human factors and driving behaviour. Only longitudinal behaviour is discussed here. Vehicles are numbered to indicate their order: n is the vehicle under consideration, $n-1$ its leader, $n+1$ its follower, etc., see Fig. 1.6. The behaviour of each individual vehicle is typically modelled in terms of the position of the front of the vehicle x_n, speed $v_n = \mathrm{d}x_n/\mathrm{d}t$ and acceleration $a_n = \mathrm{d}v_n/\mathrm{d}t = \mathrm{d}x_n^2/\mathrm{d}t^2$. The speed typically depends on a few of the following factors:

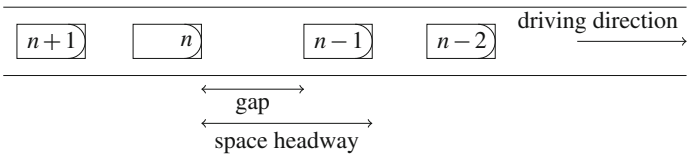

Fig. 1.6 Vehicle numbering in microscopic traffic flow models (and macroscopic models in Lagrangian formulation)

current speed of the vehicle under consideration
current speed of the leading vehicle or possibly multiple leading vehicles
space headway distance of the vehicle to its leader
individual properties of driver and vehicle e.g. desired speed, reaction time, maximum acceleration, braking power

In this book, 'space headway' (or spacing) is defined as in Fig. 1.6: the distance between the front of the leader and the front of the vehicle under consideration. Furthermore, the 'gap' is the distance *between* the two vehicles. It should be noted that some authors, exclude the vehicle length from the space headway and define it as the distance between the vehicles, or they include the vehicle length of the vehicle under consideration instead of the vehicle length of the leader.

1.3.2 Continuum Models and Edie's Definitions

Most traffic flow models are based on the assumption that there is some relation between the distance between vehicles and their speed: if headways are short, drivers tend to lower their speed. This relation can be described, or modelled through, the fundamental diagram.

Originally Greenshields studied the relation between the variables spacing and velocity. However, the fundamental diagram can also be expressed in other variables such as density (average number of vehicles per unit length of road) and flow (average number of vehicles per time unit), see Fig. 1.7. These variables were first defined rigorously by Edie (1965). Figure 1.8 illustrates the definitions. Flow is defined as the flow in an area A with length dx and duration dt which is determined by the number of vehicles $N(A)$ that travel through the area and the distance y_n they

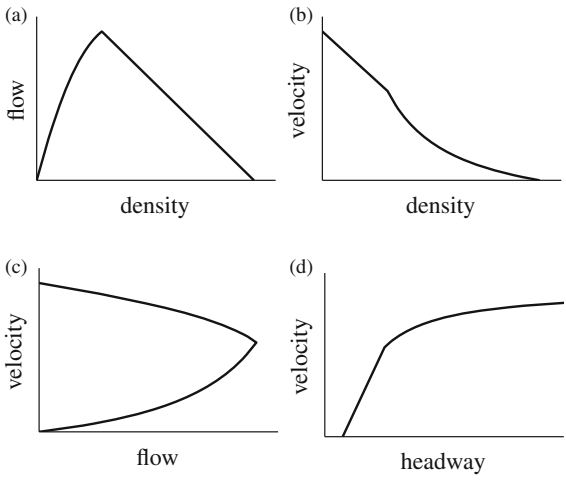

Fig. 1.7 Fundamental diagrams in different planes. (**a**) Density-flow plane. (**b**) Density-velocity plane. (**c**) Flow-velocity plane. (**d**) Spacing-velocity plane

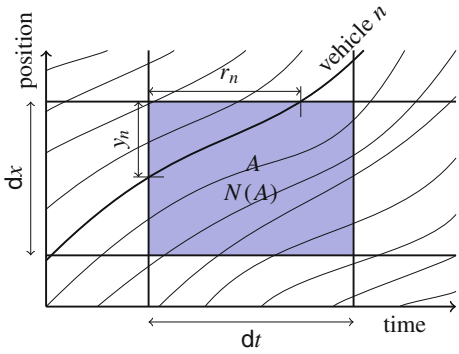

Fig. 1.8 Time-space region with some vehicle trajectories to illustrate Edie's definitions of flow and density. $N(A)$ is the number of vehicles that travel through the area A

travel through the area:

$$q_{\text{area}} = \frac{\sum_{n=1}^{N} y_n}{\mathrm{d}x\,\mathrm{d}t} \tag{1.1}$$

Similarly, density is defined as the density in an area using the time r_n vehicle n is present in the area:

$$\rho_{\text{area}} = \frac{\sum_{n=1}^{N} r_n}{\mathrm{d}x\,\mathrm{d}t} \tag{1.2}$$

Finally, this leads to the intuitive definition of velocity in an area by dividing the total distance traveled by the total time spent:

$$v_{\text{area}} = \frac{q_{\text{area}}}{\rho_{\text{area}}} = \frac{\sum_{n=1}^{N} y_n}{\sum_{n=1}^{N} r_n} \tag{1.3}$$

These are workable definitions to extract flow, density and velocity from observations of a large area A with many vehicles N. They can even be applied to long road sections observed over a short period of time or, vice versa, short road sections observed over a long period of time. However, for other applications such as macroscopic traffic flow models, flows, densities and velocities at points in (x, t) are considered. Therefore, we have to assume that traffic is a continuum flow. In Sect. 1.3.4 we argue why this is a reasonable assumption. The assumption implies that N becomes continuous (instead of discrete). Furthermore, N is assumed to be continuously differentiable in x and t. Edie's definitions are then not applicable directly. However, by decreasing the area A such that it becomes a point, the definitions of flow, density and velocity become meaningful at points.

The local and instantaneous flow, density and velocity are found using the procedure described by Leutzbach (1988). To find the local and instantaneous flow (the flow at a point in (x, t)) we decrease the length of the road section: $\mathrm{d}x \to 0$.

This yields the local flow through a cross section x. Afterwards, we decrease the time $\mathrm{d}t \to 0$ and find:

Definition 1.1 ((Local and Instantaneous) Flow)

$$q(x,t) = \lim_{\mathrm{d}t\to 0} \lim_{\mathrm{d}x\to 0} \frac{\sum_{n=1}^{N} y_n}{\mathrm{d}x\,\mathrm{d}t} = \lim_{\mathrm{d}t\to 0} \underbrace{\frac{N(x,[t,t+\mathrm{d}t])}{\mathrm{d}t}}_{=q_{\mathrm{local}}(x)} \tag{1.4}$$

To find the local and instantaneous density we decrease the time: $\mathrm{d}t \to 0$. This yields the instantaneous density through a cross section t. Afterwards, we decrease the length $\mathrm{d}x \to 0$ and find:

Definition 1.2 ((Local and Instantaneous) Density)

$$\rho(x,t) = \lim_{\mathrm{d}x\to 0} \lim_{\mathrm{d}t\to 0} \frac{\sum_{n=1}^{N} r_n}{\mathrm{d}x\,\mathrm{d}t} = \lim_{\mathrm{d}x\to 0} \underbrace{\frac{N([x,x+\mathrm{d}x],t)}{\mathrm{d}x}}_{=\rho_{\mathrm{instant}}(x)} \tag{1.5}$$

Finally, similar to Edie's definition of velocity (1.3), we define the local and instantaneous velocity:

Definition 1.3 ((Local and Instantaneous) Vehicle Velocity)

$$v(x,t) = \frac{q(x,t)}{\rho(x,t)} \tag{1.6}$$

In addition, we define local and instantaneous spacing:

Definition 1.4 ((Local and Instantaneous) Vehicle Spacing)

$$s(x,t) = \frac{1}{\rho(x,t)} \tag{1.7}$$

The above definitions of flow, density, speed, and spacing are used throughout this book. They form an essential ingredient for mesoscopic and macroscopic models.

1.3.3 Classifications of Models

To get better insight in traffic flow models and their usefulness to certain applications, they can be classified into groups with similar properties. Many classifications of traffic flow models have been proposed, including classifications based on the type of variables and equations that are used to describe the processes:

Scale of independent variables continuous, discrete, semi-discrete (independent variables are usually time and space, or sometimes vehicle count);
Stochasticity deterministic or stochastic variables and processes;
Type of model equations (partial) differential equations, discrete or static models;
Operationalization analytical or simulation, where simulation often involves discretization of the model equations;
Number of variables and parameters to distinguish between 'efficient' models with few variables and parameters but still able to reproduce and predict traffic realistically and 'inefficient' models.

Other classifications are based on how detailed traffic and driver behavior is described and potential applications:

Level of detail of representation sub-microscopic, microscopic (agent-based), mesoscopic, macroscopic (continuum), network-wide or hybrid models combining different levels of detail;
Level of detail of underlying behavioral rules individual, collective
Scale and type of application networks, links, intersections, urban roads, freeways;
Number of phases described by the model mainly to distinguish between models that show states such as free flow, congestion, stop-and-go traffic differently.
Phenomena that can be explained or reproduced by the model

Throughout the book, some categories listed above are used for sub-classification of models. Furthermore, the concepts have been used as criteria to assess traffic flow models, with properties that are often considered to be desirable such as:

1. The model only has few parameters.
2. Parameters are (easily) observable and have realistic values.
3. Relevant phenomena are reproduced and predicted by the model.
4. The model allows fast computations for state estimation or prediction.

To establish the genealogy of traffic flow models, we mainly use the classifications based on the type of model equations (static vs dynamic, with discrete or continuous flow) and the level of detail, as discussed further below. The interested reader is referred to e.g. Hoogendoorn and Bovy (2001b); Lesort et al. (2003); van Wageningen-Kessels et al. (2011); Bellomo and Dogbe (2011); van Wageningen-Kessels et al. (2015) for a more detailed discussion of classifications and reviews of traffic flow models.

1.3.4 Traffic Flow, Fluid Flow and Other Complex Systems

Traffic flow models are often related to and derived in analogy with models for fluid flow. For example, the seminal paper on macroscopic traffic flow modelling (Lighthill and Whitham 1955b), was published as 'On Kinematic Waves Part 2'

together with Part 1 discussing flood movement in rivers (Lighthill and Whitham 1955a). In turn, traffic flow models have recently inspired researchers to model pedestrian crowds and animal swarms in a similar way, cf. Bellomo and Brezzi (2008), other articles in that special issue of Mathematical Models and Methods in Applied Sciences on Traffic, Crowd, and Swarms, and Bellomo and Dogbe (2011). Furthermore, similarities between vehicular traffic, pedestrian and granular flow have been recognized and conferences on Traffic and Granular Flow are organized bi-annually, the most recent ones being held in Delft (The Netherlands) in 2015 and in Washington D.C. in 2017 (Knoop and Daamen 2016; Transportation Engineering Group at the George Washington University 2017). Finally, Helbing (2008) relates traffic flow to systems that might even seem more diverse such as those related to collective decision making, risk management, supply systems and management strategies.

1.4 Approach and Scope of This Book

In this book, we discuss the traffic flow models and some of its underlying theories and numerical methods for computer simulation. The main modelling approaches are introduced and positioned in the genealogical tree of traffic flow models, which shows the historical development of traffic flow modelling, see page 15. For most models, this book also introduces the reader to useful approaches for computer simulations.

1.4.1 The Genealogical Model Tree

The main part of this book follows the historical lines of the development of traffic flow models since they were first studied in the 1930s. This approach shows better how traffic flow models have developed and how different types of models are related to each other. To show the historical development of traffic flow models we introduce a genealogical tree of traffic flow models, see page 15.

The historical development of traffic flow models shows the emergence of four families. All models in the tree have one common ancestor: the fundamental relation (or fundamental diagram). The other three families consist of micro-, meso- and macroscopic models. After the introduction of the fundamental diagram in the 1930s, microscopic and macroscopic models were introduced simultaneously in the 1950s. Mesoscopic models are about a decade younger. Particularly over the

last two decades, the fundamental diagram and all three types of models have been developed further and many offshoots can be recognized.

The fundamental diagram family is the only one with static models. The fundamental diagram, which constitutes a family of its own, does not describe any changes in traffic state, but only links how 'busy' the road is (usually in terms of number of vehicles per kilometer) to how fast the vehicles are driving. In other words: the fundamental diagram relates the vehicle headway (front-to-front following distance) to vehicle speed, in a static way. How headways and speeds change is described by micro-, meso- and macroscopic models. These models are dynamic: they describe how traffic states change over time, for example when congestion is created and how it dissolves. Those three types of models are categorised further according to their level of aggregation of the variables. Microscopic models describe vehicles as individual agents, each with their own headway and speed, they distinguish and trace the behaviour of each individual vehicle. Macroscopic models aggregate the vehicles into a continuum flow approximation, with variables averaged over multiple vehicles, e.g. average speed of vehicles on a certain section, or average number of vehicles passing that section per time unit. Mesoscopic models have an aggregation level in between those of microscopic and macroscopic models or combine both approaches. Classical mesoscopic models describe vehicle behaviour in aggregate terms such as in probability distributions, while behaviour rules are defined as individual vehicles. Hybrid models are a much younger branch of mesoscopic models. They model traffic at different scales: adapting the scale according to the needs for accuracy and computational speed in that area.

1.4.2 Numerical Methods for Computer Simulation

To apply a traffic flow model, it is often included in a computer simulation. Therefore, the dynamic model is discretised in time. The traffic state is not computed for every moment in time, but instead only at discrete instances, with time steps of usually 0.5–2 s. In microscopic models, the traffic state consists of the position of the vehicles, usually in combination with their speed and possibly other variables. In macroscopic models, the traffic state consists of variables like density and speed. Mesoscopic models use combinations of those variables or even other variables. When doing a time step, the current state (at time t) is used to approximate the state at the next time step (at time $t + \Delta t$). This way, when the initial state is known, subsequent time stepping can predict future traffic states.

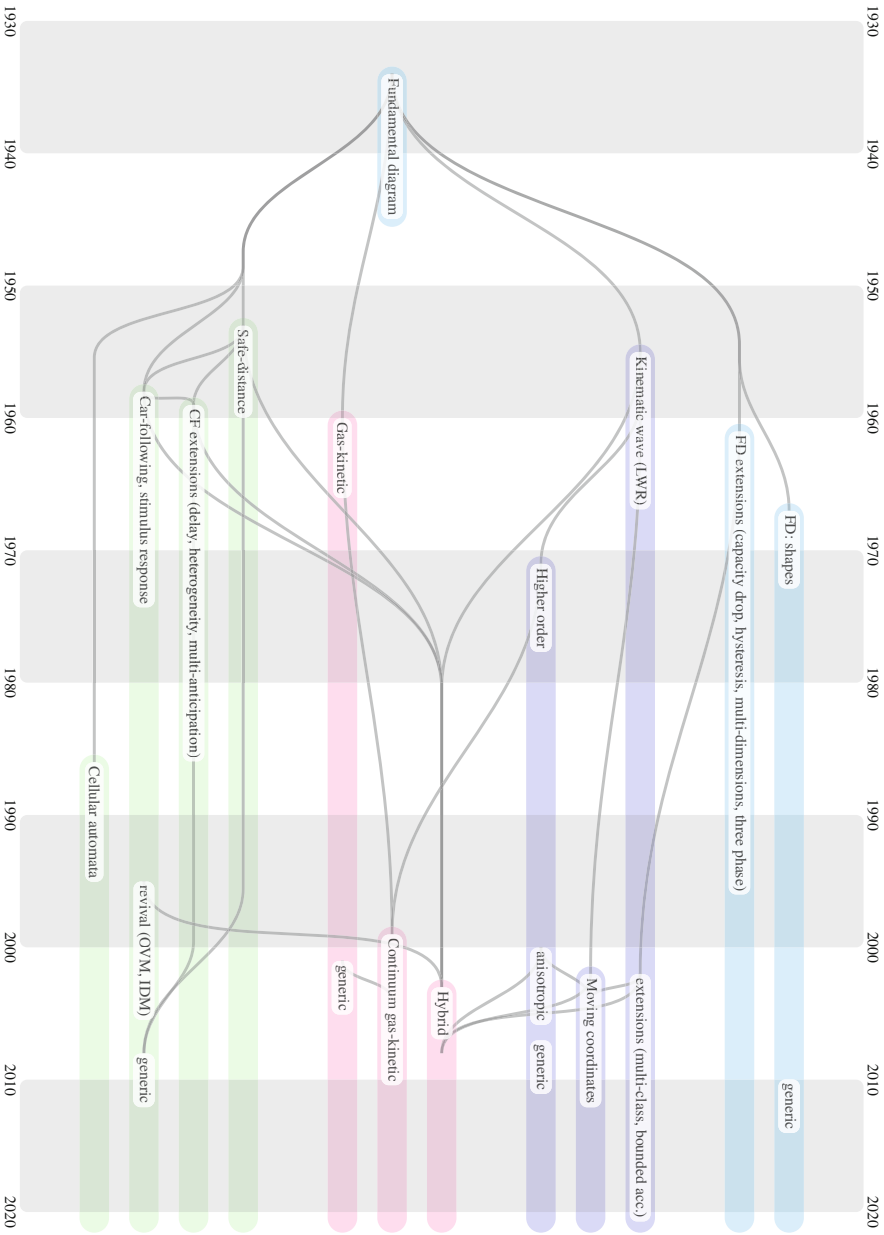
1930
1940
1950
1960
1970
1980
1990
2000
2010
2020
Fundamental diagram
FD: shapes
generic
FD extensions (capacity drop, hysteresis, multi-dimensions, three phase)
Kinematic wave (LWR)
extensions (multi-class, bounded acc.)
Moving coordinates
Higher order
anisotropic
generic
Hybrid
Gas-kinetic
generic
Continuum gas-kinetic
Safe-distance
CF extensions (delay, heterogeneity, multi-anticipation)
Car-following, stimulus response
revival (OVM, IDM)
generic
Cellular automata

How exactly the discretisation in time and—where applicable in space or an other independent variable—is approached and how the new state is computed for each time step, is discussed for some of the most widely used models.

1.4.3 Other Aspects of Traffic Flow Modelling

We focus on models that include a clear set of rules describing the behaviour of drivers, vehicles and/or traffic flows. These models are usually relatively easy to understand and are shaped by a set of mathematical equations, that can often be solved analytically for (very) simple problems. However, the human behaviour in traffic is often much more complex than can be described by these models. Therefore, artificial intelligence models have been developed (Aghabayk et al. 2015). They describe traffic flow using for example fuzzy logic or neural networks. Artificial intelligence models are not discussed in detail in this book.

Furthermore, this book focusses on models and simulation methods for longitudinal traffic flow on homogenous roads. We aim to provide the reader with knowledge and tools to be able to build their own model and simulation of a heterogeneous road with no entries, exits or intersection. Aspects of traffic modelling that are not discussed in detail in this book are:

- models for lateral behavior (lane changing) that can be included in microscopic models
- node models to include intersections, merges and diverges in traffic flow models
- demand and origin destination modelling: we assume that in the applications the number of vehicles that want to travel over a certain road is given.
- calibration and validation of models and simulation tools: we focus on the qualitative aspects of the models and refer the reader to other publications for details on how to properly estimate parameter values.
- details of applications: there is a broad variety of applications of traffic flow model and we suggest the reader—where applicable—to refer to other publications specifically dealing with their application.
- network flows: there is a steady growth in the literature about how to model flows in networks, without modelling each road individually, but instead using network (or macroscopic) fundamental diagrams. We consider this scale too course for the scope of this book.
- psychology and decision making of the driver, technology of the vehicle and their interaction: again, these topics are gaining more and more research interest but we consider this scale to detailed for the scope of this book.

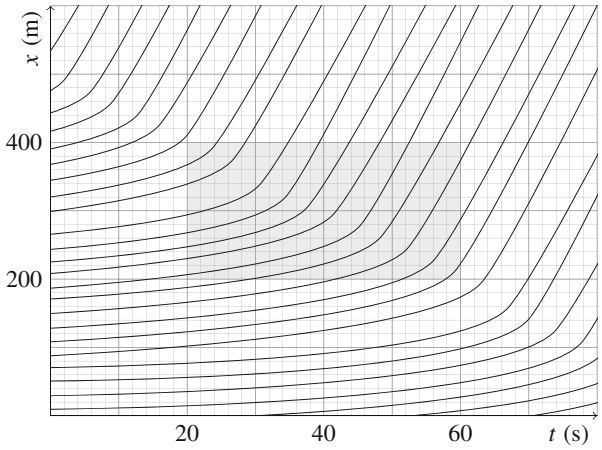

Fig. 1.9 Example of observed trajectories

Problem Set

Calculating Traffic Variables

Consider the trajectories in Fig. 1.9.

1.1 Use Edie's definitions to calculate the average density, speed and flow in the grey area from $t = 20\,\text{s}$ to $t = 60\,\text{s}$ and from $x = 200\,\text{m}$ to $x = 400\,\text{m}$.

1.2 Use Edie's definitions to calculate the instantaneous density at the boundaries of the grey area, i.e. at $t = 20\,\text{s}$ and at $t = 60\,\text{s}$.

1.3 Use Edie's definitions to calculate the local flow at the boundaries of the grey area, i.e. at $x = 200\,\text{m}$ and at $x = 400\,\text{m}$.

Wardrop User Equilibrium and Braess Paradox

This problem set is based on the ideas on user equilibrium introduced by Wardrop (1952) and the Braess paradox (Braess 1968). Consider a simple road network consisting of 4 roads, as in Fig. 1.10a. The travel times on the links from A to C and from B to D are always 15 min. The travel times on the other links (from A to B and from C to D) are longer when the number of vehicles on those links (q_{AB} and q_{CD}, respectively) are higher. To be precise, the travel time in minutes is $T_{AB} = q_{AB}/10$ and $T_{CD} = q_{CD}/10$, respectively. 100 vehicles and their drivers want to travel from A to B. Finally, assume a user equilibrium (Wardrop's first principle): there is no driver for which the travel time would decrease if they would chose a different route.

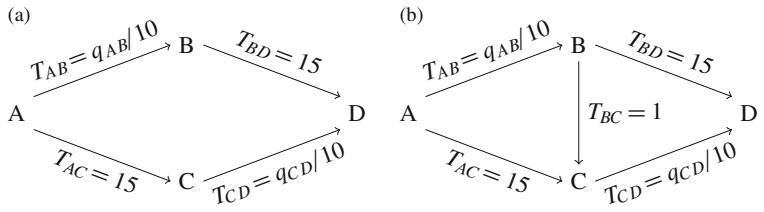

Fig. 1.10 Networks illustrating Wardrop's principle and the Braess paradox. (**a**) Initial network (**b**) Network with extra link added

1.4 (Advanced) In a user equilibrium, how many of the 100 drivers travel via B and how many travel via C? What is their travel time?

Now consider a fifth road being build, as in Fig. 1.10b. It connects B with C, only taking one minute to travel.

1.5 (Advanced) In a user equilibrium, how many of the 100 drivers travel stay on the original routes via B and C, respectively (i.e. not making use of the new route) and how many take the new route and travel $A \to B \to C \to D$? What are their travel times?

The 'traffic flow models', relating the travel time with the number of vehicles on the road, or even using a constant travel time, are very simplistic. Using more advanced and realistic models—as introduced in the next chapters—will also give more realistic travel times and it will be harder to find an example of the Braess paradox.

Identifying Phenomena in Data

There are many online tools to view current or previous traffic states, such as Google Maps (maps.google.com) or the collection of traffic states at http//traffic-flow-dynamics.org/traffic-states.

1.6 (Advanced) Go to any of these websites and identify instances of congestion, free flow, capacity drop and stop-and-go-waves.

Further Reading

Aghabayk K, Sarvi M, Young W (2015) A state-of-the-art review of car-following models with particular considerations of heavy vehicles. Transp Rev 35(1):82–105

Barceló J (ed) (2010) Fundamentals of traffic simulation. International Series in Operations Research & Management Science, vol 145, Springer, Berlin

Bellomo N, Dogbe C (2011) On the modeling of traffic and crowds: a survey of models, speculations, and perspectives. SIAM Rev 53:409–463

Daamen W, Buisson C, Hoogendoorn SP (eds) (2014) Traffic simulation and data: validation methods and applications. CRC Press, West Palm Beach

Flötteröd G, Rohde J (2011) Operational macroscopic modeling of complex urban road intersections. Transp Res B Methodol 45(6):903–922

Garavello M, Piccoli B (2006) Traffic flow on networks. Applied mathematics, American Institute of Mathematical Sciences, Springfield

Ni D (2015) Traffic flow theory: characteristics, experimental methods, and numerical techniques. Elsevier, Amsterdam

Rahman M, Chowdhury M, Xie Y, He Y (2013) Review of microscopic lane-changing models and future research opportunities. IEEE Trans Intell Transp Syst 14(3):1942–1956

Tampère CMJ, Corthout R, Cattrysse D, Immers LH (2011) A generic class of first order node models for dynamic macroscopic simulation of traffic flows. Transp Res B Methodol 45(1):289–309

van Wageningen-Kessels FLM, van Lint JWC, Vuik C, Hoogendoorn SP (2015) Genealogy of traffic flow models. EURO J Transp Logist 4:445–473

Chapter 2
The Fundamental Diagram

In the previous chapter, the main variables in traffic flow modelling were introduced. In this chapter, we discuss how they are related: obviously, high speeds seldom occur together with short headways, similarly, low densities create room for high speeds. Traffic flow models are based on the assumption that there is some relation between these variables. The relation between distance and velocity was first studied by Greenshields (1934) and called the fundamental relation (or fundamental diagram) later. Therefore, Greenshields is often regarded as the founder of traffic flow theory, and the fundamental diagram is the first model in the genealogical tree of traffic flow models (see Page 15).

The reader of this chapter is introduced to the concept of the fundamental diagram. After reading this chapter, they will be able to explain the typical shape of a fundamental diagram and why and how the basic shape can be adapted to reflect observations, such as scattered data. Furthermore, the reader will be able to link characteristics of microscopic driving behaviour (e.g. low speed at small headway and vice versa, (non)-equilibrium, hysteresis, capacity drop and heterogeneity in driving behaviour) to the shape of a fundamental diagram. Finally, they will be able to reflect on the desired properties of a fundamental diagram and assess whether a given diagram satisfies the requirements.

2.1 High Densities, Low Speeds and Vice Versa

Common observations of traffic show that at high densities, such as in (heavy) congestion, speeds are low. Conversely, when there are few vehicles on the road, headways are large and speeds are high. This is partially due to simple human behaviour: drivers tend to chose a speed that is as high as possible, while still safe. Therefore, traffic flow models commonly use a decreasing—or at least non-increasing—relationship between density and speed.

F. Kessels, *Traffic Flow Modelling*, EURO Advanced Tutorials
on Operational Research, https://doi.org/10.1007/978-3-319-78695-7_2

Because of this decreasing density-speed relationship, the maximum flow (density × speed) occurs at some intermediate density and speed values. This gives rise to one of the main challenges in traffic flow modelling: when densities are low, flows increase with increasing densities, however, at high densities, an increased density leads to a reduction in flow. See Fig. 2.1 for an example. This is different from, for example water flow (in the same figure), which is incompressible and the speed of the flow (i.e. the flow rate) does not depend on the density (Fig. 2.2). The precise relationship between variables such as density, headway, speed and flow, is an important subarea of traffic flow research. The main insights developed over the decades are discussed in the following sections of this chapter.

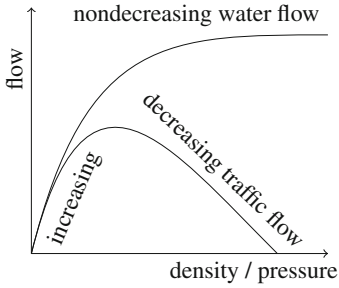

Fig. 2.1 Traffic vs. water flow: increasing and decreasing flow vs. nondecreasing flow

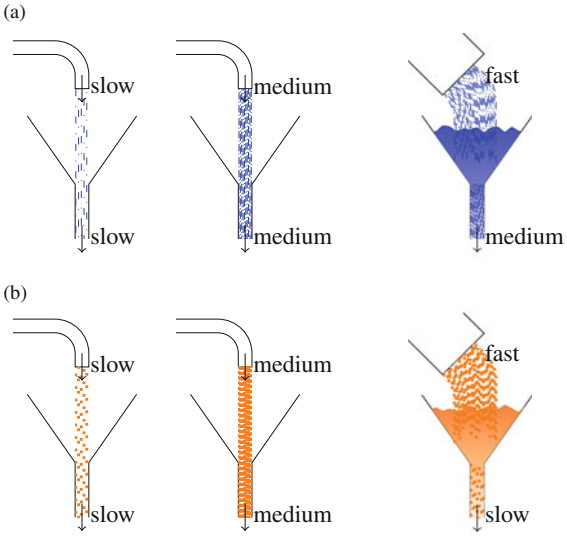

Fig. 2.2 Comparison of water and granular flow: inflows versus outflows. (**a**) Water: outflow equals inflow, up to a maximum. (**b**) Granular: at low inflows, outflow equals inflow. When inflow is too high, particles 'get stuck' in bottleneck and outflow is low, lower than with a medium inflow

2.2 Shapes of the Fundamental Diagram

The original fundamental diagram proposed by Greenshields (1934), is linear in the spacing-velocity plane. However, his name has now been linked to the fundamental diagram that he proposed one year later (Greenshields 1935). This fundamental diagram is linear in the density-velocity plane and thus parabolic in the density-flow plane (see Fig. 2.3):

$$V(\rho) = v_{\max} - \frac{v_{\max}}{\rho_{\text{jam}}}\rho, \tag{2.1}$$

with v_{max} the maximum speed and ρ_{jam} the jam density. Note the use of capital V to indicate that the speed is expressed as a function of density ρ. Therefore, $V(\rho)$ is the density-speed fundamental diagram and later we will also encounter $Q(\rho)$ as the density-flow diagram, $V(s)$ as the spacing-speed diagram and $S(v)$ as the speed-spacing diagram.

2.2.1 Fundamental Diagrams in Macroscopic Models

The model tree shows that since the 1930s, many other shapes of fundamental diagrams have been proposed, mostly for use in combination with macroscopic models. The Daganzo (1994) fundamental diagram is probably the most widespread due to its simplicity. It is bi-linear (triangular) in the density-flow plane (see Fig. 2.4):

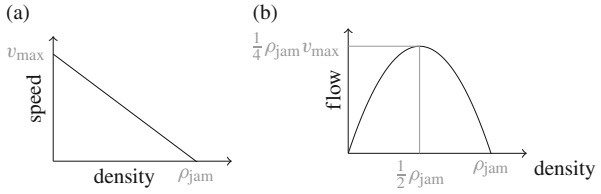

Fig. 2.3 The Greenshields fundamental diagram. (**a**) Density-speed. (**b**) Density-flow

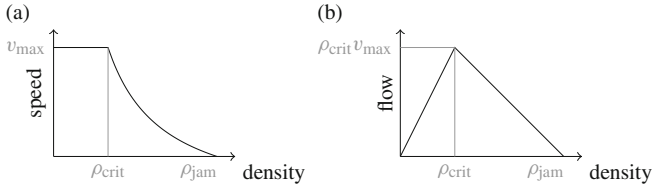

Fig. 2.4 The Daganzo fundamental diagram. (**a**) Density-speed. (**b**) Density-flow

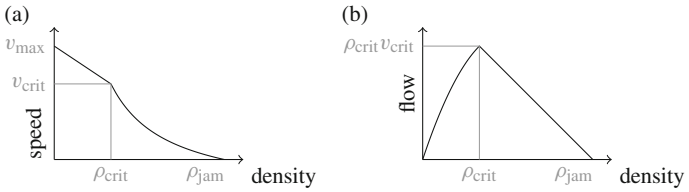

Fig. 2.5 The Smulders fundamental diagram. (**a**) Density-speed. (**b**) Density-flow

$$Q(\rho) = \begin{cases} v_{\max}\rho & \text{if } \rho < \rho_{\text{crit}} \\ \frac{\rho_{\text{crit}} v_{\max}}{\rho_{\text{jam}} - \rho_{\text{crit}}} \left(\rho_{\text{jam}} - \rho\right) & \text{if } \rho \geq \rho_{\text{crit}} \end{cases} \tag{2.2}$$

with v_{max}, v_{crit} the maximum and critical speed, respectively, ρ_{jam}, ρ_{crit}, the jam and critical density, respectively. A single parameter $w = \frac{\rho_{crit} v_{max}}{\rho_{jam} - \rho_{crit}}$ is sometimes used to denote the congestion wave speed. Figure 2.5 shows the Smulders fundamental diagram (Smulders 1990), which is a combination of the previous two: it is parabolic for low densities and linear for high densities (parabolic-linear):

$$Q(\rho) = \begin{cases} v_{\max}\rho - \frac{v_{\max} - v_{\text{crit}}}{\rho_{\text{crit}}}\rho^2 & \text{if } \rho < \rho_{\text{crit}} \\ \frac{\rho_{\text{crit}} v_{\max}}{\rho_{\text{jam}} - \rho_{\text{crit}}} \left(\rho_{\text{jam}} - \rho\right) & \text{if } \rho \geq \rho_{\text{crit}} \end{cases} \tag{2.3}$$

It still debated what is the best shape for a fundamental diagram, and how that relates to the applications. This has led to the development of even more shapes such as the exponential and power fundamental diagrams, named after their shape (del Castillo 2012). These are further generalized into a generic model, which also includes the bilinear fundamental diagram for certain parameter choices. The main advantage of the generic model (and also the exponential and power models), lies in the fact that it can be expressed in a single formula, i.e. not consisting of two branches that need to be defined separately such as in the bi-linear or parabolic-linear fundamental diagram. Furthermore, by restricting the choice of the invertible function ϕ and the model parameters, the models satisfy the requirements that will be discussed later (Sect. 2.3). The generic model is as follows:

$$\hat{q}(\hat{\rho}) = b + (a - b)\hat{\rho} - \phi^{-1}(\phi(a\hat{\rho}) + \phi(b(1 - \hat{\rho})) - \phi(0)) \tag{2.4}$$

with parameters $a > 0, b > 0$. $\hat{\rho} = \rho/\rho_{\text{jam}}$ and $\hat{q} = q/q_0$ are introduced to make the variables dimensionless. q_0 is a reference flow and not directly related to a certain traffic flow property.

If the function ϕ is chosen appropriately, then the generic model leads to a realistic and useful fundamental diagram. Examples for 'sound' functions ϕ and parameters are the power function (see Fig. 2.6):

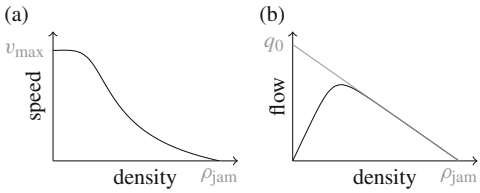

Fig. 2.6 The Power function fundamental diagram, with shape parameter $\theta = 5$. (**a**) Density-speed. (**b**) Density-flow

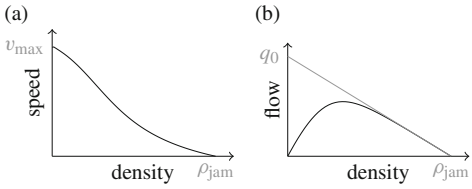

Fig. 2.7 The Exponential fundamental diagram, with shape parameter $\alpha = 2$. (**a**) Density-speed. (**b**) Density-flow

$$\phi(\rho) = \rho^{\theta} \tag{2.5}$$

with $\theta > 1$, $a = v_{\text{free}}/w$, $b = 1$ and $q_0 = w\rho_{\text{jam}}$, and exponential function (see Fig. 2.7):

$$\phi(\rho) = e^{\alpha\rho} - 1 \tag{2.6}$$

with $\alpha > 0$, $a = \frac{v_{\text{free}}}{w(1-e^{-\alpha b})}$, $b = \frac{1}{1-e^{-\alpha a}}$ and $q_0 = w\rho_{\text{jam}}$.

2.2.2 *Fundamental Diagrams in Microscopic Models*

The fundamental diagrams discussed above, are mostly applied in macroscopic traffic flow models. However, many microscopic traffic flow models also include a fundamental diagram. In this case, it is usually 'hidden' in the formulation of the car-following model. Furthermore, in microscopic models, spacing and speed are often used as main variables, and therefore it is more natural to express the fundamental diagram in these terms. As an example, the Optimal Velocity Model (OVM, Sect. 3.2.1, (Bando et al. 1995)) includes a fundamental diagram with a hyperbolic tangent function in the spacing-speed plane:

$$V(s) = c_1\big(\tanh[c_2(s - c_3)] + c_4\big) \tag{2.7}$$

c_1, c_2, c_3 and c_4 all nonnegative scaling parameters, see Fig. 2.8. The parameters are not straightforward to interpret, but Fig. 2.9 gives some indications of their relevance.

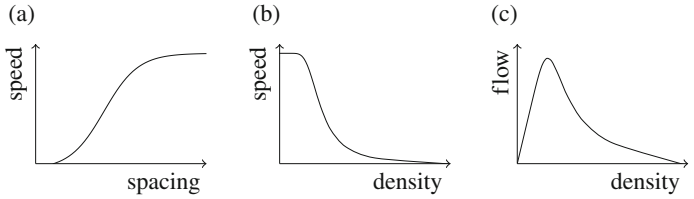

Fig. 2.8 The fundamental diagram of the Optimal Velocity Model (OVM). (**a**) Spacing-speed. (**b**) Density-speed. (**c**) Density-flow

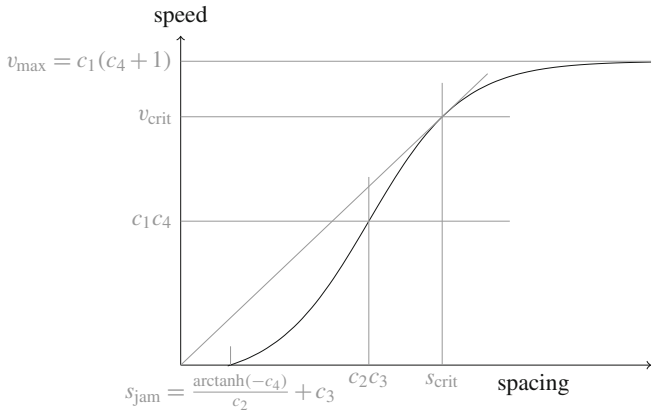

Fig. 2.9 The optimal velocity function used in OVM, with indications of the interpretation of the parameters

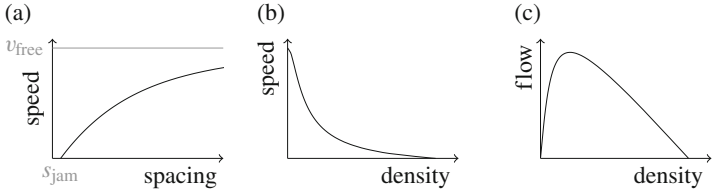

Fig. 2.10 The fundamental diagram of the Intelligent Driver Model (IDM). (**a**) Spacing-speed. (**b**) Density-speed. (**c**) Density-flow

The Intelligent Driver Model (IDM, Sect. 3.2.1, (Treiber et al. 2000)) includes a fundamental diagram that expresses the (equilibrium) headway as a function of the speed:

$$S(v) = \left(s_{\text{jam}} + T\,v\right)\left[1 - \left(\frac{v}{v_{\text{free}}}\right)^{\delta}\right]^{-1/2} \tag{2.8}$$

with s_{jam} the jam spacing and T the minimum time headway, v_{free} the free flow velocity (desired maximum speed) and δ the acceleration exponent, see Fig. 2.10.

2.3 Properties and Requirements

The previous section suggests that there are many different possible shapes of fundamental diagrams, and a few more will be introduced in the next section. Some are more popular than others, however, there is some agreement on basic requirements for the fundamental diagrams.

2.3.1 Requirements

We refer to Fig. 2.11 for an illustration of some of the properties of and requirements for fundamental diagrams. The three most important requirements for their shape are as follows:

1. A finite maximum speed exists and it is reached when density approaches zero: $V(\rho)_{\lim \rho \to 0} = v_{\max}$, with $v_{\max}$ finite.
2. A finite maximum density exists and at this density the speed is zero: $V(\rho_{\text{jam}}) = 0$, with ρ_{jam} finite.
3. When density increases, speed does not increase, and when density decreases speed does not decrease: $\frac{\mathrm{d}V}{\mathrm{d}\rho} \leq 0$ for all feasible densities $\rho \in (0, \rho_{\text{jam}}]$.

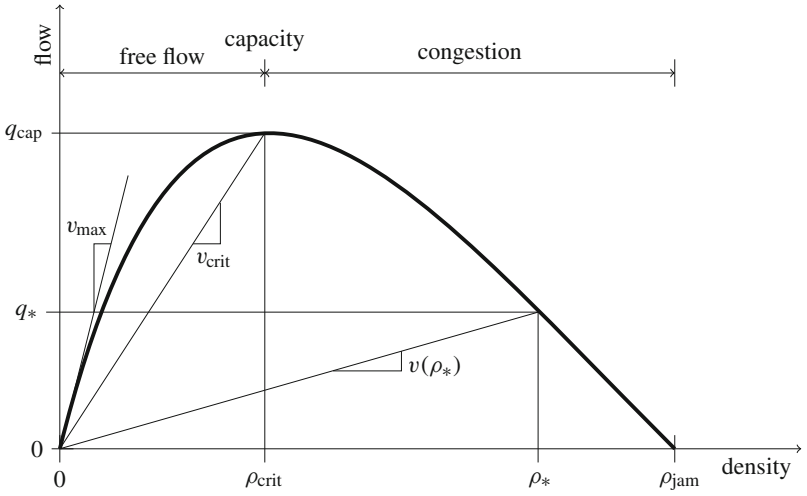

Fig. 2.11 Example of a fundamental diagram and its properties

2.3.2 Properties: Capacity, Free Flow and Congestion

When the requirements are combined with the definition of flow ($q = \rho v$), we also find that the flow is zero at the density extremes $\rho = 0$ and $\rho = \rho_{\text{jam}}$. Furthermore, there is a maximum flow, known as the capacity flow, at some density between both extremes. The corresponding density and speed are called the critical density (ρ_{crit}) and the critical speed (v_{crit}), respectively. This also splits the fundamental diagram into two branches: (1) a free flow branch with densities below critical, velocities above critical and increasing flow for increasing density and (2) a congestion branch with densities above critical, velocities below critical and a decreasing flow for increasing density.

2.3.3 Additional Requirements

In some cases, additional requirements are proposed:

1. The fundamental diagram must define speed as a unique function of density.
2. The fundamental diagram must be continuous.
3. The $Q(\rho)$ fundamental diagram must be concave, or even strictly concave.

The first additional requirement excludes fundamental diagrams that allow different speeds for the same density, such as those used to model hysteresis (see Sect. 2.4). The second additional requirement excludes fundamental diagrams with a discontinuity around capacity, such as those used to model a capacity drop (see Sect. 2.4). The third additional requirement excludes $Q(\rho)$ fundamental diagrams that are linear for a certain portion of the density domain (they are not strictly concave) and those that are convex for a certain portion of the density domain. This includes some of the fundamental diagrams in the next section, but the strict concavity requirement also excludes widespread ones such as the bi-linear and the linear-parabolic fundamental diagrams.

The main argument behind all these requirements originates from the possibility of non-unique solutions to simple problems. More specifically, when a fundamental diagram that does not satisfy the requirements is applied in a simple macroscopic model to calculate traffic states, the solution could be non-unique, i.e. multiple solutions to the same problem exist. For example, it is possible that a simple problem describing the growth of the queue upstream from a traffic light, does not have a unique solution. This issue will be explored deeper in Sect. 4.1.2.

Furthermore, the slope of a realistic $Q(\rho)$ fundamental diagram corresponds with the propagation speed of information at the corresponding density. In particular: the slope at zero density $Q'(0)$ equals the maximum vehicle speed and the slope at jam density $Q'(\rho)$ equals the congestion wave propagation velocity $-w$. This is, for example, the speed at which the front of the queue propagates upstream after a traffic light turns green. This all relates to the characteristic speed, which will also be discussed in more detail in Sect. 4.1.2.

2.4 Scatter in the Fundamental Diagram

Observed density-flow plots usually show a wide scatter, see Fig. 2.12. Much of the scatter can be explained by non-equilibrium traffic conditions (Zhang 1999; Laval 2011; Schnetzler and Louis 2013). When vehicles accelerate or decelerate, or when their headways change, their (and their drivers') behavior may be different from what may be observed when all of these variables are constant. E.g. when headways increase, a relatively high speed may still be perceived as 'safe' and thus acceptable. Zhang defines traffic to be in equilibrium if over a sufficiently long time (t) and road length (space x), velocity and density do not change: $\partial v/\partial t = 0$, $\partial \rho/\partial t = 0$, $\partial v/\partial x = 0$ and $\partial \rho/\partial x = 0$. Only points in the scatter plot that satisfy these criteria can be used to fit the fundamental diagram. Furthermore, lane changes also influence speeds and densities, and traffic can be considered to be out of equilibrium when vehicles are moving from one lane to the other. Certain branches of the family of fundamental diagrams in the model tree try to explain scatter in different ways, regardless of biased observations.

Scatter is mostly explained through vehicle properties and driver behaviour:

Capacity drop and hysteresis Scatter can be (partially) explained by a capacity drop: just before the onset of congestion, the outflow out of a bottleneck is known to be higher than in congestion, see Figs. 1.4 and 2.13a. The capacity drop has been explained by a low acceleration rate of vehicles leaving congestion, while

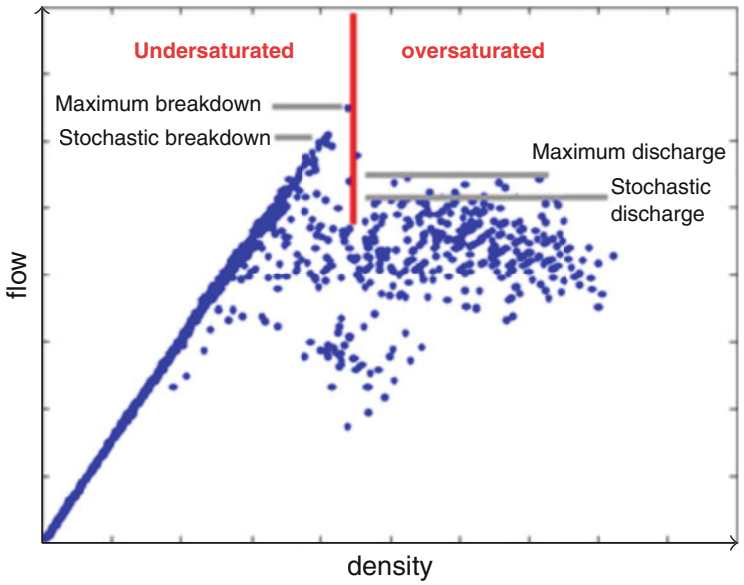

Fig. 2.12 Scatter in an observed density-flow plot, also showing a capacity drop (picture adapted from Calvert et al. (2016))

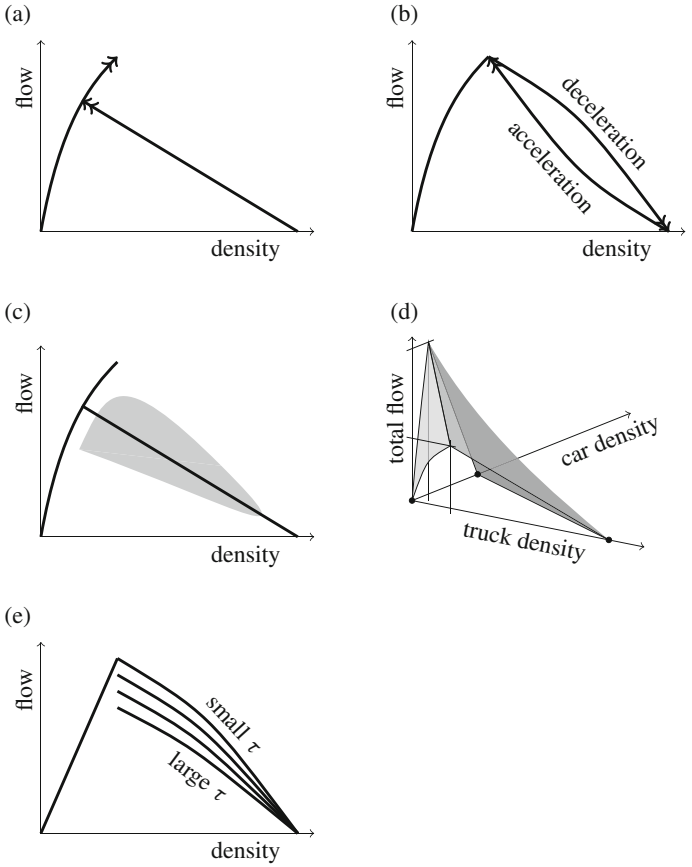

Fig. 2.13 Fundamental 'relations' based on scatter in observations. (**a**) Fundamental diagram with capacity drop. (**b**) Fundamental diagram with hysteresis. (**c**) 3-phase fundamental 'relation': lines and gray area are admissible traffic states. (**d**) 3-dimensional fundamental diagram with multi-class approach. (**e**) Fundamental diagram with capacity drop explained through difference in net time headway τ

vehicles decelerate at a higher rate when entering congestion (Edie 1961; Cassidy and Bertini 1999). Similar explanations including differences in acceleration and deceleration lead to fundamental diagrams with hysteresis (Newell 1965; Treiterer and Myers 1974; Zhang 1999), see Fig. 2.13b.

Heterogeneity An other approach to varying capacities is introduced in multi-class models. The fundamental diagram takes into account heterogeneity among vehicles and drivers. For example, trucks may be slower than cars, but occupy more space, leading to a lower jam density when there are many trucks. Therefore, the flow is a function of both the density of cars and the density of trucks. For example, Chanut and Buisson (2003) propose a three-dimensional

fundamental diagram, see Fig. 2.13d. The figure shows that if truck densities are relatively high, capacity is low.

From a different perspective, it has been argued that observations show too much scatter to derive a unique fundamental diagram from (Kerner and Rehborn 1996; Kerner 2009). It is proposed to use a three-phase approach characterized by the existence of three phases, one of them featuring wide scatter in the density-flow plane, see Fig. 2.13c. As a result, the maximum flow (capacity) of a road may vary over time. The idea of stochastic capacity is also explored by Srivastava and Geroliminis (2013); Calvert et al. (2016). The fundamental diagram including capacity drop and hysteresis are non-unique: in a region around capacity the flow is not uniquely defined by the density, but also depends on previous traffic states. Therefore, for a unique solution of the model when it is applied in a dynamic setting, additional assumptions on the transitions between the branches are needed (Zhang 2001).

The approach to including heterogeneity in the fundamental diagram by Chanut and Buisson (2003) makes very clear how the traffic throughput not only depends on density, but also depends on the composition of traffic. It is found that a large fraction of trucks, which—at least in Europe—drive at low speeds results in a lower flow. While, if there are only fewer trucks, cars and possibly also trucks drive at higher speeds. This approach leads to a unique flow, when densities of each type of vehicle are given. The core ideas have been implemented in many multi-class macroscopic traffic flow models, which are discussed in Chap. 4.

Schnetzler and Louis (2013) take a similar approach: explaining scatter through differences between cars and trucks. However, they also include a capacity drop, explaining this through differences in net time headway. This results in a fundamental diagram with a congestion branch (and congestion capacity) dependent on the net time headway, see Fig. 2.13e.

Problem Set

Assessment of the Fundamental Diagrams

Consider the fundamental diagrams discussed in this chapter, in particular:

1. The Greenshields fundamental diagram (parabolic in $Q(\rho)$)
2. The Daganzo fundamental diagram (bi-linear in $Q(\rho)$)
3. The Smulders fundamental diagram (parabolic-linear in $Q(\rho)$)
4. The OVM fundamental diagram (hyperbolic tangent in $V(s)$)
5. The IDM fundamental diagram
6. The power function fundamental diagram
7. The exponential fundamental diagram

2.1 Do the fundamental diagrams satisfy the requirements in Sect. 2.3.1? Does this depend on the parameter values, and if so, how?

2.2 For which fundamental diagrams are the critical density and critical speed explicitly defined as parameters? For the other models: what are the critical density, critical speed and capacity? How do they depend on other parameters?

2.3 Do the first five fundamental diagrams satisfy the additional requirements in Sect. 2.3.1? Does this depend on the parameter values, and if so, how?

Power and Exponential Fundamental Diagram

Consider the power and exponential fundamental diagram as discussed in Sect. 2.2.

2.4 Choose either of these fundamental diagrams and:

1. Draw the fundamental diagram using your method of choice (by hand or using a computer program like Octave or Matlab).
2. Change the parameters and see how the fundamental diagram changes.
3. Which parameter settings recover the bi-linear (Daganzo) fundamental diagram?

For better insight into the interpretation of the parameters, it can be useful to rewrite the fundamental diagram (2.4) such that it again expresses the flow as a function of the density (instead of the dimensionless flow as a function of the dimensionless density).

2.5 (Advanced) Rewrite (2.4) expressing flow as a function of density, i.e. find $Q(\rho)$.

del Castillo (2012) proves that when the following conditions all hold, then the generic model (2.4) is strictly concave:

- $\phi(0) \geq 0$
- $\phi' \geq 0$
- $\phi'' \geq 0$

We encourage the interested reader to study this proof.

2.6 (Advanced) Proof that the power and exponential fundamental diagrams are strictly concave.

Heterogeneity in the Fundamental Diagram

Consider the multi-class fundamental diagram as introduced in Chanut and Buisson (2003). It applies a Smulders fundamental diagram, with maximum speed parameter $v_{\max}$ unequal for cars ($v_{\max,\text{car}}$) and trucks ($v_{\max,\text{truck}}$). Furthermore, the other

parameters of the fundamental diagram depend on the car density ρ_{car} (the average number of cars per unit length) and the truck density ρ_{truck} (the average number of trucks per unit length):

$$\rho_{\text{crit}} = \beta\rho_{\text{jam}} \quad \text{and} \quad \rho_{\text{jam}} = \frac{\rho_{\text{car}} + \rho_{\text{truck}}}{L_{\text{car}}\rho_{\text{car}} + L_{\text{truck}}\rho_{\text{truck}}} \tag{2.9}$$

with L_{car} and L_{truck} the gross vehicle lengths of cars and trucks, respectively. I.e. L_{car} is the front to front distance between 2 cars in a queue (at standstill). Note that the critical speed v_{crit} is equal for both classes and independent of the traffic state.

2.7 Use these parameter values $v_{\text{max,car}} = 30$ m/s, $v_{\text{max,truck}} = 25$ m/s, $v_{\text{crit}} = 20$ m/s, $\beta = 0.2$, $L_{\text{car}} = 6$ m, $L_{\text{truck}} = 18$ m to calculate jam density ρ_{jam} and critical density ρ_{crit} in the following situations:

(a) only cars on the road
(b) only trucks on the road
(c) 10% trucks, 90% cars
(d) 50% trucks, 50% cars

2.8 Draw the axes for a density-speed fundamental diagram with on the horizontal axis the total density (cars and trucks), on the vertical axis speed.

- Draw the fundamental diagrams of cases (a) and (b).
- Add the fundamental diagrams for both cars and trucks for cases (c) and (d).
- Under which conditions do the car and truck fundamental diagrams overlap? I.e., when are the speeds of the cars equal to those of trucks?

2.9 Answer the questions below using the graph from the previous problem.

- Under which traffic conditions do the car and truck fundamental diagrams overlap? I.e., when are the speeds of the cars equal to those of trucks?
- Is this realistic? Why (not)?

Fundamental Diagrams Explaining Scatter

Consider the fundamental diagrams that explain scatter in Sect. 2.4.

2.10 (Advanced) Reflect on whether these models satisfy the requirements in Sect. 2.3.1.

Further Reading

del Castillo J (2012) Three new models for the flow-density relationship: derivation and testing for freeway and urban data. Transportmetrica 8(6):443–465

Kerner BS (2009) Introduction to modern traffic flow theory and control: the long road to three-phase traffic theory. Springer, Berlin

Li MZF (2008) A generic characterization of equilibrium speed-flow curves. Transp Sci 42(2):220–235

Zhang HM (1999) A mathematical theory of traffic hysteresis. Transp Res B Methodol 33(1):1–23

Chapter 3
Microscopic Models

The earliest family in the model tree incorporating dynamics are microscopic models. They are based on the assumption that drivers adjust their behaviour to that of the leading vehicle. Microscopic modelling has shown to be a fruitful line of thought, which is illustrated by the large part of the model tree taken up by this family (see the model tree on page 15). Microscopic models describe the longitudinal (car-following) and lateral (lane-changing) behaviour of individual vehicles. We focus on longitudinal behaviour.

Most microscopic models are car-following models: they describe the movement of each vehicle based on the behavior (movements) of the vehicle(s) in front of it. This chapters also discusses the most recent branch of microscopic models, namely cellular-automata and numerical methods for microscopic models.

After reading this chapter, the reader will understand the basics of the most popular microscopic models, including their main features. They understand how extensions of microscopic models to include heterogeneity, multi-anticipation and time delay will improve them and being able to adapt a simple model in these directions. They can reflect on the desired properties of such models, including stability, and are able to assess simple models. Finally, the reader learns about the application of numerical methods applied to microscopic models, understand the impact of the choice of numerical method on stability and accuracy and they will be able to apply simple methods themselves.

3.1 Safe-Distance Models

In microscopic models, vehicles are numbered to indicate their order: n is the vehicle under consideration, $n-1$ its leader, $n+1$ its follower, etc., see Fig. 1.6. The state of each individual vehicle n is modelled in terms of the position of the front of the vehicle x_n at time t. Different types of models have different ways to describe or

F. Kessels, *Traffic Flow Modelling*, EURO Advanced Tutorials
on Operational Research, https://doi.org/10.1007/978-3-319-78695-7_3

predict the movement of the vehicles, and thus how their position changes over time. Most models reflect human factors and behaviour, and are built using assumptions on how humans react and drive (Saifuzzaman and Zheng 2014).

The earliest car-following models include a car-following rule based on safe following distance. Pipes (1953) proposes to express the position of the leader as a function of the position of its follower:

$$x_{n-1} = x_n + T v_n + s_{n,\text{jam}} \tag{3.1}$$

with $s_{n,\text{jam}} = l_n + d$ the minimum rear-to-rear headway, i.e. the distance between the rear of the leader $n-1$ and the vehicle under consideration n in a jam. This is also illustrated in Fig. 3.1. $T v_n$ is interpreted as the 'legal distance' *between* vehicle $n-1$ and n: the extra distance that—together with the minimum rear-to-rear headway $s_{n,\text{jam}}$—makes up the actual rear-to-rear headway.

Assuming $s_{n,\text{jam}} = s_{\text{jam}}$ equal for all vehicles n, the model can be reformulated expressing the speed v_n as a function of the position x_n and the leaders' position x_{n-1}, or of the space headway (spacing) $s_n = x_{n-1} - x_n$:

$$v_n = \frac{x_{n-1} - x_n - s_{\text{jam}}}{T} = \frac{s_n - s_{\text{jam}}}{T} \tag{3.2}$$

which then leads to the following spacing-speed and density-speed relation:

$$V^*(s) = \frac{1}{T}(s - s_{\text{jam}}) \quad \text{or} \quad V(\rho) = \frac{1}{T\rho_{\text{jam}}}\left(\frac{\rho_{\text{jam}}}{\rho} - 1\right) \tag{3.3}$$

The 'fundamental diagrams' are shown in Fig. 3.2. Note that for low densities, the fundamental diagram is not realistic as the speed goes to infinity.

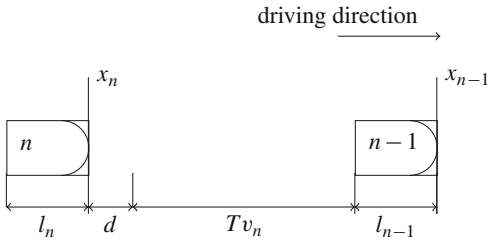

Fig. 3.1 Parameters of Pipes' safe-distance model

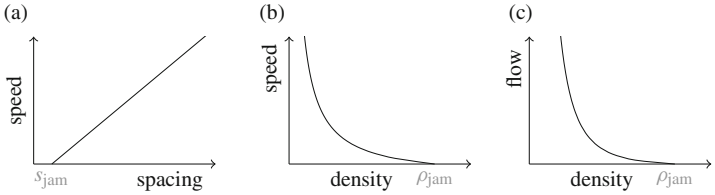

Fig. 3.2 The fundamental diagram of Pipes' safe-distance model. (**a**) Spacing-speed. (**b**) Density-speed. (**c**) Density-flow

3.1.1 Safe-Distance Models with Delay

Safety is closely related with delay: car-following behaviour is only safe when the delayed response to a change is taken into account. The first models including delay were introduced around 1960 (Kometani and Sasaki 1961; Newell 1961). Kometani and Sasaki's model is derived from basic Newtonian equations of motion. It is assumed that a drivers act such that they can avoid a collision even if their leader would act 'unpredictable'. Effectively, jam spacing s_{jam} in Pipes's model is replaced with a velocity-dependent term. Furthermore, their formulation includes a time delay τ. A positive τ represents that it takes some time between a change in the behaviour of a vehicle and the actual reaction of its follower to this change. The time delay τ includes the reaction time of the driver, but it can also depend on their perception and the time it takes between noticing that action is needed/desired and actual braking or accelerating due to limitations of the vehicle.

Several decades after the introduction of Newell's 1961 model, it was simplified (Newell 2002):

$$x_n(t + \tau_n) = x_{n-1}(t) - s_{\text{jam},n} \tag{3.4}$$

In this model, a vehicle follows the trajectory of its leader, translated by delay time τ_n and jam spacing $s_{\text{jam},n}$. Delay time τ_n and jam spacing $s_{\text{jam},n}$ may differ for each vehicle and driver. This model was later extended to include differences between 'timid' and 'aggressive' drivers (Laval and Leclercq 2010). Timid drivers would keep a longer distance when the leader decelerates into congestion, while aggressive drivers tend to keep shorter following distances, see Fig. 3.3. The formulation clearly shows that delay leads to hysteresis: the current behaviour of a vehicle/current traffic state depends on previous behaviours/states. With the correct parameter settings, the timid/aggressive car-following models gives simulation results showing stop-and-go waves.

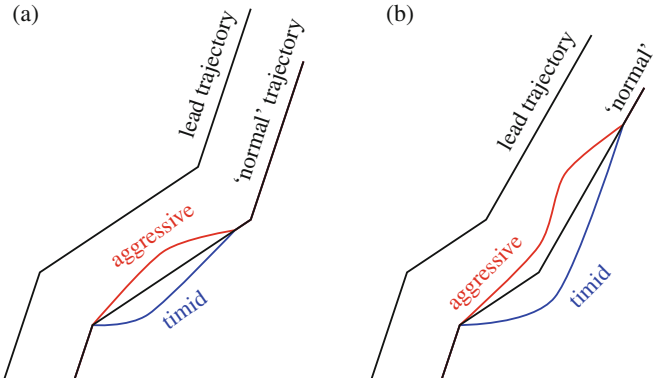

Fig. 3.3 Trajectories in the timid/aggressive model. Timid drivers decelerate and accelerate fast and therefore keep longer headways throughout a congestion wave. Aggressive drivers keep shorter headways. (**a**) Long wave. (**b**) Short wave

3.1.2 High Speeds Versus Safety

Gipps (1981) refines safe-distance car-following models with delay by assuming that 'the driver travels as fast as safety and the limitations of the vehicle permit':

$$v_n(t+\tau) = \min \left\{ \overbrace{v_n(t) + 2.5 a_{\max}\tau \left(1 - \frac{v_n(t)}{v_{\max}}\right)\sqrt{0.025 - \frac{v_n(t)}{v_{\max}}}}^{\text{limited by self}}, \right.$$
$$\left. \underbrace{a_{\min}\tau + \sqrt{a_{\min}^2\tau^2 - a_{\min}\left(2\left(s_n(t) - s_{\text{jam}}\right) - v_n(t)\tau - \frac{v_{n-1}(t)^2}{a_{\min}}\right)}}_{\text{limited by safe distance}} \right\} \tag{3.5}$$

with $a_{\max}$ maximum acceleration, $a_{\min}$ maximum deceleration (minimum acceleration), $v_{\max}$ the desired (maximum) velocity and s_{jam} jam spacing. Jam spacing is the front-to-front distance between two vehicles at standstill. Effectively, this approach introduces two regimes: one in which the vehicle itself limits its velocity (the upper part in Eq. (3.5)), and one in which the safe distance to the leader limits velocity (the lower part in the equation).

An other approach to model 'safe' behaviour is to include the collision probability in a model for acceleration (Hamdar et al. 2008). The authors propose to model the probability of a collision and adjust the acceleration (or deceleration)

accordingly. The main idea is as follows: Driver behaviour is influenced by

1. the predicted velocity distribution of the leading vehicle
2. the speed of the leading vehicle relative to the own speed
3. the gap between the rear bumper of the leading vehicle and the own front bumper.

These three factors determine the probability of a collision, for any given acceleration. However, accelerating also gives a certain utility: e.g. driving at a speed close to the maximum speed. A combined utility function is proposed to weigh the collision probability against the utility of accelerating. Finally, the utility is maximized and the vehicle is modelled to accelerate or decelerate with the corresponding optimal acceleration/deceleration.

3.2 Stimulus-Response Models

The second branch of car-following models consists of stimulus-response models. It is assumed that drivers accelerate (or decelerate) as a reaction to three stimuli:

1. own current velocity $v_n = \frac{\mathrm{d}x_n}{\mathrm{d}t}$
2. spacing with respect to leader $s_n = x_{n-1} - x_n$
3. relative velocity with respect to leader (receding rate) $\dot{s}_n = \frac{\mathrm{d}s_n}{\mathrm{d}t} = v_{n-1} - v_n$

In the late 1950s and early 1960s there was a rapid development of stimulus-response models and the efforts consolidated in the now famous GHR-model, named after Gazis et al. (1961):

$$\underbrace{a_n(t)}_{\text{response}} = \underbrace{\gamma \frac{\big(v_{n-1}(t)\big)^{c_1}}{\big(s_n(t-\tau)\big)^{c_2}}}_{\text{sensitivity}} \underbrace{\dot{s}_n(t-\tau)}_{\text{stimulus}} \tag{3.6}$$

$\gamma \frac{(v_{n-1}(t))^{c_1}}{(s_n(t-\tau))^{c_2}}$ is considered as the sensitivity of vehicle/driver n. γ is the sensitivity parameter and c_1 and c_2 are parameters that are used to fit the model to data. The receding rate $\dot{s}_n(t-\tau)$ is observed at delay time τ ago and is considered as the stimulus, the acceleration $a_n(t)$ as the response, hence the name 'stimulus-response' model.

Since those early developments, a lot of work has been done in calibrating and validating this and other similar models. However, in 1999, Brackstone and McDonald concluded that stimulus-response models are being used less frequently, mainly because of contradictory findings on parameter values. Nevertheless, since the mid 1990s many new models have been developed and stimulus-response models are popular again.

3.2.1 More Recent Stimulus-Response Models: OVM and IDM

Bando et al. (1995) introduce the optimal velocity model assuming that drivers accelerate (or decelerate) to their optimal velocity, which is a function of the headway:

$$a_n(t) = \gamma \left(V\big(s_n(t)\big) - v_n(t) \right) \tag{3.7a}$$

$$V(s) = c_1 \big(\tanh[c_2(s - c_3)] + c_4 \big) \tag{3.7b}$$

with γ the sensitivity parameter and c_1, c_2, c_3 and c_4 parameters of the optimal velocity function $V(s)$. As discussed in more detail in Sect. 2.2.2, the optimal velocity function can be interpreted as the fundamental diagram of the model: it represents the spacing-speed relationship at equilibrium.

In the intelligent driver model by Treiber et al. (2000) the acceleration function includes two important components:

1. acceleration towards the maximum speed $v_{\max}$
2. acceleration/deceleration to obtain the space gap that is desired at the current speed and current change in gap (e.g. deceleration/lower acceleration when approaching the leader).

The acceleration function is described by:

$$a = a_{\max} \left(1 - \left(\frac{v}{v_{\max}} \right)^{\delta} - \left(\frac{S(v, \dot{s})}{s} \right)^2 \right) \tag{3.8}$$

with $a_{\max}$ the maximum acceleration, v_{free} the free flow velocity (desired maximum speed) and δ the acceleration exponent. $S(v, \dot{s})$ denotes the space gap function, describing the desired spacing as a function of the speed and the change in spacing (i.e. difference in speed with leader):

$$S(v, \dot{s}) = s_{\text{jam}} + T v - \frac{v \dot{s}}{2\sqrt{a_{\max} a_{\min}}} \tag{3.9}$$

with $a_{\min}$ the maximum deceleration (minimum acceleration), s_{jam} the jam spacing and T the minimum time headway.

The fundamental diagram (2.8) can be derived using the acceleration equation (3.8) and the space gap function (3.9). At equilibrium both the acceleration a and the change in spacing $\dot{s}$ are zero. Substituting this into (3.8) and subsequently substituting (3.9) gives:

$$a = a_{\max} \left(1 - \left(\frac{v}{v_{\max}} \right)^{\delta} - \left(\frac{s_{\text{jam}} + T v}{s} \right)^2 \right) = 0 \tag{3.10}$$

Table 3.1 Typical parameter values of the IDM

Maximum speed $v_{\max}$	30 m/s
Jam spacing s_{jam}	7 m
Reaction time T	1.5 s
Maximum acceleration $a_{\max}$	1 m/s^2
Maximum deceleration $a_{\min}$	1.5 m/s^2
FD shape parameter δ	1

Rewriting gives the fundamental diagram (2.8):

$$S(v) = \left(s_{\text{jam}} + T\,v\right)\left[1 - \left(\frac{v}{v_{\max}}\right)^{\delta}\right]^{-1/2} \tag{3.11}$$

with s_{jam} the jam spacing and T the minimum time headway, v_{free} the free flow velocity (desired maximum speed) and δ the acceleration exponent, see Fig. 2.10.

Typical values for parameters in the IDM are given in Table 3.1. They are used in the simulations to produce the figures in this chapter. Readers are encouraged to play around with the parameter settings in the Problem Set at the end of this chapter.

3.2.2 Simulation Results with a Stimulus Response Model

The results of a simple simulation using IDM are shown in Fig. 3.4. It shows 15 vehicles on a 800 m long ring road. They are waiting in a queue until the first one starts driving at $t = 0$. Because they drive on a ring road, the first vehicle catches up with the last one and after about 1 min, the spacing and speeds are almost equal for all vehicles. The parameters of the model are given in Table 3.1. Furthermore, for the numerical method, an explicit Euler scheme with time step size $\Delta t = 0.5$ s were used. The relevance of the numerical method is discussed in Sect. 3.6.

3.2.3 Generic Model and Stability

Already in the earliest days of stimulus-response models Chandler et al. (1958) introduced a generic formulation:

$$a(t) = f\left(v(t), s(t), \dot{s}(t)\right) \tag{3.12}$$

In this formulation, it clear to see that the acceleration a is a response to the stimuli speed v, spacing s and change in spacing $\dot{s}$. It is interesting to note that, after reformulation, most safe-distance models also fit in this framework.

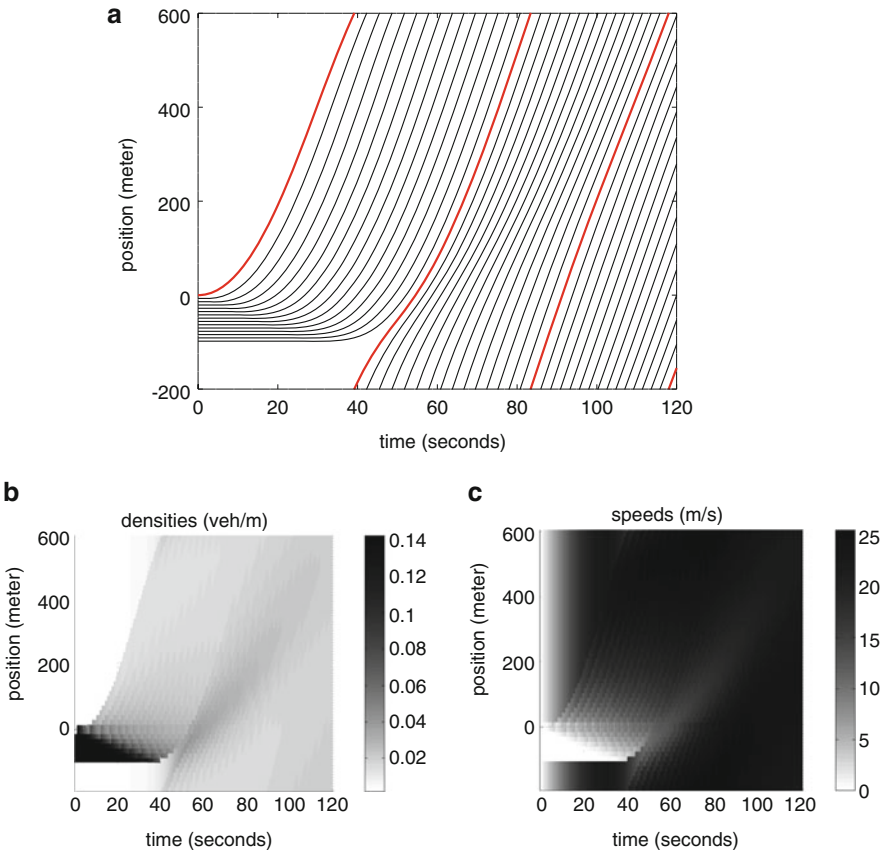

Fig. 3.4 Simulation results with IDM on a ring road, with an initial queue that dissolves, as described in Sect. 3.2.2. The same results are presented in different ways. (**a**) Trajectories: thick red trajectory is that of the first vehicle that starts driving at $t = 0$. The other trajectories (black) are of vehicles that were waiting in a queue behind the first one. (**b**) Densities. (**c**) Speeds

3.2.3.1 Requirements for Car-Following Models

More recently, Wilson (2008), Wilson and Ward (2011) use the generic formulation (3.12) to qualitatively asses stimulus-response models. They perform stability analyses and put forward constraints on the function f and its parameters. Firstly, for any car-following model, it should be possible to derive an equilibrium fundamental relation from the steady state solution of f:

$$\forall s > 0, \ \exists v = V(s) > 0 \text{ such that } f(v, s, 0) = 0 \tag{3.13}$$

Secondly, driving behaviour should be 'rational':

1. If velocity increases, the vehicle accelerates less (or decelerates more): $\mathrm{d}f/\mathrm{d}v < 0$.
2. If headway increases, the vehicle accelerates more (or decelerates less): $\mathrm{d}f/\mathrm{d}s \geq 0$.
3. If relative velocity increases, the vehicle accelerates more (or decelerates less): $\mathrm{d}f/\mathrm{d}\dot{s} \geq 0$.

If these conditions are satisfied, the model satisfies certain desirable stability conditions, as discussed in more detail below.

3.2.3.2 Stability of Car-Following Models

When looking at the dynamics of a system, it is important to know whether it is stable. In general, a system is stable if, when it is brought out of its current state, it will go back to that state (see Fig. 3.5a). In a traffic flow context, this means that when there is a perturbation (e.g. one driver suddenly brakes), traffic is stable when all vehicles will return to their initial speed. There are three types of questions to ask about the stability:

1. Does the fluctuation grow over time, will it stay within certain limits, or will it 'die out'?
2. Does the fluctuation stay at the same position or does it move, does it also affect other vehicles?
3. If the fluctuation moves, does it move with the vehicle that initially experienced the perturbation or does it move with a different speed, maybe even in the other direction?

These kind of questions are addressed by defining two types of stability that are of special interest in traffic flow: local stability and string stability. Local stability is about a perturbation growing both in amplitude and number of affected vehicles and becoming permanent, see Fig. 3.5b. If the flow is locally unstable, it will not return to its original, unperturbed state, and this type of instability is undesired. Wilson and Ward (2011) show that if the rational driving behaviour conditions are satisfied, then the car-following model is local stable. It is important to note, however, that, for a given model, the rational driving conditions may be satisfied for certain parameter values, but not for others.

The second type of stability is string stability , which is about a perturbation that might grow but each vehicle themselves will eventually return to the original unperturbed state Fig. 3.5c. This type of stability is linked to stop-and-go waves. The idea is that if a model is string unstable, then the fluctuation will grow and after it has passed tens or hundreds of cars, nonlinear effects will take over and trigger stop-and-go waves. The key difference with local stability is that the frame of reference is permitted to move: the fluctuation will remain, but it is allowed to move upstream, leading to recovery from the perturbation by vehicles that were affected

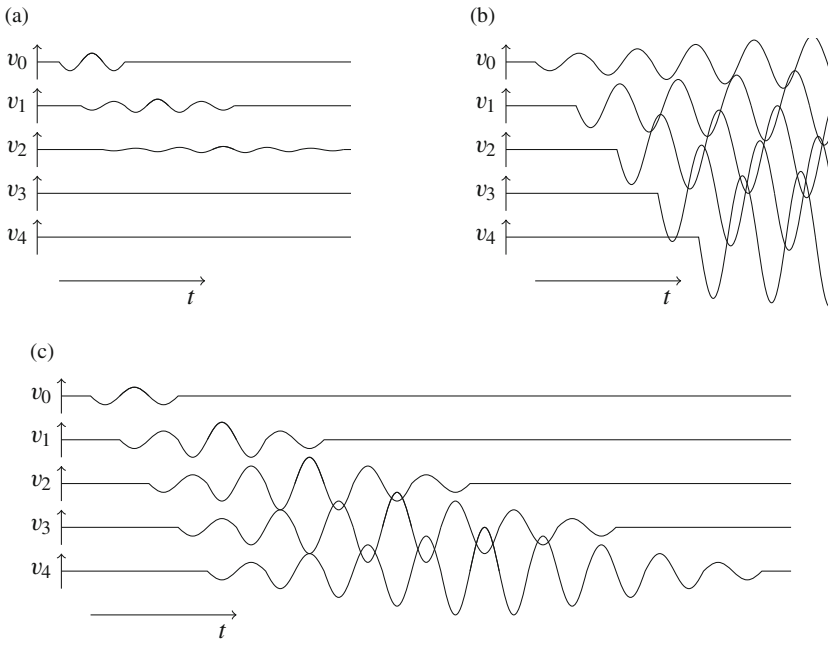

Fig. 3.5 Stability in car-following. The top line indicates the development of the speed (v_0) of the leading vehicle, which has a small perturbation. The other lines indicate the development of the speed of the following vehicles. (**a**) Stability. (**b**) Local instability (**c**) String instability

before. Wilson and Ward (2011) show that it largely depends on its parameter values whether the model will exhibit string instability. The problem set at the end of this chapter will explore this further and challenge the reader to do some stability analysis themselves.

Except for the type of stability, also its propagation direction is important. Will any propagation move downstream, in the driving direction of the vehicles, at the same speed, faster or slower? Or will it stay at the same location or move upstream, and at which speed? To model stop-and-go waves realistically, the string instability should propagate upstream, at the same speed as an observed stop-and-go wave, which is more or less equal to the slope of the congestion branch of the fundamental diagram. This could be checked by simulation, but a more rigorous approach is, again, based on analysis of the acceleration function f in (3.12). However, the analysis is beyond the scope of this book. The interested reader is referred to Wilson and Ward (2011), Ward and Wilson (2011) for more details.

3.3 Action Point Models

The third, and last, branch of car-following models consists of action point models, first introduced by Wiedemann (1974). However, a decade earlier, Michaels (1965) discussed the underlying concept that drivers would only react if they perceive that they approach a vehicle. Therefore, the approach rate or the headway must reach some perception threshold before a driver reacts. The main advantage of action point models is that they incorporate, in contrast to other car-following models, that:

1. at large headways driving behaviour is not influenced by that of other vehicles, and
2. at small headways driving behaviour is only influenced by that of other vehicles if changes in relative velocity and headway are large enough to be perceived.

If driving behaviour is influenced by that of others, any of the previously introduced safe-distance or stimulus-response models can be used to describe the influence quantitatively.

3.4 Cellular-Automata Models

Cellular-automata models are usually categorized as microscopic models, even though they are a different, and much younger, branch of the model tree. Just as in car-following models, the movement of individual vehicles is modelled. The main difference with car-following models is that space, and sometimes time, is discretized. Moreover, the velocity is discretized. Therefore, they are in general computationally more efficient.

In a cellular-automata model, the road is partitioned into cells of usually 7.5 m long. In a cell either a vehicle might be present or not. The model consists of a set of rules, that determine when the vehicle will move to the next (downstream) cell. The rules may be stochastic or deterministic. The model by Nagel and Schreckenberg (1992) is regarded as the prototype cellular-automata model. In this model, each time step each vehicle is advanced a few (or zero) cells according to the following algorithm:

1. If velocity is below maximum velocity, then accelerate: $\tilde{v} \rightarrow \min(\tilde{v} + 1, v_{\max})$.
2. If headway is too small, then decelerate: $\tilde{v} \rightarrow \min(\tilde{v}, \tilde{s}_{\text{jam}} - 1)$.
3. Decelerate at random: $\tilde{v} \rightarrow \max(\tilde{v} - 1, 0)$ with probability π.
4. Move: $\tilde{x} \rightarrow \tilde{x} + \tilde{v}$.

In the algorithm, $\tilde{v}$ denotes the normalized vehicle velocity in number of cells per time step, $\tilde{v}_{\max}$ denotes the normalized maximum vehicle velocity and $\tilde{s}_{\text{jam}}$ the normalized jam spacing in number of cells. $\tilde{x}$ is the cell number and π is the deceleration probability.

More recent developments combine cellular-automata models with the optimal velocity car-following model (Helbing and Schreckenberg 1999) or three phase theory (Kerner et al. 2002). Some of the most popular cellular-automata models are compared by Knospe et al. (2004).

3.5 Extensions

Microscopic models can relatively easily be adopted to other (assumed) behaviours of vehicles and drivers. Extra variables or parameters are added to reflect differences between types of vehicles, to reflect look-ahead behaviour, to reflect reaction-time delays or to include lane changes and lateral behaviour.

3.5.1 Heterogeneity

Most car-following models described and analysed in literature assume homogeneous vehicle-driver units, that is: vehicles and drivers all behave identically. However, since each vehicle is modelled and simulated individually, it is relatively straightforward to take into account heterogeneity. In that case model parameters such as desired (maximum) velocity, sensitivity and reaction time may vary over vehicles and drivers. In fact, most simulation tools based on car-following models are multi-class, that is: they do take into account heterogeneity.

3.5.2 Multi-Anticipation

Simple car-following models only take into account reaction to the immediate leader. However, in multi-anticipation models more than one leading vehicle influences the behaviour of a driver. For example, the generic model (3.12) with multi-anticipation would then be:

$$a_n(t) = f\big(v_n(t), s_n(t), \dot{s}_n(t), s_{n-1}(t), \dot{s}_{n-1}(t), \ldots, s_{n-N}(t), \dot{s}_{n-N}(t), \big) \quad (3.14)$$

The index n is used to denote the vehicle under consideration, $n-1$ is its leader, etc. N is the number of leaders that may influence the behaviour.

3.5.3 Time Delay

Time delay is introduced to reflect that drivers do not instantaneously react to any changes, but instead take a while to change their behavior (Bando et al. 1998; Treiber et al. 2006; Yu et al. 2014). For example, the generic model (3.12) with delay would then be:

$$a_n(t) = f\big(v(t-\tau), s(t-\tau), \dot{s}(t-\tau)\big) \tag{3.15}$$

with $\tau \geq 0$ the delay time. This is a commonly used extension of the models. However, including delay has a big impact on the mathematical properties of the model, and especially on the stability. However, this is beyond the scope of this book. The interested reader is referred to Wilson and Ward (2011), Ward and Wilson (2011) for more details about the theory. They are also encouraged to explore the issues using simulations, described in the Problem Set at the end of this chapter.

3.5.4 Lateral Movements

Until now, we have only discussed longitudinal (car-following) behaviour. However, an agent based traffic flow simulation for multi-lane roads is not complete without a model for lateral movements (lane changes). There are many models for lane changing, most of them making a distinction between:

mandatory lane change occurs when a driver moves to a different lane because of their route choice, e.g. from on ramp to main road to enter the freeway, from main road to off ramp to leave the freeway, from one lane to the next because the first lane will end or is blocked.

discretionary lane change occurs when a driver seeks a speed advantage, this often includes overtaking.

Other types of lane change in models can include random lane change (without apparent reason) or forced merging (when a driver creates a gap to enter a congested lane). Most lane change models consist of the following three steps:

1. Decide about necessity of lane change
2. Choose target lane
3. Decide whether to accept gap

Gap acceptance models include choices about whether the gap (distance between new leader and new follower) is big enough, but also about whether the necessary deceleration or acceleration are acceptable. A more detailed review of lane change models can be found in Rahman et al. (2013), Treiber and Kesting (2013).

3.6 Numerical Methods for Car-Following Models

The previously introduced car-following models are continuous in time and space. Therefore, for any case or simulation that is not very simple or even trivial, numerical integration needs to be used. Time is sliced into discrete time steps and the positions, and possibly states like velocity, acceleration and lane of all vehicles are computed.

One of the most simple and widely applied schemes is the Euler method:

$$x_n^{k+1} = x_n^k + \Delta t v_n^k \tag{3.16a}$$

$$v_n^{k+1} = v_n^k + \Delta t a_n^k \tag{3.16b}$$

Where k indicates the previous time step and $k+1$ the new time step: x_n^k, v_n^k and a_n^k are the position, speed and acceleration, respectively, of the n-th vehicle at time $t = t_0 + k\Delta t$. a_n^k is calculated according to the car-following model, e.g.

$$a_n^k = f\left(v_n^k, x_{n-1}^k - x_n^k, v_{n-1}^k - v_n^k\right) \tag{3.17}$$

with function f as the generic model as in (3.12). Furthermore, $v_{n-1} - v_n$ approximates the change in spacing because $\dot{s} = \frac{\mathrm{d}s}{\mathrm{d}t} \approx \frac{\mathrm{d}}{\mathrm{d}t}(x_{n-1} - x_n) = v_{n-1} - v_n$. This method is, for example, applied in the traffic simulators SUMO (Krajzewicz et al. 2012) and AIMSUN (Casas et al. 2010).

3.6.1 Advanced Numerical Methods

Other, more advance methods have been proposed and compared by Treiber and Kanagaraj (2015). The most promising of them is the ballistic update scheme which uses the same Euler update for the velocity (3.16b). The position is updated using the average of the velocity at the old time and that of the new time:

$$\begin{aligned} x_n^{k+1} &= x_n^k + \Delta t \frac{v_n^k + v_n^{k+1}}{2} \\ &= x_n^k + \Delta t v_n^k + \frac{(\Delta t)^2}{2} a_n^k \end{aligned} \tag{3.18}$$

The ballistic method outperforms the Euler method in terms of accuracy and computational complexity. Furthermore, they show that other methods (such as Runge Kutta) that are often used for ordinary differential equations resulting from other types of systems, perform worse because of the lack of 'smoothness' in traffic flow. Traffic is not 'smooth' in the sense that oftentimes there are sudden changes in traffic state such as a decrease in speed and increase in density at the upstream front

of congestion. In fact, the non-smoothness can even in the most simple numerical methods lead to negative velocities. Therefore, in simulations, heuristics are applied to ensure that vehicles stop behind their leader without driving backward.

3.6.2 Numerical Methods and Delay

Many car-following models include a delay term, such as in (3.15). Therefore, the time step Δt needs to be taken such that the delay τ is a multiple thereof: $\tau = r\Delta t$, with r integer. When including delay, the acceleration function f is not considered at current time t, but at the earlier time $t - \tau = t - r\Delta t$, which leads to the following formula for the acceleration:

$$a_n^k = F\left(v_n^{k-r}, x_{n-1}^{k-r} - x_n^{k-r}, v_{n-1}^{k-r} - v_n^{k-r}\right) \tag{3.19}$$

The difference between time delay τ and time step size Δt is important. Even though they have the same dimension (time) and can be of similar size ($\approx$0.1–1.5 s), they have a different interpretation and changing them should affect simulation results in a different way. τ is a model parameter—reflecting a time delay that is present in real car-following behaviour. τ should be small (or zero) when one wants to model that drivers (and vehicles) react quickly (or instantaneously) to a change in their leaders' behaviour, it should be large when the reaction takes longer. Δt is a parameter of the numerical method: indicating the size of the time steps in the simulation. A very small time step (approaching zero) gives a very accurate approximation of the time-continuous model. A somewhat larger time step size will give less accurate approximation but in many cases also shorter computation times. This difference is explored further in the Problem Set.

Problem Set

Microscopic Model and Fundamental Diagram

Consider Gipps' Safe-Distance model with delay as in Sect. 3.1.2. We modify the equation slightly to allow speed to become zero:

$$v_n(t+\tau) = \min\left\{ v_n(t) + 2.5a_{\max}\tau\left(1 - \frac{v_n(t)}{v_{\max}}\right), \right.$$
$$\left. a_{\min}\tau + \sqrt{a_{\min}^2\tau^2 - a_{\min}\left(2\big(s_n(t) - s_{\text{jam}}\big) - v_n(t)\tau - \frac{v_{n-1}(t)^2}{a_{\min}}\right)} \right\} \tag{3.20}$$

This adaptation may lead to unrealistic acceleration/deceleration behaviour at very low speeds, but that does not interfere with our current goal of deriving and understanding the fundamental diagram.

3.1 Consider only the safe distance branch of (3.20) (that is the lower part of the equation). Derive the spacing-speed fundamental diagram and draw it.

The other ('free') branch introduces more realistic behaviour at high spacings.

3.2 What is the speed at very high spacings, according to (3.20)? Note: consider the free branch (the upper part).

3.3 Add the free flow branch to the previously drawn fundamental diagram (Problem 3.1).

Simulations

Simulations can give better insights into models. Sample code can be found on the website (http://extras.springer.com) of this book.

3.4 Run a simulation to reproduce the results in Fig. 3.4.

3.5 Adapt the provided code in one or more of these directions:

- make the initial queue longer
- change parameter values of the model parameters (maximum speed, jam spacing, reaction time, maximum and minimum acceleration shape parameter δ)
- replace the IDM with the OVM
- include delay
- change the time step size
- replace the Euler explicit time stepping method with the ballistic update scheme.

Compare the results of different setups and reflect on your insights: is this more (or less) realistic? Do you see other phenomena? Compare your results with those in literature.

Stability in IDM

As a base case, we consider the Intelligent Driver Models as introduced in Sect. 3.2.1, with the parameters as in Table 3.1. Again, we refer to the sample code available on the website.

3.6 Assess the platoon stability of the model by determining the sign of the derivatives of the acceleration function.

3.7 (Advanced) Asses the string stability of the model using simulations:

- Simulate vehicles driving over a ring road, using the default parameters.
- Vary the initial state of the vehicles to find when the model is string stable and when it is string unstable.
- When the results show instability, does the instability propagate upstream and/or downstream? Is this realistic?

Stability in Other Models

3.8 (Advanced) Use the adaptations in Problem 3.5 to explore (string) stability of:

- IDM with different parameter values
- OVM
- IDM or OVM with delay

and the interplay between the time step size or the numerical method and stability.

Simulations of Other Models

Problem 3.1 (Advanced) Adapt the simulation of IDM for a simple cellular automata model (see Sect. 3.4). Use the same queue test case and compare the results with those of other simulations that you have done.

Further Reading

Aghabayk K, Sarvi M, Young W (2015) A state-of-the-art review of car-following models with particular considerations of heavy vehicles. Transp Rev 35(1):82–105

Brackstone M, McDonald M (1999) Car-following: a historical review. Transp Res F Traffic Psychol Behav 2(4):181–196

Knospe W, Santen L, Schadschneider A, Schreckenberg M (2004) Empirical test for cellular automaton models of traffic flow. Phys Rev E Stat Nonlinear Soft Matter Phys 70(1):016115

Orosz G, Wilson RE, Stépán G (2010) Traffic jams: dynamics and control. Philos Trans R Soc A Math Phys Eng Sci 368:4455–4479

Rahman M, Chowdhury M, Xie Y, He Y (2013) Review of microscopic lane-changing models and future research opportunities. IEEE Trans Intell Transp Syst 14(3):1942–1956

Saifuzzaman M, Zheng Z (2014) Incorporating human-factors in car-following models: a review of recent developments and research needs. Transp Res Part C Emerg Technol 48:379–403

Treiber M, Kanagaraj V (2015) Comparing numerical integration schemes for time-continuous car-following models. Phys A Stat Mech Appl 419:183–195

Wilson RE, Ward JA (2011) Car-following models: fifty years of linear stability analysis: a mathematical perspective. Transp Plan Technol 34(1):3–18

Chapter 4
Macroscopic Models

Macroscopic traffic flow models forms arguably the largest family in the model tree, see page 15. They describe traffic flow as if it were a continuum flow and are often compared to, or derived in analogy with, continuum models for fluids. Individual vehicles are not modeled, however aggregated variables such as (average) density and (average) flow are used.

After reading this chapter, the reader will understand the basics of the most popular macroscopic models, including their main features. They understand why and how extensions of macroscopic models such as higher order models, multi-class models and extensions using bounded acceleration or capacity drop, will improve them. The reader will also be able to adapt a simple model in these directions. They can reflect on desired properties of such models, including anisotropy. Finally, the reader will become familiar with the Eulerian and Lagrangian coordinate systems and will be able to reflect on their (dis)advantages.

4.1 Kinematic Wave Models

Macroscopic traffic flow models were first introduced by Lighthill and Whitham (1955b) and, independently (Richards 1956). Their model is the prototype kinematic wave model and was named the LWR model later. The dynamics of traffic is described by a partial differential equation, which models the conservation of vehicles:

$$\frac{\partial \rho}{\partial t} + \frac{\partial q}{\partial x} = 0 \tag{4.1}$$

and a fundamental relation $q = Q(\rho)$. The system of equations is closed with the relation between flow q, density ρ and speed v: $q = \rho v$. This model is closely related to other models for fluid flow, which often look very similar, with just an

F. Kessels, *Traffic Flow Modelling*, EURO Advanced Tutorials
on Operational Research, https://doi.org/10.1007/978-3-319-78695-7_4

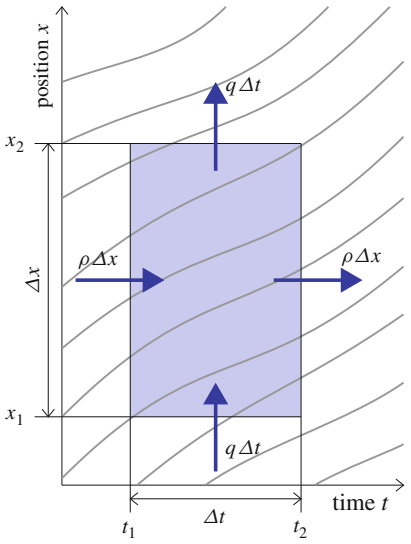

Fig. 4.1 Graphical derivation of the conservation equation in the kinematic wave model using vehicle trajectories and a control volume

other type of density-flow relation. The LWR model, was even introduced as Part 2 (Lighthill and Whitham 1955b) of a pair of articles, the first one titled 'On kinematic waves I: Flood movement in long rivers' (Lighthill and Whitham 1955a).

4.1.1 Graphical Derivation

The vehicle conservation equation (4.1) can be derived using vehicle trajectories in a control volume as illustrated in Fig. 4.1. The number of vehicles entering the control volume (inflow) equals the number of vehicles leaving it (outflow). This can be written as:

$$\underbrace{\int_{x_1}^{x_2} \rho(t_1, x)\,\mathrm{d}x}_{\text{inflow from left}} + \underbrace{\int_{t_1}^{t_2} q(t, x_1)\,\mathrm{d}t}_{\text{inflow from below}} = \underbrace{\int_{x_1}^{x_2} \rho(t_2, x)\,\mathrm{d}x}_{\text{outflow to right}} + \underbrace{\int_{t_1}^{t_2} q(t, x_2)\,\mathrm{d}t}_{\text{outflow to above}} \tag{4.2}$$

We decrease the control volume to an infinitesimal volume: $x_2 = x_1 + \Delta x \to x_1$ and $t_2 = t_1 + \Delta t \to t_1$. Because the volume is small, we may assume density ρ and flow q are constant.[1] Consequently, $\int_{x_1}^{x_2} \rho(t, x)\mathrm{d}x \to \rho(t, x_1)\Delta x$ and $\int_{t_1}^{t_2} q(t, x)\mathrm{d}t \to q(t_1, x)\Delta t$. Furthermore, rewriting (4.2) yields:

$$\frac{\rho(t_1 + \Delta t, x) - \rho(t_1, x)}{\Delta t} + \frac{q(t, x_1 + \Delta x) - q(t, x_1)}{\Delta x} = 0 \tag{4.3}$$

[1] This assumption is related to the continuum assumption, stating that the flow can be described as if it were a continuum instead of individual particles. The validity of this assumption is discussed in more detail in Sect. 7.1.1.

We now recall the definition of the partial derivatives of $f = f(y, z)$:

$$\frac{\partial}{\partial y} f(y,z) = \lim_{\Delta y \to 0} \frac{f(y+\Delta y, z) - f(y,z)}{\Delta y},$$
$$\frac{\partial}{\partial z} f(y,z) = \lim_{\Delta z \to 0} \frac{f(y, z+\Delta z) - f(y,z)}{\Delta z} \tag{4.4}$$

We apply this definition (4.4) to the infinitesimal control volume and find the conservation equation (4.1).

4.1.2 Method of Characteristics

To solve the equations of the kinematic wave model, different methods can be applied. We introduce the method of characteristics because it gives a good insight into the behaviour of the model and into how the model can be extended for more realistic results. Furthermore, Chap. 5 will discuss numerical methods that can be applied in computer simulations.

4.1.2.1 Characteristics

An important property of any traffic flow model is the speed and direction of information: if there is a discontinuity or a disturbance, at which speed does it travel to influence other vehicles, and in which direction? Sometimes, it travels with the vehicles, in other cases information will travel upstream, against the travel direction of the vehicles.

In the kinematic wave model, it is relatively easy to analyse the characteristic velocity. In this context, characteristics are lines of constant density. In general, in partial differential equations, characteristics, or characteristic waves, or characteristic curves, are curves in the (t, x) plane along which the equation simplifies in a certain way. This touches upon an important difference between the kinematic wave model and other non-linear hyperbolic partial differential equations, on one hand, and linear constant-coefficient hyperbolic partial differential equations such as the advection equation on the other hand:

$$\frac{\partial \rho}{\partial t} + v \frac{\partial \rho}{\partial x} = 0 \tag{4.5}$$

In the advection equation (4.5), the characteristic velocity equals the flow velocity v and characteristic curves are straight lines at which density is constant. However, in the kinematic wave model (4.1), characteristic velocity depends on the actual traffic state. To see this, we rewrite the conservation equation (4.1) in quasilinear form:

$$\frac{\partial \rho}{\partial t} + \frac{\partial q}{\partial x} = \frac{\partial \rho}{\partial t} + \frac{\mathrm{d}Q}{\mathrm{d}\rho} \frac{\partial \rho}{\partial x} = 0 \tag{4.6}$$

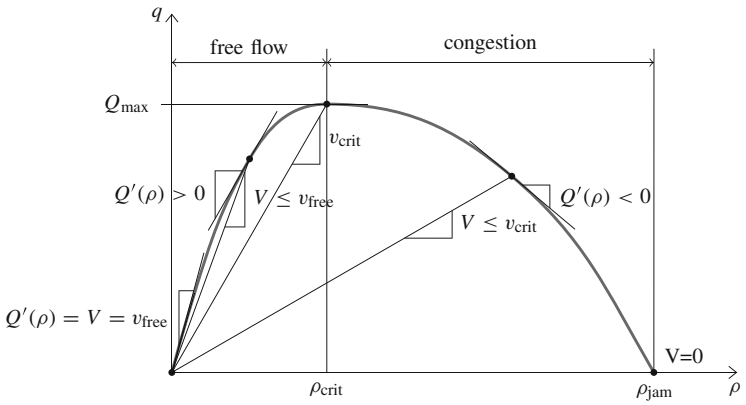

Fig. 4.2 Fundamental diagram with indication of characteristic velocities: in free flow, characteristic velocities are positive, in the congestion branch, they are negative

Again, at the characteristic curves, density is constant. However, the characteristic velocity does not always equal the flow velocity, instead it is:

$$\frac{\mathrm{d}Q}{\mathrm{d}\rho} = Q'(\rho) = V(\rho) + \rho V'(\rho) \tag{4.7}$$

We note that the characteristic velocity thus equates to the slope of the $Q(\rho)$ fundamental diagram. Assuming a traditionally shaped continuous and concave fundamental diagram (see Fig. 4.2) with an increasing free flow branch and a decreasing congestion branch the following holds:

- At zero density ($\rho = 0$), vehicle velocity equals characteristic velocity: $\left.\frac{\mathrm{d}Q}{\mathrm{d}\rho}\right|_{\rho=0} = V(0) = v_{max}$.
- If traffic is in free flow ($\rho \leq \rho_{crit}$), then the slope of the characteristic curve is positive and information moves in the same direction as the vehicles.
- If traffic is in congestion ($\rho > \rho_{crit}$), then the slope of the characteristic curve is negative and information moves in the direction opposite of the direction of the vehicles.

4.1.2.2 Shock Waves

Characteristics, as described in the previous paragraph, can move in either direction: upstream or downstream—backward or forward and at various speeds. Therefore, if the above is applied in a naive way to an initial value problem with increasing densities, characteristics may also intersect, see e.g. Fig. 4.3. An other way of looking at this is shown in Fig. 4.4. The initial densities propagate at different

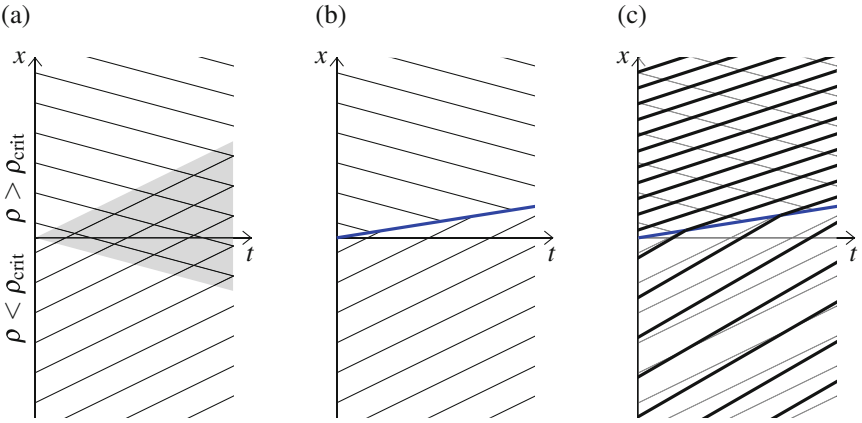

Fig. 4.3 Example of intersecting characteristics and the creation of a shock wave. (**a**) Intersecting characteristics (gray area). (**b**) Characteristics and shock wave (thick blue line). (**c**) Characteristics, shock wave and vehicle trajectories (thick lines)

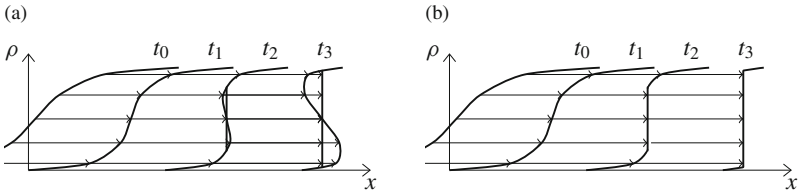

Fig. 4.4 Example of focussing of a deceleration wave, resulting in (unrealistic) triple valued solutions and a (realistic) shock. (**a**) Triple valued solution at $t = t_2$ and $t = t_3$. (**b**) Shock

speeds, leading to triple valued solutions. This is where shock wave theory comes into play. Shock waves—also known as kinematic waves—are formed at the boundary between characteristics that would otherwise intersect or lead to triple valued solutions.

To calculate the velocity of a shock wave, we first observe that vehicles may—and often do—travel at a velocity unequal to the shock wave velocity v_{shock}. Furthermore, the flux into the shock $\rho_{\text{upstream}}(v_{\text{upstream}} - v_{\text{shock}})$, must equal the flux leaving the shock $\rho_{\text{downstream}}(v_{\text{downstream}} - v_{\text{shock}})$. Therefore, the velocity of the shock wave is:

$$\begin{aligned} v_{\text{shock}} &= \frac{\rho_{\text{upstream}} v_{\text{upstream}} - \rho_{\text{downstream}} v_{\text{downstream}}}{\rho_{\text{upstream}} - \rho_{\text{downstream}}} \\ &= \frac{q_{\text{upstream}} - q_{\text{downstream}}}{\rho_{\text{upstream}} - \rho_{\text{downstream}}} \end{aligned} \tag{4.8}$$

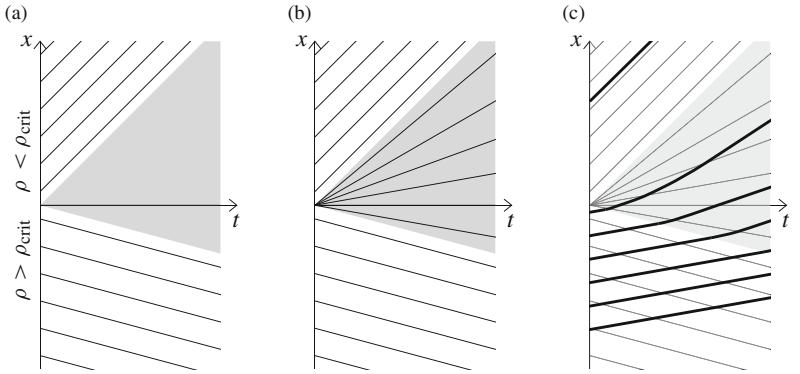

Fig. 4.5 Example of 'missing' characteristics and the creation of a rarefaction wave. (**a**) Characteristics (lines) and area with unknown characteristics (gray). (**b**) Characteristics, also in the rarefaction wave area. (**c**) Characteristics and trajectories (thick lines)

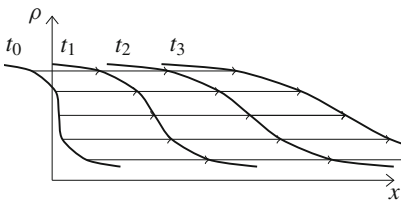

Fig. 4.6 Example of a rarefaction wave

4.1.2.3 Rarefaction Waves

Finally, it can also occur that characteristics move away from each other, yielding no solution at all in certain areas, see e.g. Figs. 4.5 and 4.6. It occurs at a discontinuity with a decreasing density in x-direction. This is where the concept of entropy maximisation comes into play. In these areas, entropy maximisation yields that vehicles drive as fast as possible, given the traffic state. This is also called the 'drive impulse' (Ansorge 1990). The traffic state at (t, x)—any point between the characteristics emanating from either the downstream or the upstream region—can now be determined by solving:

$$\frac{x - x_0}{t - t_0} = Q'(\rho) \tag{4.9}$$

with an initial discontinuity at (t_0, x_0). This equation has a unique solution if and only if the $Q(\rho)$ fundamental relation is strictly concave. If, however, it is concave, but not strictly concave, the entropy condition states that the solution with the highest flux is chosen, i.e. the state that corresponds to the state on the fundamental diagram closest to capacity.

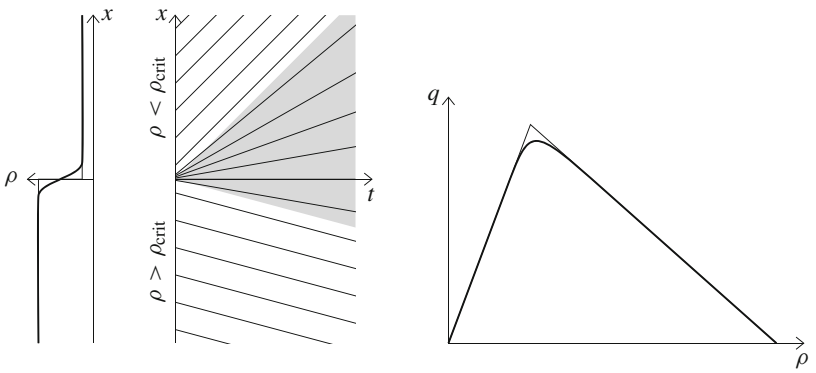

Fig. 4.7 Example a rarefaction wave constructed using a smooth approximation of the initial conditions (on the left) and of the fundamental diagram (on the right)

An other way to approach the issue with the lack of characteristics emanating from the initial conditions, is to use a smooth approximation, see Fig. 4.7. A discontinuity in the initial density at location $x = 0$ is approximated as:

$$\rho(0,x) = \begin{cases} \rho_{\text{upstream}} & \text{if } x \leq -\varepsilon \\ \frac{\rho_{\text{upstream}}+\rho_{\text{upstream}}}{2\varepsilon} x & \text{if } -\varepsilon < x < \varepsilon \\ \rho_{\text{downstream}} & \text{if } x \geq \varepsilon \end{cases} \tag{4.10}$$

With small $\varepsilon > 0$. Note that if $\varepsilon \to 0$, we get back a discontinuity, with on one side $\rho = \rho_{\text{upstream}}$ and on the other side $\rho = \rho_{\text{downstream}}$. Furthermore, any discontinuity in the differentiability of the fundamental relation, is approximated as being continuously differentiable. For example, the bilinear fundamental relation would be approximated as:

$$Q(\rho) = \begin{cases} \rho v_{\text{free}} & \text{if } \rho \leq \rho_{\text{crit}} - \delta \\ \tilde{Q}(\rho) & \text{if } \rho_{\text{crit}} - \delta < \rho < \rho_{\text{crit}} + \delta \\ \frac{\rho_{\text{crit}} v_{\text{free}}}{\rho_{\text{jam}} - \rho_{\text{crit}}} (\rho_{\text{jam}} - \rho) & \text{if } \rho \geq \rho_{\text{crit}} + \delta \end{cases} \tag{4.11}$$

With small $\delta > 0$. $\tilde{Q}(\rho)$ is chosen such that $Q(\rho)$ is continuous and continuously differentiable. If we now apply the method of characteristics, we find characteristics with all slopes between v_{free} and $-\frac{\rho_{\text{crit}} v_{\text{free}}}{\rho_{\text{jam}} - \rho_{\text{crit}}}$ emanating from the (now smoothened) discontinuity at $x = 0$. And the expansion wave becomes apparent.

4.1.2.4 Constructing Solutions

The method of characteristics as described above is applied to the typical test case of a traffic light problem. It is formulated as an initial value on an infinitely long road:

$$\rho(0,x) = \begin{cases} 0 & \text{if } x > 0 \\ \rho_{\text{jam}} & \text{if } -L < x \leq 0 \\ \rho_{\text{upstream}} & \text{if } x \leq -L \end{cases} \tag{4.12}$$

with L the length of the queue of vehicles waiting for the traffic light to turn green at $t = 0$ and $\rho_{\text{upstream}} < \rho_{\text{crit}}$ the density upstream of the queue. See also Fig. 4.8a. To simplify calculations, a bilinear fundamental diagram is applied. The solution—as shown in Fig. 4.8—is constructed with the following steps:

1. Determine characteristic velocities at time $t = 0$.
2. Identify initial locations of shock and expansion waves.
3. Determine the shock wave velocity.
4. Find whether and where the shock wave and the expansion wave meet and the behaviour after this.
5. Fill in all traffic states between the boundaries that were just determined.

Other typical problems that can be solved using the method of characteristics are Riemann initial value problems and certain boundary value problems. The interested reader is encouraged to practice with these cases in the problem set (Problems 4.1 and 4.2).

4.1.3 Simulation Results with the Kinematic Wave Model

The results of a simple simulation are shown in Fig. 4.9. The test case is the same as used for microscopic models in the previous chapter, most notably Sect. 3.2.2. It shows vehicles on a 800 meter long ring road. They are waiting in a queue of length 200 meters until the first one starts driving at $t = 0$. They drive on a ring road and thus the first vehicle essentially follows the last one. A linear-parabolic fundamental diagram is applied, with parameters as in Table 4.1. Furthermore, the table also shows the parameter values of the numerical method, an explicit Lagrangian scheme. The relevance of the numerical method is discussed in Chap. 5.

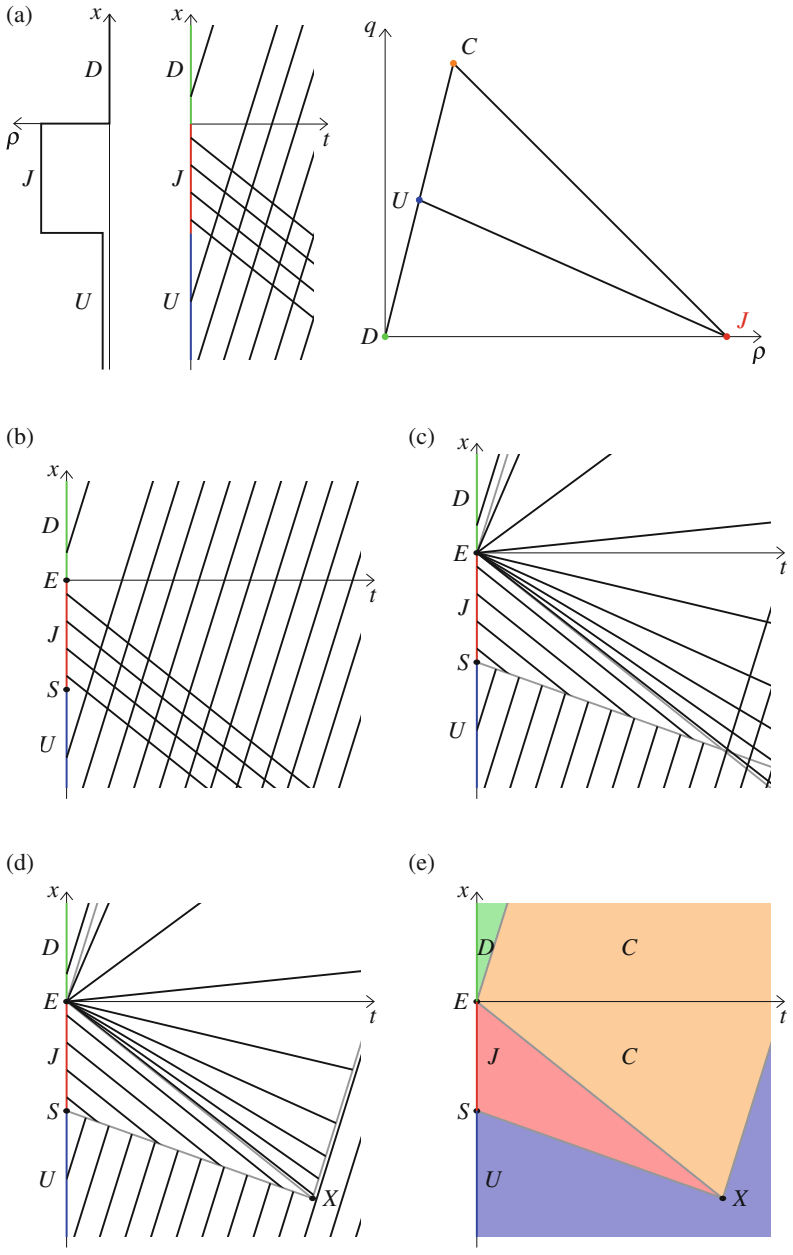

Fig. 4.8 Example of the application of the method of characteristics to a traffic light problem. (**a**) Step 1: initial conditions (left), fundamental diagram (right) and characteristics (center). (**b**) Step 2: locations of shock and expansion wave. (**c**) Step 3: shock wave velocity and expansion wave. (**d**) Step 4: after shock and expansion wave meet (X). (**e**) Step 5: solution in the form of traffic state

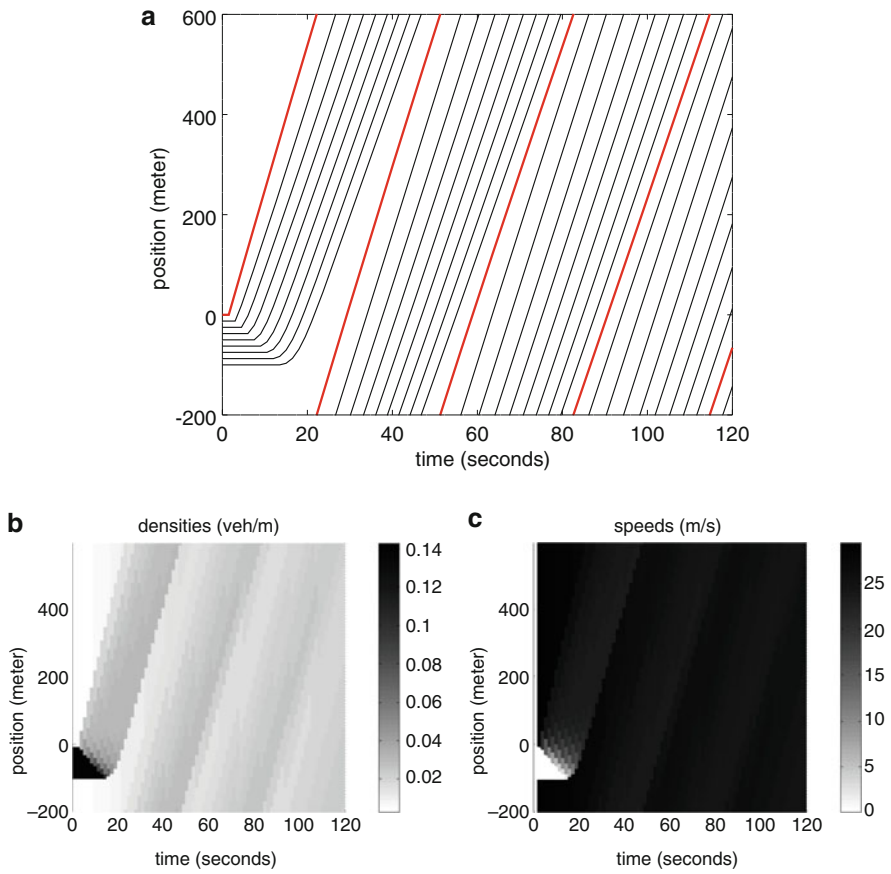

Fig. 4.9 Simulation results with the kinematic wave model with parabolic-linear fundamental diagram. The test case is a ring road, with an initial queue that dissolves, as described in Sect. 4.1.3. The same results are presented in different ways. (**a**) Trajectories of 'vehicle groups': they are not actual vehicle trajectories, but of groups of $\Delta n \approx 1.79$ vehicles. The thick red trajectory is that of the first vehicle group that starts driving at $t = 0$. The other trajectories (black) are of groups that were waiting in a queue behind the first one. (**b**) Densities. (**c**) Speeds

Table 4.1 Parameter values of the linear-parabolic fundamental diagram and numerical scheme applied to the kinematic wave model

Maximum speed $v_{\max}$	30 m/s
Critical speed v_{crit}	$\frac{4}{5}v_{\max} = 24$ m/s
Jam density ρ_{jam}	$\frac{1}{7} \approx 0.14$ veh/m
Critical density ρ_{jam}	$\frac{1}{5}\rho_{\text{jam}} \approx 0.029$ veh/m
Time step size Δt	1.5 s
Vehicle group size Δn	≈ 1.79
CFL number ν	0.9

4.1.4 Critique and Adaptations of the Kinematic Wave Model

Because of its simplicity the LWR model has received both much attention and critique. The model tree shows that this resulted in many offshoots. The main drawback is that vehicles are assumed to attain the new equilibrium velocity immediately after a change in the traffic state, which implies infinite acceleration. This problem is addressed by:

higher order models with an added speed equation, see Sect. 4.3
bounded acceleration and hysteresis as extension to LWR, sometimes modelled as a capacity drop, see Sect. 4.5

An other drawback of the LWR model is that breakdown (the transition from the free flow regime to the congestion regime) always occurs at the same density and leads to the same outflow after breakdown. This is addressed by:

heterogeneity by introducing different types of vehicles or drivers, driving according to different fundamental diagrams, see Sect. 4.2
stochasticity using breakdown probabilities (Hoogendoorn et al. 2009) or via other probability distributions (Jabari and Liu 2012, 2013) (not discussed in detail in this book).
multi-lane kinematic wave models in which vehicle flow is separated into flows on each lane and between the lanes—as opposed to a 'single pipe flow'. The multi-class model (Daganzo et al. 1997) is an example. Other multi-lane models (Laval and Daganzo 2006; Jin 2010) are not discussed in detail in this book.

Finally, the approaches can be combined, for example by multi-class or higher order models with capacity drop. We will not discuss these models in detail because combining multiple extensions is usually rather straightforward and does not add much extra theoretical insights. However, combining approaches can be useful to obtain realistic simulation results for a wider range of applications and scenarios.

4.2 Multi-Class Kinematic Wave Models

In the last one to two decades, the branch of multi-class kinematic wave models has developed quickly. This follows the earlier development of other types of multi-class models (micro- and mesoscopic, higher-order macroscopic).

Multi-class kinematic wave models all consist of a system of conservation equations. There is one conservation equation for each of the U classes:

$$\frac{\partial \rho_u}{\partial t} + \frac{\partial q_u}{\partial x} = 0 \tag{4.13}$$

with ρ_u the class specific density of class u, $q_u = \rho_u v_u$ the class specific flow and v_u the class specific velocity. The class specific velocity is defined differently for

each model, but they can all be cast into the following form:

$$v_u = V_u(\rho_1, \rho_2, \ldots, \rho_U) \tag{4.14}$$

This implies that the class specific velocity only depends on the current class specific densities, and not on any previous state. Therefore, these models are classified as kinematic wave models.

In the simplest—and oldest—multi-class kinematic wave models the speed depends on the total density:

$$v_u = V_u\left(\rho_1, \rho_2, \ldots, \rho_U\right) = V_u\left(\sum_{u=1}^{U} \rho_u\right) \tag{4.15}$$

Furthermore, the fundamental relation is scaled differently for each class, see Fig. 4.10a:

$$v_u = V_u\left(\sum_{u=1}^{U} \rho_u\right) = \frac{v_{u,\max}}{v_{1,\max}} V_1\left(\sum_{u=1}^{U} \rho_u\right) \tag{4.16}$$

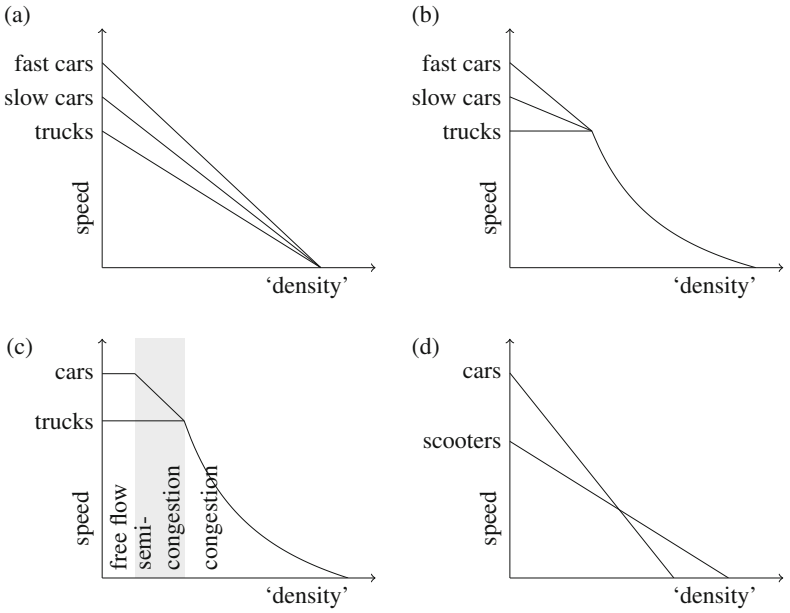

Fig. 4.10 Typical density-speed fundamental diagrams of multi-class macroscopic models. The precise definition of 'density' differs per model: it could be the total density $\sum_u \rho_u$, the weighted sum of the class specific densities, $\sum_u \eta_u \rho_u$, or even some other increasing density function $\rho(\rho_1, ..., \rho_U)$. (**a**) Basic multi-class model with scaled fundamental diagram. (**b**) Fastlane or cross section of multi-dimensional fundamental diagram. (**c**) Three regime model. (**d**) Porous flow model

The model tree shows that Wong and Wong (2002) were the first to introduce such a multi-class kinematic wave model.

4.2.1 Multi-Dimensional Fundamental Diagram

Later models apply a multi-dimensional fundamental diagram, to include the difference in length between the classes. Effectively, these models scale both axes of the fundamental relation differently for each class. In the case of two classes, this leads to a three dimensional fundamental relation (see Figs. 2.13(d), 4.10b). For example, the fundamental diagram introduced by Chanut and Buisson (2003) is a scaled version of the linear-parabolic fundamental diagram (2.3):

$$v_u = V_u(\rho_1, \rho_2) \begin{cases} v_{u,\max} - \frac{v_{u,\max} - v_{\text{crit}}}{\rho_{\text{crit}}(\rho_1,\rho_2)} & \text{if } \rho_1+\rho_2 < \rho_{\text{crit}}(\rho_1, \rho_2) \\ \frac{\rho_{\text{crit}}(\rho_1,\rho_2) v_{\text{crit}}}{\rho_{\text{jam}}(\rho_1,\rho_2)\rho_{\text{crit}}(\rho_1,\rho_2)} \left(\frac{\rho_{\text{jam}}(\rho_1,\rho_2)}{\rho_1+\rho_2} - 1 \right) & \text{if } \rho_1+\rho_2 \geq \rho_{\text{crit}}(\rho_1, \rho_2) \end{cases} \tag{4.17}$$

with state dependent (scaled) critical density and jam density, respectively:

$$\rho_{\text{crit}}(\rho_1, \rho_2) = \beta \rho_{\text{jam}}(\rho_1, \rho_2) \quad \text{and} \quad \rho_{\text{jam}}(\rho_1, \rho_2) = \frac{\rho_1 + \rho_2}{L_1\rho_1 + L_2\rho_2} \tag{4.18}$$

with $\beta < 0.5$ and L_1 and L_2 the gross vehicle lengths of class 1 and 2, respectively. Therefore, when there are no vehicles of class 2 present (i.e. $\rho_2 = 0$), then the jam density parameter is the inverse of the vehicle length of class 1: $\rho_{\text{jam}}(\rho_1, 0) = 1/L_1$. Similarly, when there are no vehicles of class 1, then $\rho_{\text{jam}}(0, \rho_2) = 1/L_2$.

4.2.2 Fastlane

Fastlane is an other offshoot in the branch of multi-class kinematic wave models (van Lint et al. 2008; van Wageningen-Kessels et al. 2014). An 'effective density' is computed and this is used as input for the fundamental relation. The fundamental relation now expresses the class specific velocity as a function of the effective density, see Fig. 4.10b. The effective density is a weighted summation of all class specific densities:

$$\rho = \sum_u \eta_u(\rho)\rho_u \tag{4.19}$$

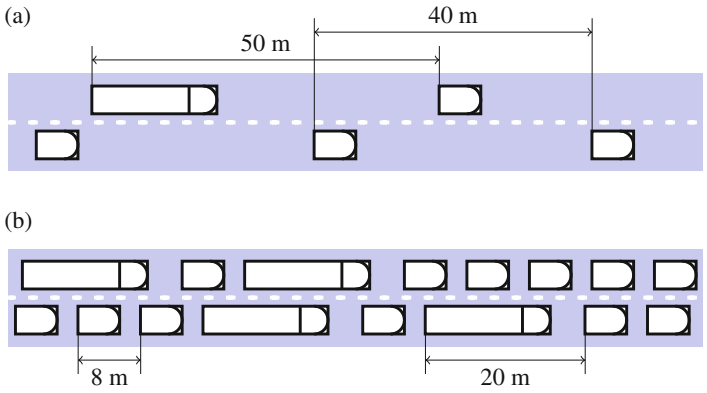

Fig. 4.11 Example illustrations of pce-values. Vehicles drive to the right, cars (short) and trucks (long) are present. In both examples, the truck is longer than the car and the gap (distance *between* two vehicles) is similar for cars and trucks. (**a**) Few vehicles with large spacings: free flow. The space occupancy of a truck (50 m) is a bit higher than that of a car (40 m). This is because the gap is much higher than the vehicle length and thus the vehicle length contributes relatively little to the space occupancy. In this example, the pce value of a truck is $\eta_{\text{truck}} = 50/40 = 1.25$. (**b**) Many vehicles, with small spacings: congestion. The space occupancy of a truck (20 m) is much higher than that of a car (8 m). This is because the truck is longer, but the gap is very similar for both cars and trucks. In this example, the pce value of a truck is be $\eta_{\text{truck}} = 20/8 = 2.5$

with η_u the state-dependent passenger car equivalent (pce) value:

$$\eta_u(\rho) = \frac{L_u + T_u v_u(\rho)}{L_1 + T_1 v_1(\rho)} \tag{4.20}$$

The idea behind the pce value is as follows: Passenger cars have a pce value of 1. Other pce values in Fastlane depend on the actual traffic state. The approach takes into account that adding one truck into the mix, will have a larger effect on the flow than adding one car. Furthermore, and this is unique for Fastlane, a truck takes up more space than a car, but this effect is much larger at high densities and low speeds than it is at low densities and high speeds. This is illustrated in Fig. 4.11.

We note that the presented formulation of Fastlane includes an implicit density function (4.19): to calculate the density, the pce values need to be known, for which the densities are needed (4.20). An alternative formulation of Fastlane that is more practical to apply and more theoretically sound (because it does not have this implicit self-reference)—albeit much more complicated at first sight—is presented by van Wageningen-Kessels et al. (2014).

4.2.3 Models with Three Regimes

A different approach to modelling the behaviour of classes that share a (multi-lane) road is by assuming that the flow is always in a 'lane distribution equilibrium'. In this equilibrium, the vehicles distribute themselves over the lanes in such a way that any other distribution would lead to lower speeds for at least one of the classes. Furthermore, all vehicles drive as fast as possible, on the fraction of the road that is available to them. The most simple of this type of models is the two-class and two-lane model by Daganzo (2002). The terminology of 'slugs' (slow cars) and 'rabbits' (fast cars) is used. Slugs always stay on the outer lane. Rabbits can use both lanes and chose among them based on a user equilibrium. This gives rise to 3 possible 'regimes', see also Fig. 4.10c:

free flow If there are few cars, fast cars will remain on the inner lane and drive at their maximum speed.

semi-congestion If the number of fast cars increases slightly above the density threshold for their maximum speed (critical density), then their speed decreases, but they will stay in the inner lane.

congestion If the number of fast cars increases even more and their speed drops below the maximum speed of the slow cars, there is no advantage anymore in only staying in the inner lane. In fact, the fastest cars will start sharing the outer lane with the slow cars. In this situation, both types of cars will drive at the same speed.

This leads to the following density speed relationships:

$$\begin{aligned} &v_1 = v_{1,\max}, \quad v_2 = v_{2,\max} && \text{free flow, 2 pipe} \\ &v_1 = w_1 \left(\tfrac{\rho_{\text{jam}}}{\rho_1} - 1 \right), \quad v_2 = v_{2,\max} && \text{semi-congestion, 2 pipe} \\ &v_1 = v_2 = \tfrac{w_1 w_2}{w_1 + w_2} \left(\left(\tfrac{1}{\rho_1} + \tfrac{1}{\rho_2} \right) \rho_{\text{jam}} - 1 \right) && \text{congestion, 1 pipe} \end{aligned} \tag{4.21a}$$

with congestion wave speed:

$$w_u = \frac{\rho_{\text{crit}} v_{u,\max}}{\rho_{\text{jam}} - \rho_{\text{crit}}} \tag{4.22}$$

and ρ_{jam} and ρ_{crit} per lane jam density and critical density, respectively. Traffic is in 2 pipe free flow regime when $\rho_1 < \rho_{\text{crit}}$. It is in 2 pipe semi-congestion regime when $\rho_{\text{crit}} \leq \rho_1 < \frac{w_1 \rho_{\text{jam}}}{v_{2,\max} + w_1}$. It is in 1 pipe congestion regime when $\rho_1 \geq \frac{w_1 \rho_{\text{jam}}}{v_{2,\max} + w_1}$. Furthermore, it is assumed that $\rho_2 < \rho_{\text{crit}}$ in the 2 pipe regimes and $\rho_2 < \rho_{\text{jam}}$ in the 1 pipe regime. Therefore, the slow cars will always stay in the outer lane and never enter the inner lane.

4.2.4 Porous Flow Models

The most recent multi-class kinematic wave model are the porous flow models. They consider heterogeneous traffic on a two dimensional roadway. Small vehicles can drive ('creep') through openings ('pores') between other vehicles. It is developed to model disordered traffic flow with different types of vehicles such as cars, scooters and bikes and without lanes. The main idea that if overall densities are low, large vehicles with high maximum velocities (e.g. cars) are faster than smaller vehicles with low maximum velocities (e.g. two-wheelers). However, when the road gets busier, cars are less able to manoeuvre between the other vehicles and two-wheelers are better able to maintain their velocity. The resulting 2-class model by Fan and Work (2015) is very similar to previously developed models with a fundamental diagram that is linear in the density-velocity plane:

$$v_u = \left(1 - \frac{\rho}{\rho_{u,\text{jam}}}\right) v_{u,\max} \tag{4.23}$$

However, class 1 (cars) has a speed in low densities, class 2 (scooters) has a higher velocity in high densities: $v_{1,\max} > v_{2,\max}$ and $\rho_{1,\text{jam}} < \rho_{2,\text{jam}}$, see also Fig. 4.10d. Other examples of porous flow models (Nair et al. 2011; Gashaw et al. 2017) use the same principles but their approach leads to fundamental diagrams with different shapes. However, all porous flow models share the property that at low density one class is faster, while at high density, an other class is faster.

4.2.5 Requirements of Multi-Class Models

Along the same lines of the requirements for fundamental diagrams (Sect. 2.3) and microscopic models (Sect. 3.2.3), requirements for multi-class kinematic wave models are proposed:

1. When the density reaches a certain threshold (which may depend on the traffic composition), all class specific vehicle speeds are zero.
2. When a single vehicle of any class is added to the flow, neither of the class specific speeds will increase.
3. Information travels at finite speed.
4. Information travels at a velocity not larger than that of vehicles.

The first two requirements are similar to the requirements put forward for fundamental diagrams in Sect. 2.3. Especially, the second requirements may seem obvious: when there are more vehicles on the road, they drive slower (or certainly not faster). However, it has been shown that not all multi-class models satisfy this requirements (Van Wageningen-Kessels 2016). Furthermore, the last two requirements relate to hyperbolicity and anisotropy, and 'plausible driver behaviour', like the requirements

in Sect. 3.2.3. A traffic flow model is hyperbolic when it takes time for traffic at some distance to an event, to react to that event: i.e. drivers do not react instantaneously, but after a nonzero reaction time. Along the same lines, drivers only react to their leaders and not to their followers. This is also called anisotropy, as discussed in more detail in Sect. 4.3.1. Some of these requirements are not straightforward to check. However, a step-by-step plan (Van Wageningen-Kessels 2016) can be followed. Application of the plan shows that most models satisfy the requirements, but some only conditionally.

4.3 Higher-Order Models

Higher-order models form the last branch of macroscopic traffic flow models. They include an equation describing the acceleration ('velocity dynamics') towards the equilibrium velocity described by a fundamental relation. In 1971, Payne derived a macroscopic traffic flow model from a simple stimulus-response car-following model. It yields a model consisting of a fundamental relation and two coupled partial differential equations, hence the name higher-order model. The partial differential equations are the conservation of vehicles equation (4.1) and an equation describing the velocity dynamics:

$$\frac{\partial v}{\partial t} + v\frac{\partial v}{\partial x} = \frac{V(\rho) - v}{\tau} - \frac{c^2}{\rho}\frac{\partial \rho}{\partial x} \tag{4.24}$$

with $V(\rho)$ the equilibrium velocity described by the fundamental relation and τ can be interpreted as reaction or relaxation time, because of its relation with the reaction time in the car-following model. c^2 is a diffusion parameter and can for example be chosen to be $c^2 = \mu/\tau$ μ the anticipation coefficient.

4.3.1 Critique on Higher Order Models

Daganzo (1995) has argued that higher-order models are flawed because they are not anisotropic. The main implication of non-anisotropic models is that vehicles may drive backward. To understand this, we note that the term 'anisotropy' in traffic flow theory is used in a slightly different way than usual in fluid dynamics:

Isotropy The fluid flow has no directional preference, e.g. in a water flow, water molecules react the same to their neighbouring molecules independent of in which direction the other molecules are located.

Anisotropy in fluid flows There is a directional preference, e.g. a gravitational force only acts in one direction.

Anisotropy in traffic flows There is a directional preference and vehicles only react on what is happening in front of them, not on what is behind them.

Non-anisotropy in traffic flows There may be a directional preference but vehicles both react to changes in front and behind.

We use the definitions common to traffic flow. In an anisotropic traffic flow, vehicles do not react to what happens behind them. This implies that if a vehicle is in a queue, it does not matter whether there is an other vehicle behind them or not, it will just stay in the queue and only start moving once the vehicles in front start moving. In a non-anisotropic traffic flow, however, this same vehicle in a queue may behave differently depending on what happens behind them. If there is no vehicle behind them, in a non-anisotropic model, the vehicle may start to drive backward. This is usually due to the diffusion term $-\frac{c^2}{\rho}\frac{\partial \rho}{\partial x}$. An other property of non-anisotropic traffic flow models is related to the characteristic velocity at low densities and high vehicle speeds. In a non-anisotropic model, again the diffusion term $-\frac{c^2}{\rho}\frac{\partial \rho}{\partial x}$ causes behaviour that is considered unrealistic, namely characteristics travelling faster than the average vehicle speed. This is explored further in Problems 4.6 and 4.8.

The introduction of the concept of anisotropy in traffic flow by Daganzo (1995) sparked a long debate on whether or not traffic flow models should be anisotropic, in which Helbing (2009) gave the final contribution. Some authors (e.g. Zhang (2003)) argue that in multi-lane traffic, the average vehicle speed can be below the speed of the fastest vehicles and therefore, those fastest vehicles can carry information with them at a speed higher than the average vehicle speed. This would make characteristics travelling faster than the average speed realistic on multi-lane roads, as long as the characteristics are not faster than the fastest vehicles.

4.3.2 Anisotropic Higher Order Models

In the time Daganzo's article was written, existing higher-order models were indeed not anisotropic. The publication has lead to rapid developments of new higher order models that resolve the problems by including an other speed equation. Probably the most well-known of them is the ARZ model by Aw and Rascle (2000); Zhang (2002) with:

$$\frac{\partial v}{\partial t} + v\frac{\partial v}{\partial x} = -c(\rho)\frac{\partial v}{\partial x} \tag{4.25}$$

with $c(\rho) = \rho V'(\rho)$ the 'sound speed': the speed at which a small perturbation travels. In this and similar models, when parameters have been chosen reasonably, characteristic waves can not be faster than vehicles. This is explored further in Problems 4.6, 4.7 and 4.8. Extended versions of this model have been proposed to include multiple classes or multiple lanes.

4.3.3 Generic Higher Order Model

Lebacque et al. (2007) develop a generalized higher-order model (GSOM) that includes the models such as those by Aw and Rascle (2000); Zhang (2002) as special cases. It includes a 'generic invariant' I, which is attached to the vehicle stream and could thus be seen as a property of a vehicle or driver: every vehicle may have a different function $\tilde{I}(t, x)$. The main idea is that $\tilde{I}$ may depend on the actual traffic state $\tilde{I}(t, x) = I(\rho(t, x), v(t, x))$, but this function I travels with the vehicles. For example, I could model slow acceleration for some vehicles and fast acceleration for others, and thus changing the fundamental diagram.

The generalized model is as follows:

$$\frac{\partial \rho}{\partial t} + \frac{\partial q}{\partial x} = 0 \tag{4.26a}$$

$$\frac{\partial}{\partial t}(\rho I) + \frac{\partial}{\partial x}(q I) = -\rho g(I) \tag{4.26b}$$

$$I = I(\rho, v) \tag{4.26c}$$

Note that only if $f(I) = 0$, the invariant is actually conserved over vehicle trajectories. If the relaxation function $f(I)$ is nonzero, than I is not conserved but, depending on the choice of the relaxation function, it changes slowly. A slight adaptation of the ARZ model is presented as a typical example within the GSOM with the invariant the distance to the equilibrium fundamental relation:

$$I = v - V(\rho) \tag{4.27}$$

and the relaxation term models acceleration/deceleration towards the equilibrium fundamental relation:

$$g(I) = \frac{I}{\tau} \tag{4.28}$$

For later reference, we note that the generic model (4.26) can be reformulated as a system of conservation equations:

$$\frac{\partial \mathbf{u}}{\partial t} + \mathrm{J}(\mathbf{u}) \frac{\partial \mathbf{u}}{\partial \mathrm{x}} = s(\mathbf{u}) \tag{4.29}$$

with state vector, Jacobian and source function, respectively:

$$\mathbf{u} = \begin{pmatrix} \rho \\ I \end{pmatrix}, \quad \mathrm{J}(\mathbf{u}) = \begin{pmatrix} \frac{\mathrm{d}q}{\mathrm{d}\rho} & 0 \\ 0 & v \end{pmatrix} = \begin{pmatrix} v + \rho \frac{\mathrm{d}v}{\mathrm{d}\rho} & 0 \\ 0 & v \end{pmatrix} \quad \text{and} \quad \mathrm{s}(\mathbf{u}) = \begin{pmatrix} 0 \\ -g(I) \end{pmatrix} \tag{4.30}$$

To see the equivalence between (4.26) and (4.29), we rewrite (4.26b):

$$\rho \frac{\partial I}{\partial t} + I \frac{\partial \rho}{\partial t} + q \frac{\partial I}{\partial x} + I \frac{\partial q}{\partial x} = -\rho g(I) \tag{4.31}$$

Substitution (4.26) and dividing by ρ gives:

$$\frac{\partial I}{\partial t} + v \frac{\partial I}{\partial x} = -g(I) \tag{4.32}$$

Combining (4.26) and (4.32) yields (4.29).

Furthermore, in certain cases, it is useful to rewrite the second term of (4.29) as a partial derivative of the flux function $f(\mathbf{u})$:

$$\frac{\partial f(\mathbf{u})}{\partial x} = \mathrm{J}(\mathbf{u}) \frac{\partial \mathbf{u}}{\partial \mathrm{x}} = \begin{pmatrix} \frac{\mathrm{d}q}{\mathrm{d}\rho} & 0 \\ 0 & v \end{pmatrix} \frac{\partial \mathbf{u}}{\partial \mathrm{x}} = \begin{pmatrix} \frac{\mathrm{d}q}{\mathrm{d}\rho} \frac{\partial \rho}{\partial x} \\ v \frac{\partial I}{\partial x} \end{pmatrix} \tag{4.33}$$

This then yields the conservative form of (4.26):

$$\frac{\partial \mathbf{u}}{\partial t} + \frac{\partial f(\mathbf{u})}{\partial x} = s(\mathbf{u}) \tag{4.34}$$

4.4 Moving Coordinates

Traditionally, macroscopic traffic flow models are formulated in the Eulerian—fixed—coordinate system. This is also the approach that has been taken in this chapter until now. In the fixed coordinate system, the independent variables are time t and position x, see Fig. 4.12a. Traffic state variables, such as density, flow and speed, are expressed as function of time and location. Discretizations are used in simulations (more details in Chap. 5) and involve calculating the state variables on fixed times and at fixed locations. However, this is not the only possible approach and other approaches have some advantages.

4.4.1 The Lagrangian Coordinate System

Since the early 2000s several authors have developed macroscopic models formulated in the Lagrangian—moving—coordinate system (Aw et al. 2002; Leclercq et al. 2007; van Wageningen-Kessels et al. 2010). In the moving coordinate system, the independent variables are time t and vehicle number n, see Fig. 4.12b. Traffic state variables are expressed as function of time and vehicle number. This results in the following conservation equation:

$$\frac{\mathrm{D}s}{\mathrm{D}t} + \frac{\partial v}{\partial n} = 0 \tag{4.35}$$

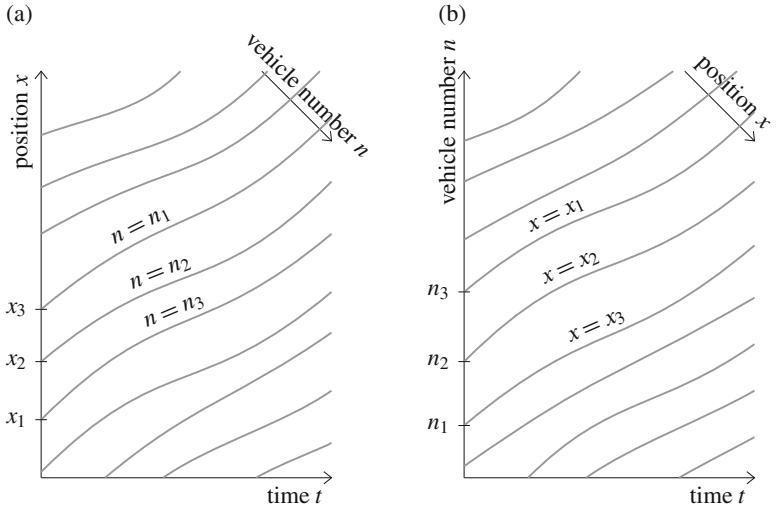

Fig. 4.12 Trajectories in Eulerian and Lagrangian coordinate system. (**a**) Eulerian coordinate system with vehicle trajectories: vehicle number n increases over time t for a fixed position x. (**b**) Lagrangian coordinate system with vehicle trajectories: position x increases over time t for a fixed vehicle number n

Table 4.2 Comparison of different formulations of the kinematic wave model

	Euler	Lagrange
Coordinates	(x, t)	(n, t)
Main state variable	$\rho = -\partial n/\partial x$	$s = -\partial x/\partial n$
Fundamental relation	$q = Q(\rho)$	$v = V(s)$
Conservation equation	$\frac{\partial \rho}{\partial t} + \frac{\partial q}{\partial x} = 0$	$\frac{\mathrm{D}s}{\mathrm{D}t} + \frac{\partial v}{\partial n} = 0$

The conservation equation in Lagrangian formulation (4.35) can be understood qualitatively by considering two vehicles: a leader and a follower. If the follower has a higher velocity than the leader, the distance between the two vehicles decreases, i.e. if $\partial v/\partial n > 0$ then $\mathrm{D}s/\mathrm{D}t < 0$. The reverse is also true: if the follower is slower than the leader the distance will increase.

For easy reference, the Eulerian and Lagrangian formulation of the kinematic wave model are summarized in Table 4.2. The advantages of this moving coordinate system include simpler extensions of the model in certain directions (e.g. including bounded acceleration, see Sect. 4.5) faster and more accurate calculations (see Sect. 5.4) and easier analysis of the models (Van Wageningen-Kessels 2016). However, there is a third formulation of the kinematic wave model—the 'T-model'—that uses space and vehicle number as independent variables (Laval and Leclercq 2013).

4.4.2 Graphical Derivation

The Lagrangian conservation equation can be derived using a similar procedure as the derivation of the kinematic wave model in Eulerian coordinates (Sect. 4.1.1). Alternatively, the model can be derived analytically from the Eulerian formulation. We focus on the graphical approach, which may be more intuitive and easy to understand. In Problem 4.14, we encourage the interested reader to also study the analytical approach, which is mathematically more rigorous.

In the Lagrangian case, the control volume is not rectangular as in Fig. 4.1 but it is a platoon of Δn vehicles that is followed over a time Δt, as in Fig. 4.13. However, the platoon is rectangular in the (t, n)-plane. The road length taken by this platoon changes over time as it travels forward. On one hand, the original length at time t_1 is increased by the distance traveled by the first vehicle n_1. On the other hand, it is decreased by the distance traveled by the last vehicle $n_2 = n_1 + \Delta n$. (Note again the order of vehicles: vehicle n_2 is behind vehicle n_1.) This can be written as:

$$\underbrace{\int_{n_1}^{n_2} s(t_2, n)\mathrm{d}n}_{\text{final length}} = \underbrace{\int_{n_1}^{n_2} s(t_1, n)\mathrm{d}n}_{\text{initial length}} + \underbrace{\int_{t_1}^{t_2} v(t, n_1)\mathrm{d}t}_{\text{distance first veh}} - \underbrace{\int_{t_1}^{t_2} v(t, n_2)\mathrm{d}t}_{\text{distance last veh}}. \quad (4.36)$$

Again, by decreasing the control volume to an infinitesimal volume we may assume spacing s and velocity v are constant within this volume. Consequently,

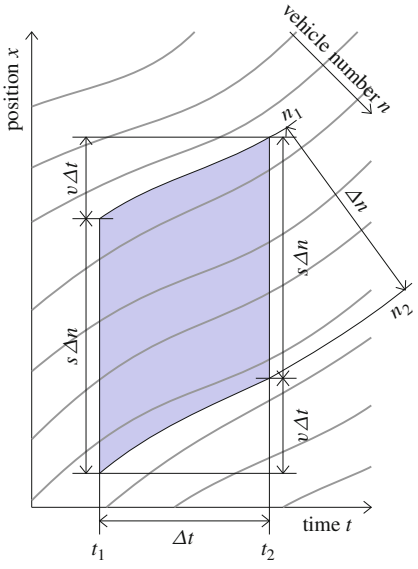

Fig. 4.13 Graphical derivation of the conservation equation in the kinematic wave model in Lagrangian coordinates, using vehicle trajectories and a control volume

$\int_{n_1}^{n_2} s(t,n)\mathrm{d}n \to s(t,n)\Delta n$ and $\int_{t_1}^{t_2} v(t,n)\mathrm{d}t \to v(t,n)\Delta t$. Furthermore, rewriting (4.36) yields:

$$\frac{s(t_2,n_1)-s(t_1,n_1)}{\Delta t}+\frac{v(t_2,n_2)-v(t_2,n_1)}{\Delta n}=0. \tag{4.37}$$

We take an infinitesimal volume, that is: we let $\Delta n \to 0$ and $\Delta t \to 0$ in (4.37). Furthermore, we use the definition of the partial derivative (4.4) to find the Lagrangian conservation equation (4.35).

4.4.3 Generic Higher Order Model in Lagrangian Coordinates

The generic higher order model (4.26) lends itself well for reformulation in the Lagrangian coordinate system. This is because the driver attribute I travels with the vehicles and thus the model becomes:

$$\frac{\mathrm{D}s}{\mathrm{D}t}+\frac{\partial v}{\partial n}=0, \tag{4.38a}$$

$$\frac{\mathrm{D}I}{\mathrm{D}t}=-g(I), \tag{4.38b}$$

$$v=V(s,I) \tag{4.38c}$$

4.5 Bounded Acceleration, Hysteresis and Capacity Drop

One of the most common critiques on the LWR model is the underlying assumption of instantaneous acceleration and deceleration. This implies, for example, that when a vehicle leaves congestion and enters a free flow region, according to the LWR model it would accelerate instantaneously to its free flow speed. This problem is fixed in higher order models, however, also more direct ways to address it have been introduced. These adaptations to the LWR model include bounded accelerations. Usually, only acceleration is bounded because instantaneous deceleration proves to be less of in issue in practise. However, the same techniques could be applied the also limit deceleration.

4.5.1 Bounded Acceleration

It is most natural to introduce bounded acceleration in the Lagrangian coordinate system. This is because the coordinates move with the vehicles and one can just

limit their change in speed. This idea was introduced by Leclercq (2009) and further developed by others including Calvert et al. (2015), Calvert et al. (2018). The simplest version of a bounded acceleration model limits the acceleration by explicitly requiring the speed to be as large as possible under the constraints of the fundamental diagram and the bounded acceleration. I.e. speed v is maximised such that both:

$$v \leq V(1/s) \quad \text{and} \quad \frac{\partial v}{\partial t} \leq a_{\max} \tag{4.39}$$

with $a_{\max} > 0$ the maximum acceleration.

The main advantage of doing this in the Lagrangian coordinate system lies in the discretisation. This is because, very much like in a car-following model, trajectories are calculated and the bounded acceleration condition makes them more smooth, as in Fig. 4.14. The discretisation will be discussed in more detail in Chap. 5.

Alternatively, bounded acceleration can be introduced in the Eulerian coordinate system, even though that is a bit more complicated. In such cases, the numerical

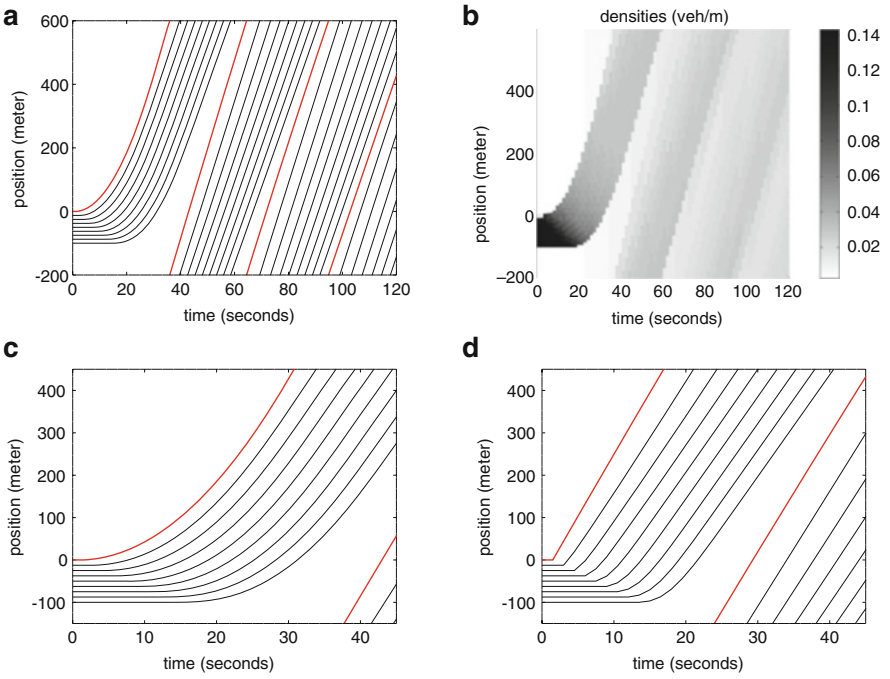

Fig. 4.14 Simulation results with bounded acceleration and comparison of trajectories (zoomed) with and without bounded acceleration. (**a**) Trajectories. (**b**) Densities. (**c**) Trajectories with bounded acceleration (zoom of (**a**). (**d**) Trajectories without bounded acceleration (zoom of Fig. 4.9a)

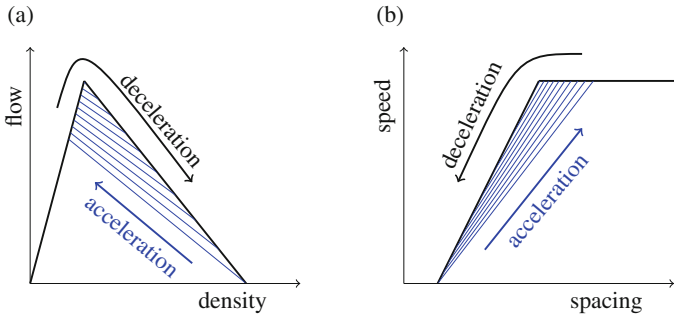

Fig. 4.15 Fundamental relation with hysteresis: the black line is the original fundamental diagram, that is active during deceleration. When traffic accelerates, however, one of the other branches—with reduced flow and speed—is followed. (**a**) Density-flow: for model in Eulerian formulation. (**b**) Speed-spacing: for model in Lagrangian formulation

solution method is altered to account for the capacity drop (Lebacque 2003; Srivastava and Geroliminis 2013).

4.5.2 Hysteresis

An other way to model the hysteresis effect, is to include multiple branches in the fundamental diagram: one congestion branch for deceleration and one (or even more) for acceleration. Instead of using the speed in the original fundamental diagram, in the acceleration phase, the speed is reduced to a lower branch, as indicated in Fig. 4.15. It is recommended that the Lagrangian coordinate system is applied for simulation (Yuan et al. 2017).

Problem Set

Method of Characteristics

Consider the following initial value problem. Initially, traffic state is as follows:

$$\rho(x,0) = \begin{cases} 0 & \text{if } x > 0 \\ \rho_{\text{jam}} & \text{if } -200 \le x \le 0 \\ 0 & \text{if } x < 200 \end{cases} \tag{4.40}$$

Furthermore, the LWR model is applied, in combination with a bilinear fundamental diagram, with parameters as in Table 4.1, except for critical speed $v_{\text{crit}} = v_{\text{max}} = 30$ m/s.

4.1 Apply the method of characteristics to solve the initial value problem. Draw the traffic states in the (t, x)-plane and answer the following questions:

1. At any $t > 0$, what is the velocity of the first vehicle that starts driving?
2. What is the velocity of the downstream front of the queue?
3. What is the velocity of the upstream front of the queue?
4. How long does it take for the queue to solve?

Consider the same problem as above, but now with – in addition to the prescribed initial densities as in (4.40) – the following upstream boundary conditions:

$$q(400, t) = \begin{cases} 0 & \text{if } 0 < t < 6.67 \\ \rho_{\text{crit}} v_{\text{max}} & \text{if } 6.67 \leq t \leq 20 \\ 0 & \text{if } t > 20 \end{cases} \quad \text{and}$$

$$\rho(400, t) = \begin{cases} 0 & \text{if } 0 < t < 6.67 \\ \rho_{\text{crit}} & \text{if } 6.67 \leq t \leq 20 \\ 0 & \text{if } t > 20 \end{cases} \tag{4.41}$$

This can be interpreted as a platoon of vehicles that approaches the queue, for example from a traffic light further upstream.

4.2 Apply the method of characteristics to solve the combined initial and boundary value problem. Draw the traffic states in the (t, x)-plane.

Simulations

Simulations can give better insights into models. Sample code can be found on the website (http://extras.springer.com) of this book.

4.3 Run a simulation to reproduce the results in Fig. 4.9.

4.4 Adapt the code to apply the bilinear fundamental diagram instead of the parabolic linear one. Reflect on the results and comment on whether they are in correspondence with the solution of problem 4.1.

4.5 Adapt the provided code in one or more of these directions:

- make the initial queue longer
- change parameter values of the model parameters (maximum speed, critical speed, jam density, critical density)
- change to yet an other fundamental diagram

Compare the results of different setups and write about your insights: is this more (or less) realistic? Do you see other phenomena? Compare your results with those in literature.

The reader is further encouraged to run different simulations in the problem set of the next chapter, after introducing the numerical methods.

Higher Order Models

As discussed in Sect. 4.3, the Payne model ((4.1) and (4.24)) is not anisotropic, while the ARZ ((4.1) and (4.25)) is. To calculate the characteristic velocities, the models are reformulated into a system of equations (4.42):

$$\frac{\partial \mathbf{u}}{\partial t} + \mathrm{J}(\mathbf{u})\frac{\partial \mathbf{u}}{\partial \mathrm{x}} = \mathrm{f}(\mathbf{u}) \tag{4.42}$$

with the state vector $\mathbf{u} = \begin{pmatrix} \rho \\ y \end{pmatrix}$, $J(\mathbf{u})$ the jacobian matrix and $f(\mathbf{u})$ the source term. The variable y and the Jacobian matrix are different for each model. The eigenvalues of the Jacobian matrix are the characteristic values.

4.6 Calculate the characteristic velocities of the Payne model by:

1. Define variable y, the Jacobian matrix $\mathrm{J}(\mathbf{u})$ and the source term $f(\mathbf{u})$ such that (4.42) defines the Payne model.
2. Determine the eigenvalues of the Jacobian matrix.

4.7 Calculate the characteristic velocities of the ARZ model.

4.8 Reflect on the difference between the Payne model and the ARZ model and on why the first one is not anisotropic and the second one is.

An other popular model is the Aw-Rascle model (Aw and Rascle 2000) with the following speed equation:

$$\frac{\partial}{\partial t}(v + p(\rho)) + v\frac{\partial}{\partial x}(v + p(\rho)) = 0 \tag{4.43}$$

with $p(\rho)$ a 'pressure term'. The (increasing) function $p(\rho)$ can have different forms, but $p(\rho) = \rho^c$ with some constant $c > 0$ is considered as the prototype.

4.9 (Advanced) Calculate the characteristic velocities of the Aw-Rascle model.

4.10 (Advanced) Define the invariant I and the source function $g(I)$ for the Aw-Rascle model, i.e.: for which functions $I(\rho, v)$ and $g(I)$ in the generic higher order model, is the Aw-Rascle model retrieved?

Models with Capacity Drop/Hysteresis

4.11 (Advanced) Run a simulation to reproduce the results in Fig. 4.14.

4.12 (Advanced) Adapt the code to use the bilinear fundamental diagram and reflect on how the results differ from the ones with the linear-parabolic fundamental diagram, and from the ones without bounded acceleration.

4.13 (Advanced) Adapt the code to apply other maximum accelerations and reflect on how the simulation results change.

The Lagrangian Coordinate System

The Lagrangian formulation of the LWR model (4.35) can be derived from its Eulerian formulation (4.1). Therefore, the definition of spacing and the Lagrangian time derivative are needed. The definition of spacing expresses spacing as the partial derivative of the position x to vehicle number n:

$$s = \frac{1}{\rho} = -\frac{\partial x}{\partial n} \tag{4.44}$$

The minus sign results from the fact that vehicles are numbered opposite to the driving direction. Furthermore, the Lagrangian time derivative is:

$$\frac{\mathrm{D}}{\mathrm{D}t} = \frac{\partial}{\partial t} + v\frac{\partial}{\partial x} \tag{4.45}$$

$\mathrm{D}/\mathrm{D}t$ is the partial derivative with respect to time in Lagrangian coordinates, that is: the derivative with respect to time t with the other coordinate (vehicle number n) fixed. As n-coordinates move with vehicle velocity, $\mathrm{D}r/\mathrm{D}t$ is the rate of change of some variable r as it is observed by a driver moving with velocity $v(n,t) = v(x(n),t) = \partial x/\partial t$. This implies that $\mathrm{D}/\mathrm{D}t$ is a directional derivative in Eulerian coordinates: it is the derivative in the direction of the moving observer (the driver). Both coordinates t and x change in this direction. Conversely, $\partial/\partial t$ is a partial derivative in Eulerian coordinates and a directional derivative in Lagrangian coordinates.

4.14 (Advanced) Derive the Lagrangian formulation of the LWR model from its Eulerian formulation. Hint: Use (4.44) to redefine density as a partial derivative and substitute it into the Eulerian conservation equation. After reordering the result, substitute the Lagrangian time derivative (4.45) and apply the definition of spacing once again.

The Lagrangian formulation can also be applied to higher order models and multi-class kinematic wave models (van Wageningen-Kessels et al. 2010).

4.15 (Advanced) Derive the Lagrangian formulation (4.38) of the generic higher order model (4.26) or of a multi-class model.

Further Reading

Aw A, Klar A, Rascle M, Materne T (2002) Derivation of continuum traffic flow models from microscopic follow-the-leader models. SIAM J Appl Math 63(1):259–278

Lebacque JP, Mammar S, Haj Salem H (2007) Generic second order traffic flow modelling. In: Allsop RE, Bell MGH, Heydecker BG (eds) Transportation and traffic theory 2007. Elsevier, Oxford, pp 755–776

Leclercq L, Laval J, Chevallier E (2007) The Lagrangian coordinates and what it means for first order traffic flow models. In: Allsop RE, Bell MGH, Heydecker BG (eds) Transportation and traffic theory 2007. Elsevier, Oxford, pp 735–753

Van Wageningen-Kessels FLM (2016) Framework to assess multi-class continuum traffic flow models. Transp Res Rec J Transp Res Board 2553:150–160

Chapter 5
Numerical Methods for Continuum Models

Numerical methods are used to approximate the solution of traffic flow models. This is needed because in most realistic cases it is impossible to solve the problems analytically. When a macroscopic model is applied, usually the space and time domains are divided into intervals: road segments (grid cells) and time steps. For each time step and at each grid cell the model equations are solved approximately using numerical methods. The result is the density in each grid cell, at each time step. Alternative methods are based on moving coordinates and will also be discussed. In this chapter, the focus is on the numerical methods themselves, with the main purpose that the reader should be able to apply the methods.

After reading this chapter the reader will understand the basics of applying numerical methods to macroscopic traffic flow models. They can apply those methods to the models and can argue about the impact of choices such as a fixed vs. moving coordinate system and grid cell and time step size.

5.1 Finite Difference Methods and Time Stepping

To build efficient numerical methods for traffic flow simulations, it is often useful to write the model in conservative shape, as in (4.34):

$$\frac{\partial \mathbf{u}}{\partial t} + \frac{\partial f(\mathbf{u})}{\partial x} = s(\mathbf{u}) \tag{5.1}$$

Most—if not all—models from the previous chapter fit into this framework.

Finite difference methods (FDM's) are often applied to solve such partial differential equations. In their most basic form, they approximate the spatial derivatives by dividing the difference in value by the distance, as illustrated in Fig. 5.1.

F. Kessels, *Traffic Flow Modelling*, EURO Advanced Tutorials
on Operational Research, https://doi.org/10.1007/978-3-319-78695-7_5

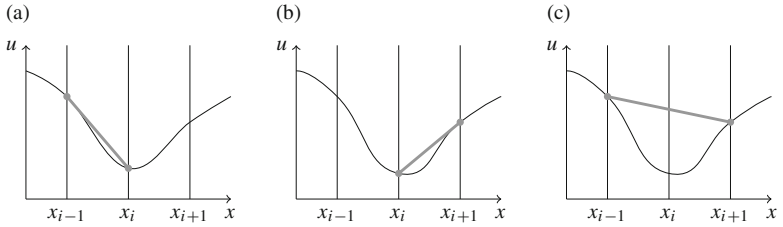

Fig. 5.1 Examples of FDM approximation of the slope of u at location x_i. (**a**) Upwind method $u'(x_i) \approx \frac{u(x_i)-u(x_{i-1})}{x_i-x_{i-1}}$. (**b**) Downwind method $u'(x_i) \approx \frac{u(x_{i+1})-u(x_i)}{x_{i+1}-x_i}$. (**c**) Central method: $u'(x_i) \approx \frac{u(x_{i+1})-u(x_{i-1})}{x_{i+1}-x_{i-1}}$

5.1.1 Explicit Time Stepping

Usually, an explicit time stepping scheme is applied. The basic idea is that it is assumed that the current state determines the flow for the duration of the whole time step. Applying the explicit time stepping method to the generic continuum traffic flow model (5.1) gives:

$$\frac{\mathbf{u}^{k+1}-\mathbf{u}^k}{\Delta t}+\left(\frac{\partial f(\mathbf{u})}{\partial x}\right)^k \approx (s(\mathbf{u}))^k \tag{5.2}$$

with superscript k a time indicator: $\mathbf{u}^k$ is the vector $\mathbf{u}$ at time t and $\mathbf{u}^{k+1}$ is the vector $\mathbf{u}$ at time $t+\Delta t$. Rewriting gives:

$$\mathbf{u}^{k+1} \approx \mathbf{u}^k + \Delta t\left[-\left(\frac{\partial f(\mathbf{u})}{\partial x}\right)^k + (s(\mathbf{u}))^k\right] \tag{5.3}$$

In contrast, an implicit scheme would solve (5.2) but with the terms $\frac{\partial f(\mathbf{u})}{\partial x}$ and $s(\mathbf{u})$ approximated at time step $k+1$ instead of k. This approach leads to more complicated equations to be solved each time step, but the time steps themselves can be larger. Especially when combined with moving coordinates, this approach seems useful, but very little research has been done (van Wageningen-Kessels et al. 2009).

5.1.2 First Order Finite Difference Methods

Combining the above, the generic continuum traffic flow model (5.1) is discretised with $\mathbf{u}_i^k$ the numerical approximation of the state vector $\mathbf{u}(x_i, t^k)$ at location x_i

and time t^k and with $\mathbf{f}_i^k = f(\mathbf{u}_i^k)$ and $\mathbf{s}_i^k = s(\mathbf{u}_i^k)$ the approximated flow and sink/source, respectively, at this location and time. Applying the first order finite difference methods with explicit time stepping gives:

Upwind method

$$\mathbf{u}_i^{k+1} = \mathbf{u}_i^k - \frac{\Delta t}{\Delta x}\left(\mathbf{f}_i^k - \mathbf{f}_{i-1}^k\right) + \Delta t \mathbf{s}_i^k \tag{5.4}$$

Downwind method

$$\mathbf{u}_i^{k+1} = \mathbf{u}_i^k - \frac{\Delta t}{\Delta x}\left(\mathbf{f}_{i+1}^k - \mathbf{f}_i^k\right) + \Delta t \mathbf{s}_i^k \tag{5.5}$$

Central method

$$\mathbf{u}_i^{k+1} = \mathbf{u}_i^k - \frac{\Delta t}{2\Delta x}\left(\mathbf{f}_{i+1}^k - \mathbf{f}_{i-1}^k\right) + \Delta t \mathbf{s}_i^k \tag{5.6}$$

As can be seen from the equations and Figs. 5.1 and 5.2, information from either upwind, downwind, or both is used to update the state vector $\mathbf{u}$. However, as discussed in Sect. 4.1.2, characteristics can move in both directions. Therefore, in some cases—when information travels downstream—an upwind method is appropriate, while in other cases—when information travels upstream—a downwind method is appropriate. And in yet other cases, when some characteristics move downstream and others upstream, it may be best to use information from both directions and apply a central method. However, it is difficult—if not impossible—to determine beforehand which method would be best. Therefore, other methods that swap directions whenever needed have been developed. Such a method, the minimum supply method, is discussed later.

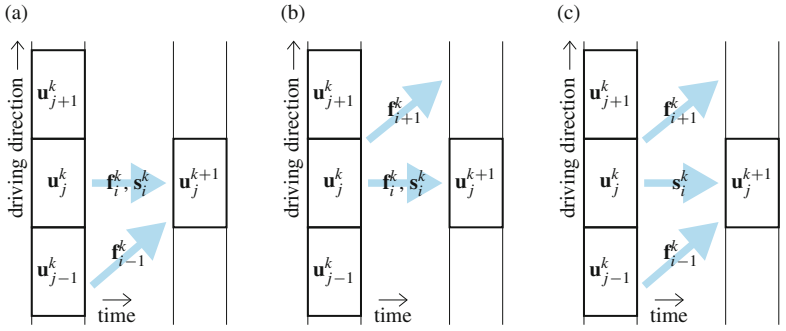

Fig. 5.2 Illustration of application of the finite difference methods in traffic flow models. (**a**) Upwind. (**b**) Downwind. (**c**) Central

5.1.3 *Stability of Numerical Methods*

Explicit time stepping methods are known to pose rather strict stability conditions. Time step sizes can not be too large, or the numerical method becomes unstable and results very unrealistic. There are different types of instability, that are relevant to different types of models and numerical methods. The most important one—that is relevant for any macroscopic traffic flow model in Eulerian formulation with explicit time stepping—is prevented by setting the time step size and grid cell size such that the Courant-Friedrichs-Lewy (CFL) number (Courant et al. 1967) ν satisfies:

$$\nu := \frac{\Delta t}{\Delta x} \max \left| \frac{\mathrm{d}Q}{\mathrm{d}\rho} \right| \leq 1 \tag{5.7}$$

Most (realistic) density-flow fundamental relations are steepest at zero density and thus the maximum slope in absolute terms is equal to the maximum velocity: $\max \|\mathrm{d}Q/\mathrm{d}\rho\| = v_{\max}$. Consequently, the CFL-condition can be interpreted as follows: within a time step, a vehicle can not cross more than the length of one cell.

5.2 Minimum Supply Demand Method for Kinematic Wave Models

The minimum supply demand method is widely used as a numerical method for the kinematic wave model. In 1994 Daganzo introduces the cell transmission model as a spatially and temporally discrete version of the LWR model. Lebacque (1996) describes the cell transmission model as a minimum supply demand method. The method is illustrated in Fig. 5.3a. This method applies explicit time stepping: within a cell and during a time step the density, flow and velocity are assumed to be constant. Each time step k, a fraction of the vehicles in the cell is transmitted to the adjacent downstream cell. The new density $\rho_j^{k+1} = \rho(j\Delta x, (k+1)\Delta t)$ of each cell j is calculated as follows:

$$\rho_j^{k+1} = \rho_j^k + \frac{\Delta t}{\Delta x} \left(q_{j-\frac{1}{2}}^k - q_{j+\frac{1}{2}}^k \right) \tag{5.8a}$$

with $q_{j-\frac{1}{2}}^k$ the inflow into and $q_{j+\frac{1}{2}}^k$ the outflow out of cell j:

$$q_{j-\frac{1}{2}}^k = \min \left(\delta_{j-1}^k, \sigma_j^k \right) \tag{5.8b}$$

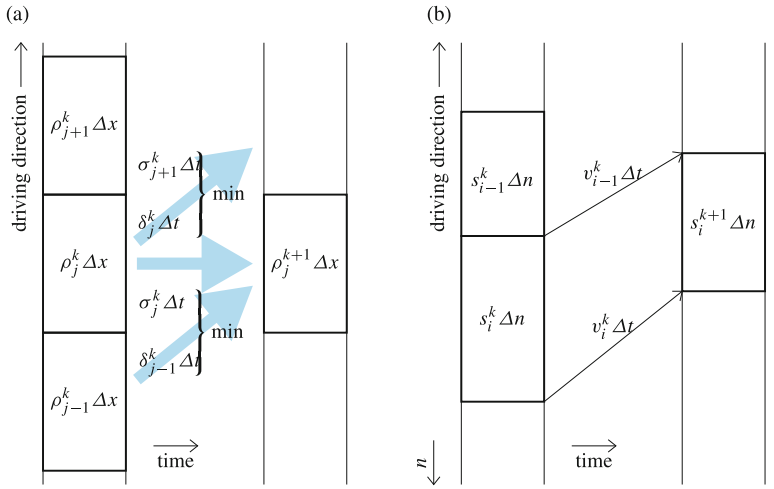

Fig. 5.3 Discretization of the LWR model in Eulerian and Lagrangian formulation. (**a**) Eulerian formulation: the minimum supply demand method leads to upwind and downwind discretization. The discretization uses the number of vehicles in each cell ($\rho \Delta x$) and the number of vehicles travelling from one cell to the next ($\min(\delta \Delta t, \sigma \Delta t)$). (**b**) Lagrangian formulation: upwind discretization. The discretization uses the road length taken by each vehicle group ($s \Delta n$) and the distance travelled by each group ($v \Delta t$)

δ_j^k the demand:

$$\delta_j^k = \begin{cases} q_j^k & \text{if } \rho_j^k \leq \rho_{\text{crit}} \\ q_{\max} & \text{if } \rho_j^k > \rho_{\text{crit}} \end{cases} \tag{5.8c}$$

σ_j^k the supply:

$$\sigma_j^k = \begin{cases} q_{\max} & \text{if } \rho_j^k \leq \rho_{\text{crit}} \\ q_j^k & \text{if } \rho_j^k > \rho_{\text{crit}} \end{cases} \tag{5.8d}$$

and $q_j^k = Q(\rho_j^k)$ the flow from the fundamental relation. Demand δ_j^k can be interpreted as the number of vehicles per time unit that want to flow from cell j to cell $j+1$ during the time step k. Supply σ_j^k can be interpreted as the number of vehicles per time unit that can be fitted in the j-th cell during time step k. Demand and supply are plotted in Fig. 5.4 together with the fundamental relation. Figure 5.5 shows simulation results for the simple test problem as described in Sect. 4.1.3. The model parameters, as well as the numerical settings are presented in Table 5.1. We note that these settings are equal to the ones applied in Chap. 4 (see Table 4.1).

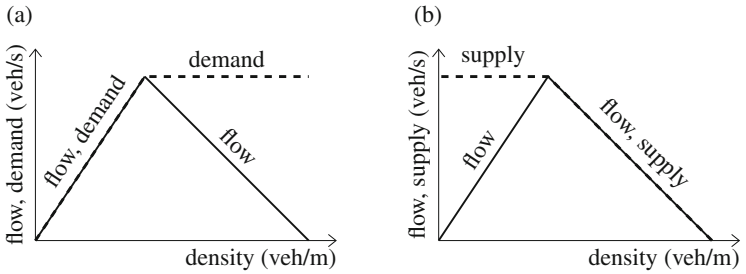

Fig. 5.4 Example of a fundamental relation (flow, solid line) with demand (broken line) and supply (broken line) as function of density. (**a**) Demand. (**b**) Supply

5.3 Methods for Higher Order Models

The basic methods in Sect. 5.1 and the minimum supply demand scheme (Sect. 5.2) can be applied to higher order models as well. However, the flux functions or supply and demand functions have to be adapted differently for each type of higher order model. Therefore, other methods are usually preferred.

The MacCormack method is one of the most popular. It consists of a predictor and a corrector step, which look as follows when applied to the generic continuum traffic flow model (5.1):

$$\tilde{\mathbf{u}}_i^{k+1} = \mathbf{u}_i^k - \frac{\Delta t}{\Delta x}\left(\mathbf{f}_i^k - \mathbf{f}_{i-1}^k\right) + \Delta t \mathbf{s}_i^k \quad \text{(predictor)} \quad (5.9)$$

$$\mathbf{u}_i^{k+1} = \frac{1}{2}\left[\tilde{\mathbf{u}}_i^{k+1} + \mathbf{u}_i^k - \frac{\Delta t}{\Delta x}\left(\tilde{\mathbf{f}}_{i+1}^{k+1} - \tilde{\mathbf{f}}_i^{k+1}\right) + \Delta t \tilde{\mathbf{s}}_i^{k+1}\right] \quad \text{(corrector)} \quad (5.10)$$

The basic idea behind the MacCormack method is that in the predictor step the upwind method with explicit time stepping is applied. But then after that, its result is averaged in the corrector step with the new state as if it was calculated using an implicit time stepping method. Furthermore, in the 'implicit' time step (corrector), a downwind FDM is used.

The MacCormack method is convectively stable if the CFL condition (5.7) is satisfied. This is a sufficient stability condition if the sink/source term $s(\mathbf{u})$ is nonzero because it dampens out numerical oscillations. When applied to a model with zero sink/source term, there is no damping and the method easily becomes unstable. In that case, the CFL number must be reduced, e.g. by reducing the time step size (Helbing and Treiber 1999). An other way to overcome this issue is to add an artificial variable $\mathbf{w}$ that suppresses oscillations (Delis et al. 2014), Mohammadian and van Wageningen-Kessels FLM (2018).

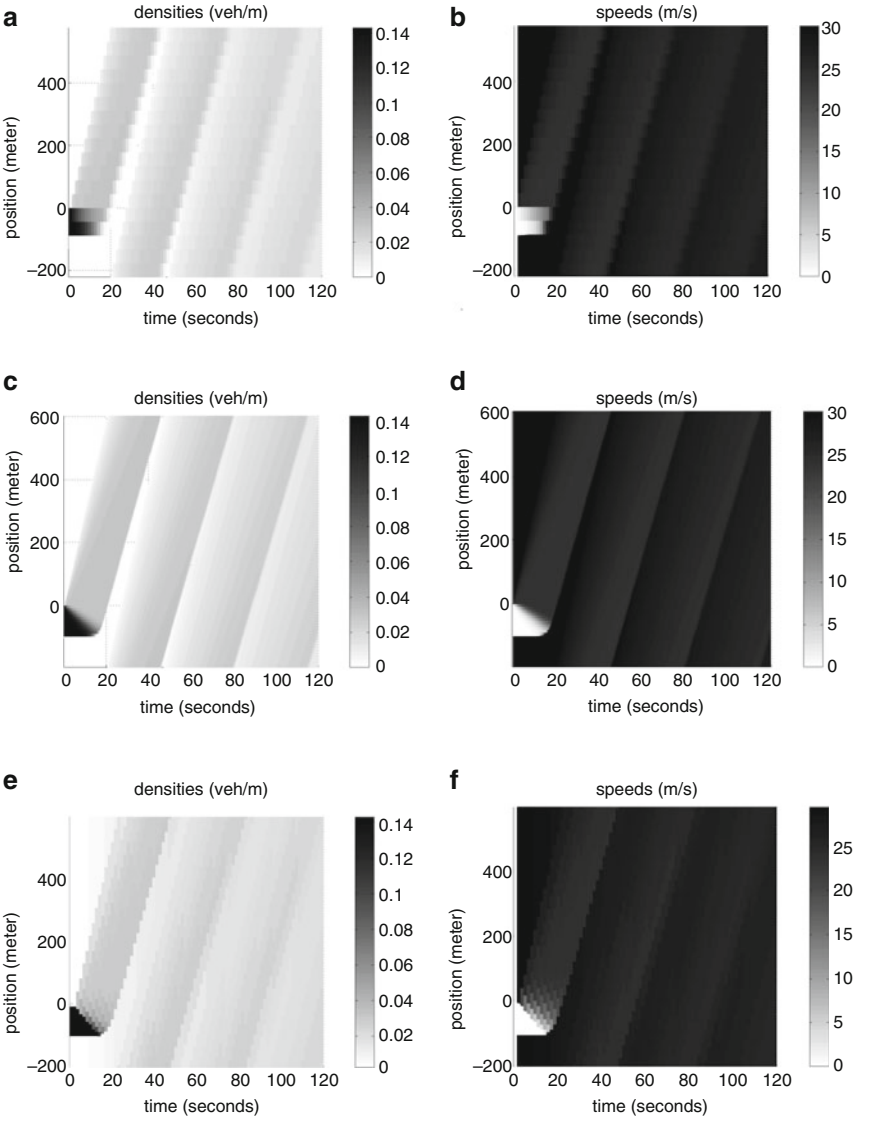

Fig. 5.5 Simulation results with the kinematic wave model with parabolic-linear fundamental diagram. The test case is a ring road, with an initial queue that dissolves, as described in Sect. 4.1.3. The Godunov and the Lagrangian numerical method are applied. (**a**) Densities, minimum supply demand method. (**b**) Speeds, minimum supply demand method. (**c**) Densities, minimum supply demand method (small time step). (**d**) Speeds, minimum supply demand method (small time step). (**e**) Densities, Lagrangian method. (**f**) Speeds, Lagrangian method

Table 5.1 Parameter values of the linear-parabolic fundamental diagram and numerical scheme applied to the kinematic wave model

Model parameters	
Maximum speed $v_{\max}$	30 m/s
Critical speed v_{crit}	$\frac{4}{5}v_{\max} = 24$ m/s
Jam density ρ_{jam}	$\frac{1}{7} \approx 0.14$ veh/m
Critical density ρ_{jam}	$\frac{1}{5}\rho_{\text{jam}} \approx 0.029$ veh/m
Minimum supply demand method	
Time step size Δt	1.5 s
Grid cell size Δx	≈ 44.4
CFL number ν	≈ 0.988
Minimum supply demand method with small time steps	
Time step size Δt	0.3 s
Grid cell size Δx	≈ 8.99
CFL number ν	≈ 0.999
Lagrangian method	
Time step size Δt	1.5 s
Vehicle group size Δn	≈ 1.79
CFL number ν	0.9

5.4 Lagrangian Simulation Methods

The Lagrangian formulation of macroscopic traffic flow models can be used to create efficient simulation methods, based on an upwind finite difference scheme. Recall that, in the Lagrangian formulation vehicle number n is an independent variable. Consequently, in the discretization, vehicles are partitioned into groups of Δn vehicles, instead of dividing the road into cells (Fig. 5.3b). Just as n, Δn is not necessarily integer, it can take any real, positive value. Again, time is partitioned into time steps of size Δt. Each time step k, each vehicle group i is moved downstream. (Or, if traffic is in complete stop, the vehicle group remains at its position.)

5.4.1 Lagrangian Method for the LWR Model

When applied to the LWR model, the following upwind discretization calculates the new position of vehicle group i:

$$s_i^{k+1} = s_i^k + \frac{\Delta t}{\Delta n}\left(v_{i-1}^k - v_i^k\right) \tag{5.11}$$

with $v_i^k = V(s_i^k)$ the velocity obtained from the fundamental relation.

The CFL-number is ν and the condition for stability and convergence is:

$$\nu := \frac{\Delta t}{\Delta n} \max \left|\frac{\mathrm{d}V}{\mathrm{d}s}\right| \leq 1 \tag{5.12}$$

Most (realistic) spacing-velocity fundamental relations are steepest at jam spacing. For example, in the linear-parabolic fundamental relation (2.3) and Fig. 2.5:

$$\max \left| \frac{\mathrm{d}V}{\mathrm{d}s} \right| = \frac{v_{\text{crit}}}{s_{\text{crit}} - s_{\text{jam}}} = w\rho_{\text{jam}} = \frac{w}{s_{\text{jam}}} \tag{5.13}$$

Consequently, the CFL-condition can be interpreted as follows. It limits the distance a vehicle groups can travel downstream within one time step. In fact, the distance between its new position (x_i^{k+1}) and the old position of the leading vehicle group (x_{i-1}^k) is at least the characteristic velocity in jam times the time step size: $w\Delta t$. To put it precisely: $x_{i-1}^k - x_i^{k+1} \geq w\Delta t$. This implies that even the fastest characteristics in the (t, n) plane, namely the characteristics related to jam, are traced with the upwind method.

Simulation results using this method were already presented in the previous chapter (Fig. 4.9). For easy comparison, they are also included in this chapter (Fig. 5.5).

5.4.2 *Simplified Lagrangian Simulation and Car-Following Models*

Finally, the discretised model can be simplified to:

$$x_i^{k+1} = x_i^k + \Delta t v_i^k = x_i^k + \Delta t V(s_i^k) \tag{5.14}$$

The velocity during the k-th time step v_i^k is determined using the fundamental relation and an upwind discretisation of the spacing:

$$s_i^k = \frac{x_{i-1} - x_i}{\Delta n} \tag{5.15}$$

This simplified method can be interpreted as follows: the new position of group i is its old position plus the distance it travels during the k-th time step: $\Delta t v_i^k$. This formulation also shows the close relation between the Lagrangian discretisation of macroscopic traffic flow models and simple car-following models, which also calculate the new position using the old position and the speed as input. This formulation is applied by Leclercq et al. (2007) to show the equivalence between the LWR model and the simplified car-following model by Newell (2002) under the following conditions:

- the fundamental relation $q(\rho)$ is triangular
- the CFL-condition (5.12) is satisfied as an equality
- the vehicle group size $\Delta n = 1$
- time parameter τ (which may be interpreted as reaction time) equals time step size $\tau = \Delta t$

Therefore, the Lagrangian coordinate system does not only lead to more efficient numerical methods, it also makes the coupling between macroscopic and microscopic regions in a hybrid model easier, as we will discuss in more detail in the next chapter (Sect. 6.3).

5.4.3 Characteristics and Numerical Methods

When comparing the minimum supply demand method (5.8) with the Lagrangian method (5.14) the difference is striking: the latter looks much less complicated. This is related to the characteristic speeds. To clarify this, let us recall the characteristic speed in the Eulerian formulation of the LWR model:

$$\frac{\mathrm{d}q}{\mathrm{d}\rho} = Q'(\rho) \tag{5.16}$$

The characteristic speed (5.16) was derived using a reformulation of the conservation equation in Eulerian coordinates (4.6). The same type of reformulation in Lagrangian coordinates gives:

$$\frac{\mathrm{D}s}{\mathrm{D}t} + \frac{\partial v}{\partial n} = 0 \quad \Rightarrow \quad \frac{\mathrm{D}s}{\mathrm{D}t} + \frac{\mathrm{d}v}{\mathrm{d}s}\frac{\partial s}{\partial n} = 0 \tag{5.17}$$

In the Lagrangian formulation, the characteristic speed is thus:

$$\frac{\mathrm{d}s}{\mathrm{d}v} = V'(s) \tag{5.18}$$

We now note that the characteristic speed in the Eulerian formulation (5.16) can be both positive (in free flow) or negative (in congestion). The characteristic speed in the Lagrangian formulation (5.18), however, is always nonnegative (for any reasonable fundamental diagram). Therefore, characteristics move in the direction of increasing vehicle number. This fact is used in the Lagrangian simulation method: it is simply an upwind method and there is no need to switch between upwind and downwind as in the minimum supply demand method.

The Lagrangian formulation yields similar benefits for numerical methods for anisotropic higher order models. However, it must be noted that for non-anisotropic models, some characteristics may be faster than vehicles and the Lagrangian simulation method will thus not be able to reproduce the fastest characteristics. Furthermore, road inhomogeneities such as intersections and ramps are more straightforward to implement in the Eulerian coordinate system, even though Lagrangian methods have been developed as well (van Wageningen-Kessels et al. 2013).

5.4.4 Lagrangian Methods for Higher Order Models

The Lagrangian coordinate system can also yield more efficient numerical methods for higher order models. We recall the GSOM in the Lagrangian coordinate system (4.38)

$$\frac{\mathrm{D}s}{\mathrm{D}t} + \frac{\partial v}{\partial n} = 0, \qquad \frac{\mathrm{D}I}{\mathrm{D}t} = -g(I), \qquad v = V(s, I) \tag{5.19a}$$

with spacing $s = 1/\rho$ and driver attribute I. Using the same discretisation approach as for the LWR model, we find:

$$I_j^{k+1} = I_j^k - \Delta t g(I_j^k), \qquad x_j^{k+1} = x_j^k + \Delta t v_j^k \tag{5.20a}$$

$$v_j^k = V\left(s_j^k, I_j^k\right), \qquad s_j^k = \frac{x_{j-1}^k - x_j^k}{\Delta n} \tag{5.20b}$$

For stability, the CFL condition has to be satisfied:

$$\nu = \frac{\Delta t}{\Delta n} \max_{s,I} \left| \frac{\mathrm{d}V(s, I)}{\mathrm{d}s} \right| \leq 1 \tag{5.21}$$

Note that the CFL number thus depends on the maximum slope of the fundamental relation, for density (or spacing s) and value of the attribute I. For more details we refer the interested reader to Khelifi et al. (2016).

5.4.5 Discretisation of Bounded Acceleration

The Lagrangian formulation is well suited for simulation of bounded acceleration. In this case, the speed is not only determined by the fundamental relation, but it is also limited from above by the maximum acceleration. Extending the simplified discretised model (5.14) yields:

$$x_j^{k+1} = x_j^k + \Delta t \ \min\left\{ V\left(s_j^k\right), v_j^{k-1} + \Delta t a_{\max} \right\} \tag{5.22}$$

Simulation results with this method are shown in the previous chapter (Fig. 4.14).

5.5 Variational Theory and Link Transmission Models

An alternative approach to numerically solve the kinematic wave model, is to use variational theory. Assuming a bilinear fundamental diagram, it exploits the fact that information can only travel at two velocities: either downstream at free flow speed, or upstream at congestion wave speed. This is used to calculate the vehicle

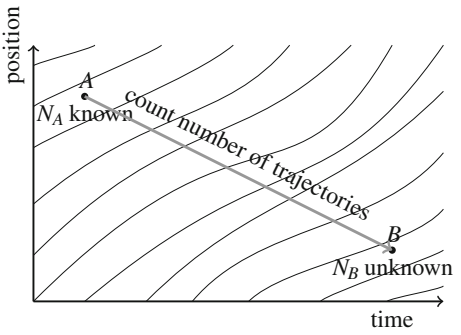

Fig. 5.6 Illustration of main principle of variational theory for traffic flow: N_B can be calculated from N_A and the number of trajectories between A and B

number n at the nodes connecting homogeneous sections of road. Just as in the Lagrangian formulation of the kinematic wave model, the vehicle number n can take any value—not necessarily integer. Furthermore, as discussed before, from the vehicle number, other variables can be derived, e.g. using Edie's definitions (see Sect. 1.3.2).

For a more detailed discussion of variational theory, we refer to Newell (1993), Daganzo (2006). Here, we restrict ourselves to its application in the Link Transmission Model (LTM) (Yperman 2007; Gentile 2010). The application of LTM to determining the vehicle number $N(x, t)$ at a node at location x and at time t consists of calculating the following:

1. The sending and receiving flows: δ and σ, respectively
2. The transition flow: f
3. The cumulative vehicle number: N

The interpretation of the sending and receiving flows are very similar to the demand and supply in the minimum supply demand method (Sect. 5.2): the sending flow is the number of vehicles in the upstream link that can reach the node (like the demand), the receiving flow is the number of vehicles that the upstream link can still accommodate (like the supply). Because of this similarity, we use the same symbols. However, they are calculated differently.

The principal idea of variational theory for traffic flow is illustrated in Fig. 5.6. The cumulative vehicle number at location B, $N_B = N(x_B, t_B)$ can be calculated once two things are known:

1. the cumulative vehicle number at location A, $N_A = N(x_A, t_A)$, and
2. the number of trajectories between A and B.

This can also be used to calculate the sending and receiving flows. This is illustrated in Fig. 5.7 and results in:

$$\delta(x_{j-1/2}, t) = \min\left[N\left(x_{j-1}, t + \Delta t - \frac{L_{i-1/2}}{v_{\max}}\right) - N\left(x_j, t\right), \Delta t\, Q_{i-1/2}\right] \tag{5.23}$$

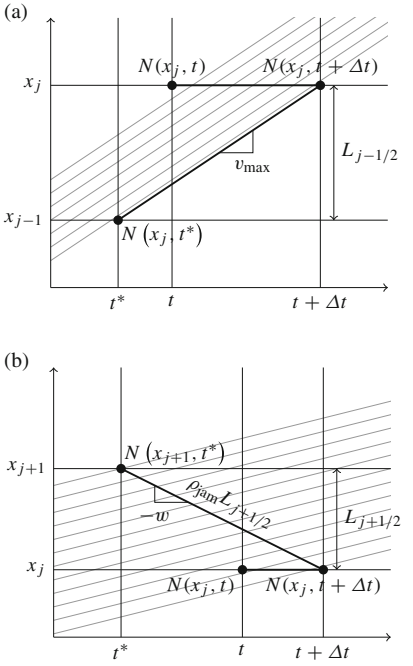

Fig. 5.7 Illustration of how the sending and receiving flows are calculated. Grey lines indicate possible vehicle trajectories. (**a**) Sending flow can not be larger than the number of vehicles that passes between (x_j, t) and $(x_j, t+\Delta t)$. The maximum number of vehicles passes when they pass at maximum speed. Therefore, the sending flow does not exceed the number of vehicles passing between (x_j, t) and (x_j, t^*), with $t^* = t + \Delta t - L_{j-1/2}/v_{\max}$. (**b**) Receiving flow can not be larger than the number of vehicles that passes between (x_j, t) and $(x_j, t+\Delta t)$ if the area is in congestion. Furthermore, the number of vehicles between (x_{j+1}, t^*) (with $t^* = t + \Delta t - L_{j+1/2}/w$) and $(x_j, t+\Delta t)$ is $\rho_{\text{jam}} L$. The proof is left as an exercise. Therefore, the receiving flow can not exceed $N\left(x_{j+1}, t^*\right) + \rho_{\text{jam}} L - N(x_j, t)$

$$\sigma(x_{j+1/2}, t) = \min\left[N\left(x_{j+1}, t + \Delta t - \frac{L_{i+1/2}}{w}\right) + \rho_{\text{jam}} L_{i+1/2} - N\left(x_j, t\right), \Delta t\, Q_{i+1/2}\right] \tag{5.24}$$

In most cases, the cumulative vehicle numbers $N\left(x_{j-1}, t + \Delta t - \frac{L_{i-1/2}}{v_{\max}}\right)$ and $N\left(x_{j+1}, t + \Delta t - \frac{L_{i+1/2}}{w}\right)$ need to be interpolated. A straightforward way to do this is to use a linear approximation at the location $x^* = x_{j-1}$ or $x^* = x_{j+1}$ at time $t^* \in (t^0, t^0 + \Delta t)$:

$$N(x^*, t^*) = (1-\alpha) N(x^*, t^0) + \alpha N(x^*, t^0 + \Delta t) \tag{5.25}$$

with $\alpha = (t^* - t^0)/\Delta t$.

Subsequently, the transition flows are the minimum of sending and receiving flows:

$$f(x_j, t) = \min[\delta(x_{j-1/2}, t), \sigma(x_{j+1/2}, t)] \tag{5.26}$$

And the new cumulative vehicle number is:

$$N(x_j, t + \Delta t) = N(x_j, t) + f(x_j, t) \tag{5.27}$$

Finally, this version of the LTM needs to satisfy a CFL condition for numerical stability:

$$\nu := \frac{\Delta t}{\min_j(L_{j+1/2})} v_{\max} \leq 1, \tag{5.28}$$

In most cases the link length $L_{j+1/2}$ is relatively large (larger than Δx in the minimum supply demand method) and therefore, time steps can also be large, resulting in fast simulations. Moreover, more efficient, iterative methods have been developed that can be applied with even larger time step sizes (Himpe et al. 2016). They are similar to implicit time stepping methods as discussed in Sect. 5.1.

Problem Set

Godunov Method for LWR

Simulations can give better insights into numerical methods. Sample code can be found on the website (http://extras.springer.com) of this book.

5.1 Run a simulation to reproduce the results in Fig. 5.5a, b.

5.2 Adapt the provided code in one or more of these directions:

- change the time step size: how do the results change for a smaller time step? And what happens if you increase the time step size?
- change the CFL number: how do the results change for a smaller CFL number? And what happens if you increase the CFL number?

Compare the results of different setups and write about your insights. Do the results look more or less accurate? Compare your results with those in literature.

Lagrangian Method for LWR

5.3 Run a simulation to reproduce the results in Fig. 5.5e, f.

5.4 Adapt the provided code in the same way as you did in Problem 5.2. Compare the results of different setups and write about your insights. Also compare the results with those obtained with the minimum supply demand method. Do the results look more or less accurate? Compare your results with those in literature.

Lagrangian Method for Bounded Acceleration and Higher Order Models

5.5 Run a simulation to reproduce the results in Fig. 4.14.

5.6 (Advanced) Adapt the provided code in one or more of these directions:

- apply a higher order model (e.g. the ARZ model)
- change parameter values of the model parameters (maximum speed, critical speed, jam density, critical density, delay time)
- change the time step size or CFL number

Compare the results of different setups and write about your insights: is this more (or less) realistic? Do you see other phenomena? Compare your results with those in literature.

LTM

Refer to Fig. 5.7b.

5.7 Show that the number of vehicles between (x_{j+1}, t^*) and $(x_j, t + \Delta t)$ equals $\rho_{\text{jam}} L_{j+1/2}$.

Further Reading

Delis A, Nikolos I, Papageorgiou M (2014) High-resolution numerical relaxation approximations to second-order macroscopic traffic flow models. Transport Res C Emerg Technol 44:318–349

Khelifi A, Haj-Salem H, Lebacque JP, Nabli L (2016) Lagrangian discretization of generic second order models: Application to traffic control. Appl Math Inf Sci Int J 10(4):1243–1254

LeVeque RJ (2002) Finite volume methods for hyperbolic problems. Cambridge texts in applied mathematics, Cambridge University Press, Cambridge

Mohammadian S, van Wageningen-Kessels FLM (2018) An improved numerical method for simulation of Aw-Rascle type second-order continuum traffic flow models. Transp Res Rec J Transp Res Board

Yperman I (2007) The link transmission model for dynamic network loading. PhD thesis, Katholieke Universiteit Leuven

Chapter 6
Mesoscopic Models

Mesoscopic traffic flow models were developed to fill the gap between the family of microscopic models that describe the behavior of individual vehicles and the family of macroscopic models that describe traffic as a continuum flow. Traditional mesoscopic models describe vehicle flow in aggregate terms such as in probability distributions. However, behavioral rules are defined for individual vehicles. The family includes headway distribution models, cluster models, gas-kinetic models and macroscopic models derived from them. Most recently, hybrid mesoscopic models have appeared as a new branch on the tree: they combine microscopic and macroscopic models.

After reading this chapter, the reader will understand the basics of the traditional mesoscopic models: headway distribution models, cluster models and gas-kinetic models. Furthermore, they will understand the basics of hybrid modelling, including interface modelling and the moving coordinate system applied to hybrid models, and are able to argue about its advantages.

6.1 Headway Distribution Models and Cluster Models

Headway distribution models calculate traffic flows using time headways. The time headways are identically distributed independent random variables. The models are part of the mesoscopic family because they describe the distribution of headways of individual vehicles, while they do not explicitly trace the individual vehicles. These models are particularly well-suited to describe stochasticity (Li and Chen 2017). Examples are Buckley's semi-Poisson model (1968) and the generalized queueing model (Branston 1976).

Cluster models describe traffic flow as a flow of clusters of vehicles. Each cluster consists of multiple vehicles and within each cluster flow properties such as velocity and headway are assumed to be homogeneous. Clusters can emerge, for example,

F. Kessels, *Traffic Flow Modelling*, EURO Advanced Tutorials
on Operational Research, https://doi.org/10.1007/978-3-319-78695-7_6

as an accumulation of vehicles behind a slow vehicles when overtaking possibilities are limited. Clusters can grow or decay. The most popular and famous cluster model is the one by Mahnke and Kühne (2007).

Since both headway distribution models and cluster models do not seem popular nowadays, we do not go into more detail here.

6.2 Gas-Kinetic Models

Gas-kinetic models were developed in analogy to models describing the motion of large numbers of small particles (atoms or molecules) in a gas. When applied to traffic flow, these models describe the dynamics of velocity distribution functions of vehicles. Prigogine and Andrews (1960), Prigogine (1961) first introduce gas-kinetic models describing traffic flow by the following partial differential equation:

$$\frac{\partial \tilde{\rho}}{\partial t} + v\frac{\partial \tilde{\rho}}{\partial x} = \left(\frac{\partial \tilde{\rho}}{\partial t}\right)_{\text{acceleration}} + \left(\frac{\partial \tilde{\rho}}{\partial t}\right)_{\text{interaction}} \tag{6.1}$$

with $\tilde{\rho}$ the reduced phase-space density which can be interpreted as follows. At time t, the expected number of vehicles between location x and $x + \mathrm{d}x$ that drive with a velocity between v and $v + \mathrm{d}v$ is the integral of the reduced phase-space density over this two-dimensional area:

$$\begin{aligned} &\text{expected \# of veh's in } [x, x+\mathrm{d}x) \text{ with velocity in } [v, v+\mathrm{d}v) \\ &= \int_x^{x+\mathrm{d}x} \int_v^{v+\mathrm{d}v} \tilde{\rho}(x, v, t)\,\mathrm{d}x\,\mathrm{d}v \;\approx\; \tilde{\rho}(x, v, t)\,\mathrm{d}x\,\mathrm{d}v \end{aligned} \tag{6.2}$$

where the approximation holds in the limit for an infinitesimal area with $\mathrm{d}x \to 0$ and $\mathrm{d}v \to 0$. Or, in other words, the reduced phase-space density is the expected number of vehicles in a small interval around location x, that travel with speed close to v at time t. The left-hand side of (6.1) consists of a time derivative and an advection term describing the propagation of the phase-space density with the vehicle velocity. At the right-hand side there is an acceleration term describing the acceleration towards the equilibrium velocity. The other term at the right-hand side is an interaction term, or collision term, describing the interaction between nearby vehicles.

6.2.1 Generic Gas-Kinetic Model

Paveri-Fontana (1975) improves this gas-kinetic model by relaxing the assumption that the behavior of nearby vehicles is uncorrelated, which results in an adapted

interaction term. In the mid 1990s a revival of gas-kinetic models started with the development of multi-lane, multi-class and generic models (Helbing 1997; Hoogendoorn and Bovy 2001). The generic model includes a distinction between lanes, user classes, state-of-driving (free flow or platooning), flow direction, destination, desired speed, angle of movement and acceleration time). As such, the authors claim that it can also be used to model other types of particle flow, including (multi-dimensional) pedestrian flows.

We limit ourselves to the generic model as proposed by Tampère et al. (2003). It includes the reduced phase-space density as in (6.2) but more variables are considered. $\mathbf{S} = (s_1, s_2, \ldots, s_n)$ is the state vector and could include, not only velocity and position, but also any of the other variables mentioned before such as lane, user class, desired velocity, etc. The generic dynamical equation for the reduced phase-space density is:

$$\frac{\partial \tilde{\rho}}{\partial t} + \nabla \mathbf{S} \cdot \left(\tilde{\rho} \frac{\mathrm{d}S}{\mathrm{d}t} \right) = \left(\frac{\mathrm{d}\tilde{\rho}}{\mathrm{d}t} \right)_{\text{events}} \tag{6.3}$$

with the nabla operator on the state vector:

$$\nabla \mathbf{S} = \left(\frac{\partial}{\partial s_1}, \frac{\partial}{\partial s_2}, \ldots, \frac{\partial}{\partial s_n} \right) \tag{6.4}$$

The reduced phase-space density $\rho(t, S) \cdot \mathrm{d}\mathbf{S}$ can now be interpreted as the expected number of vehicles in a state 'close to' S.

6.2.2 *Continuum Gas-Kinetic Models*

Gas-kinetic models are usually not applied in simulations as such because they are computationally expensive. Instead, a continuum traffic flow model is derived and simulations are based on this continuum model.

The method of moments uses integration of the gas-kinetic traffic flow model (6.1) to find a continuum model. The reformulation in a continuum model, reduces some of the accuracy of detail in the model. However, its main advantage is the relative ease with which numerical simulations can be built, once the model is reformulated as a continuum model. Methods for higher order models introduced in the previous chapter can be applied to continuum models derived from gas-kinetic models.

A detailed discussion of continuum gas kinetic models or of the method of moments is out of the scope of this chapter, but we refer the interested reader to Hoogendoorn (1999) for a derivation of a continuum traffic flow model from a gas-kinetic model. Furthermore, Tampère et al. (2003, 2005) propose a continuum gas-kinetic model that explicitly includes a simple car-following model.

6.3 Hybrid Models

Hybrid models combine modelling approaches from different branches into a new model. Most hybrid models combine a car-following model with a continuum model, and are also referred to as multi-scale models. They typically apply a microscopic model to get detail and accuracy in areas and at times where that is required, e.g. the centre of an urban area. In the surrounding areas (e.g. on a free way ring road around the urban area) less detailed results are obtained with a macroscopic model, requiring much less computation time and memory. This way, simulations take advantage of the qualities of both the microscopic model (detailed results) and the macroscopic model (fast results).

6.3.1 Lagrangian Methods for Mesoscopic Models

The modelling within the micro- or macro-regions in space-time domain is done with the models discussed before and (almost) any model could be applied. The challenge lies in the modelling of the interfaces between the regions, see Fig. 6.1. To be effective, hybrid models must have a coupling on the interface between where/when traffic flow is modelled microscopically and where/when it is done macroscopically. To simplify the coupling, the Lagrangian formulation of the macroscopic model is often used. As we already saw in the previous chapter (Sect. 5.4.2) the discretized Lagrangian model is closely related to a car-following model. This makes the coupling of a discretized Lagrangian macroscopic model with a car-following model relatively easy. The continuous formulation of the macroscopic model or a discretised version of the Eulerian macroscopic model can also be applied (Leclercq 2007).

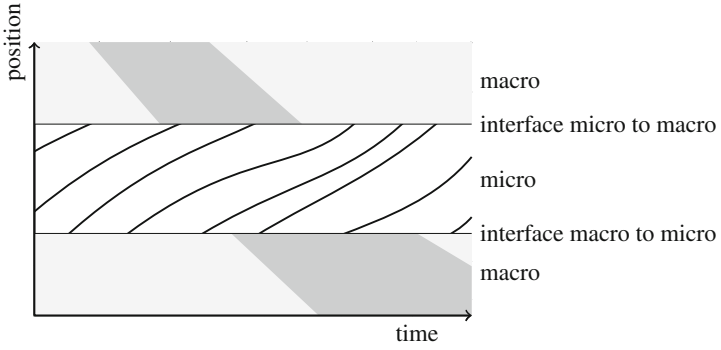

Fig. 6.1 Example of hybrid modelling: trajectories in the microscopic region and densities in the macroscopic regions

Examples of hybrid models are those combining Newell's earlier safe-distance model (Sect. 3.1.1) with the LWR model (Bourrel and Lesort 2003) and the one applying the Simplified Newell car-following model (3.4) to develop a hybrid model that couples this microscopic model with the macroscopic LWR model (Leclercq 2007). In this section, we focus on a rather generic approach as it is proposed by Moutari and Rascle (2007).

6.3.2 *Interface Modelling*

We discuss the coupling at the interface from a numerical perspective: considering how the discretized models are coupled. Therefore, at the macro-to-micro interface, groups of Δn vehicles are disaggregated into individual vehicles, while at the micro-to-macro interface, individual vehicles are aggregated into groups of Δn vehicles. For simplicity, we assume that Δn is integer, even though the method could be adjusted to also work with vehicle groups that contain any non-integer number of vehicles.

The main idea now is:

at the micro to macro interface vehicles leave the minimal microscopic region as individual vehicles. When, at time step k, Δn vehicles have left the region, they are aggregated in a vehicle group at the same location as the last vehicle in that group. See Fig. 6.2a.

at the macro to micro interface vehicles approach the minimal microscopic region as aggregated groups, but they are not allowed to enter as such. Therefore, once the front of the groups has entered at time step k, the group is disaggregated into individual vehicles, uniformly spaced over the road length that was previously taken by the group. See Fig. 6.2a.

We note that this implies that microscopic trajectories are created before the macro to micro interface and they are continued until after the micro to macro interface.

Depending on the applied microscopic and macroscopic models, the aggregated groups and the disaggregated individual vehicles inherit properties from the individual vehicles and vehicle groups, respectively. If the generic higher order macroscopic model is applied, the invariant I is inherited. The variable I can simply be averaged at the micro to macro interface: $I_j^k = \frac{1}{\Delta n} \sum_{m=1} N I_m^k$. At the macro to micro interface, the value of I_i^k for the individual vehicles equals I_j^k of the vehicle group: $I_i^k = I_j^k$.

Finally, the time step size has to satisfy the CFL condition for Lagrangian simulation (5.12). For a microscopic model with $\max \left| \frac{\mathrm{d}V}{\mathrm{d}s} \right| = v_{\max}$ and $\Delta n = 1$, the CFL condition reduces to:

$$\nu := \Delta t v_{\max} \leq 1 \tag{6.5}$$

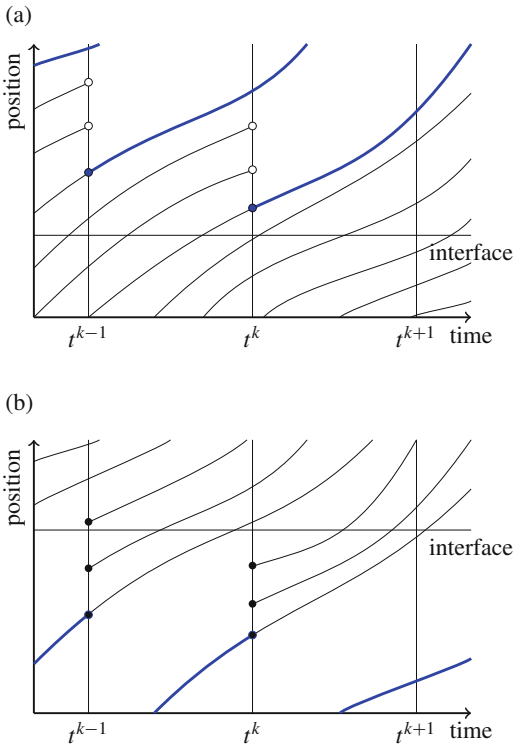

Fig. 6.2 Examples of interfaces in a hybrid model. Microscopic trajectories are indicated with thin black lines, macroscopic Lagrangian trajectories are indicated with thick blue lines. Open circles indicate the end of a trajectory, dots the start of a trajectory. The vehicle discretization in the Lagrangian model is set to $\Delta n = 3$. (**a**) In this example, every third microscopic trajectory is converted into a macroscopic Lagrangian trajectory. Whenever a new macroscopic trajectory is created, all downstream microscopic trajectories are terminated. (**b**) In this example, the macroscopic Lagrangian trajectories are converted into three microscopic trajectories. This is done when the front of the group reaches the interface, i.e. when the most upstream microscopic trajectory has left the macroscopic region. Two microscopic trajectories are created between this microscopic trajectory and the Lagrangian trajectory. Furthermore, the Lagrangian trajectory is converted into a microscopic trajectory

In most cases, this is a much stronger requirement than for the macroscopic model. This leads to a low CFL number for the macroscopic part of the simulation, which leads to added numerical diffusion and smaller times steps (and thus longer computations) than strictly necessary. Therefore, it is possible to take a larger time step only in the macroscopic region. For more details, we refer the interested reader to Moutari and Rascle (2007).

6.3.3 Moving Interfaces

In the examples, we have only shown interfaces fixed in space. However, the interface may also move, or one may be interested in more (or less) detail during a specific time interval. For example, it could be useful to apply a macroscopic model nighttime traffic, while moving to microscopic modelling in the urban areas of a network during peak hour. For more details about how to apply hybrid models in such cases, we refer to Joueiai et al. (2015).

Problem Set

Gas Kinetic Models

Consider the continuum gas-kinetic model as proposed by Treiber et al. (1999). (Refer to the original article for a detailed description.)

6.1 (Advanced) Reformulate the model in the Lagrangian coordinate system: i.e. reformulate the model such that it fits into the framework in Sect. 4.4.3 and define invariant I and source function g.

6.2 (Advanced) Adapt the code for a higher order model to simulate this model. Reflect on the results and compare them with previous simulations.[1]

Hybrid Models

6.3 (Advanced) Combine the code for microscopic and macroscopic modelling to build a hybrid simulation. Reflect on the results and compare them with previous simulations.[1]

Further Reading

Hoogendoorn SP, Bovy PHL (2001) Generic gas-kinetic traffic systems modeling with applications to vehicular traffic flow. Transp Res B Methodol 35(4):317–336

Joueiai M, Leclercq L, van Lint JWC, Hoogendoorn SP (2015) A multi-scale traffic flow model based on the mesoscopic LWR model. Transp Res Rec J Transp Res Board 2491:98–106

[1]Gas-kinetic and hybrid modelling are advanced topics. Numerical methods are not yet well-developed. The interested reader is encouraged to try to do some simulations, but it is not expected that this can be done easily.

Li L, Chen X (2017) Vehicle headway modeling and its inferences in macroscopic/microscopic traffic flow theory: a survey. Transp Res C Emerg Technol 76:170–188
Moutari S, Rascle M (2007) A hybrid Lagrangian model based on the Aw-Rascle traffic flow model. SIAM J Appl Math 68:413–436

Chapter 7
Conclusion: Convergence Versus Branching Out

In the previous chapters, four different families of traffic flow models were discussed. In this chapter we compare them, highlight their differences and discuss their applications.

After reading this chapter, the reader will be able to compare the models introduced in previous chapters with respect to important properties related to parameters, modelling scale, reproduction of phenomena and simulation speed and accuracy. They will also be able to argue about the (dis)advantages of modelling and simulation choices and they are able to make an appropriate choice for a given application. Furthermore, they are able to identify current trends in traffic flow modelling. Finally, after finishing this book, readers are able to reflect on new developments in traffic flow modelling, they are equipped with tools to grow and fill gaps in the modelling tree and contribute to future trends themselves.

7.1 Modelling Scale: Microscopic vs. Macroscopic

One of the first things to notice in the tree is the tension between, on the one hand, highly detailed models which are complex and (supposedly) describe reality very accurately and, on the other hand, simple and traceable models that are applicable in real time in applications such as traffic management. Comparisons between the modeling families are often related to the appropriate modelling scale. In the rest of this section we discuss some of the issues with microscopic and macroscopic modelling.

F. Kessels, *Traffic Flow Modelling*, EURO Advanced Tutorials
on Operational Research, https://doi.org/10.1007/978-3-319-78695-7_7

7.1.1 Macroscopic Modeling and the Continuum Assumption

It has been argued that the differences between fluid flow (including that of gasses) and traffic flow are too large to justify a continuum approach. Papageorgiou (1998) even argues that there is hardly any hope that traffic flow models will ever have the same descriptive accuracy as models in other domains such as Newtonian physics or thermodynamics. This is because:

1. vehicles and humans (drivers) all behave differently, and change there behaviour over time, unlike molecules of which the behaviour follows (usually simple and constant) physical laws, and
2. there are relatively few vehicles in the area of interest (at most a few hundred per kilometer), unlike in for example thermodynamics with around 10^{23} particles per cm^3.

The second reason is also used to argue that aggregating vehicles to develop a continuum traffic flow model is not justified (Darbha et al. 2008; Tyagi et al. 2008; Bellomo and Dogbe 2011). Furthermore, in fluid mechanics the Knudsen number is often used to choose between a continuum (macroscopic) or a particle (microscopic) approach. The Knudsen number is the ratio of the mean free path over a representative physical length scale. Only if it is much smaller than 1, can the fluid be approximated as a continuum. In vehicle flow the Knudsen number would be the following distance over a section length. Tyagi et al. (2008) argue that the Knudsen number is small enough (10^{-3}). However, in free flow (e.g., 100 m following distance) on short sections (e.g., of 100 m) the Knudsen number is much larger than 10^{-3} and the continuum approach is not justified. Still, the first observation (drivers do not behave like molecules) shows that fluid flow and traffic flow are dissimilar in other aspects. Therefore, comparison of ratios such as the Knudsen number or the number of particles per region of interest can not be the only reason to justify (or falsify) a model approach. The authors approach to this question is that the continuum assumption is reasonable for traffic flow, if one does not seek too much descriptive detail.

7.1.2 Microscopic Models and Parameters

Traffic flow models are often criticized for their parameters (Brackstone and McDonald 1999; Bellomo and Dogbe 2011):

Too many Traffic flow models have many parameters. This holds true especially for microscopic models and in particular those which include heterogeneity or stochasticity. An extreme example is the Deterministic Acceleration Time Delay Three-Phase Traffic Flow Model based on three phase theory with 19 parameters (Kerner 2009), which does not even include heterogeneity or stochasticity. Furthermore, some parameters can be different for each link of the network, for

example those related to the maximum speed/speed limit and those related to number of lanes/jam density.

Not observable Parameter values are difficult to estimate because of the dynamics of the system (Brackstone and McDonald 1999; Orosz et al. 2010; Bellomo and Dogbe 2011). Parameters are often not easily observable or even have no physical interpretation at all. For example, the constants c_1 and c_2 in the GHR model (Sect. 3.2) and the acceleration exponent δ in the IDM (Sect. 3.2.1) have no physical interpretation and are only used to fit the simulation results to data. Other parameters such as maximum and minimum acceleration $a_{\max}$ and $a_{\min}$ do have a physical interpretation but are almost impossible to observe. To observe those parameters one would need detailed trajectory data including observations where this maximum (or minimum) acceleration is realized. Similar arguments hold for models including a fundamental diagram. The critical and jam density can only be observed if the data includes situations where traffic is in such as state.

Unrealistic values Traffic flow models sometimes have unrealistic parameter values. For example, Brackstone and McDonald (1999) concluded that contradictory findings on parameter values c_1 and c_2 in the GHR model are the main reason why they were being used less frequently.

In general macroscopic models have less parameters which are more easily observable than microscopic models.

7.2 Model Choice Considerations

When one is choosing a traffic flow model, it is important to consider its application. For example, descriptive and predictive accuracy have to be weighted against the need for fast simulations.

7.2.1 Predictive Accuracy

Some authors argue that all experimentally observed features, including stop-and-go waves should be reproduced by a traffic flow model (Helbing 2001; Kerner 2009; Bellomo and Dogbe 2011). However, we believe that it largely depends on the model application whether such more complex phenomena need to be reproduced (Papageorgiou 1998; van Wageningen-Kessels et al. 2011).

Let us make a comparison with fluid models. In some applications, such as the design of the propeller of a ship, it is very useful to know the details about turbulence and a fluid flow model should include turbulence. In other applications, such as weather predictions only large scale effects of turbulence need to be taken into account. Similarly, predicting the emergence and propagation of stop-and-go

waves can be useful in some situations, for example, if one wants to warn drivers of approaching a stop-and-go wave. However, for relatively coarse predictions on large networks to estimate the level of congestion during a given peak hour, it is probably not useful to predict individual stop-and-go waves.

A macroscopic model is often a good choice for application when the model needs to allow for fast simulations. If optimal control is applied, it is furthermore desirable that the model has a simple mathematical formulation, for example allowing linearisation. Moreover, though new computers will be faster than current ones, the need for fast simulations will remain, e.g. for the comparison of many scenarios on ever larger networks.

Microscopic models are often the more obvious choice for smaller networks and when there is not such a strict limit on computation time. They also allow for the predictive accuracy that can be useful for in-car information such as warnings for stop-and-go waves ahead and for applications in (semi-)automated vehicles or driver simulators.

7.2.2 Numerical Methods

There are many considerations for choosing an appropriate numerical method and its settings (e.g. time step size) for a given application. Some of the main considerations are:

Computational speed How fast will the simulation run? And which speed is required by the application?

Memory usage How much computer memory is used? And how much memory is available?

Accuracy How accurately do the simulation results reflect the analytical solution to the problem? And what accuracy level is required?

Ease of implementation Can the method be implemented easily and quickly, possibly building on previously developed simulation tools?

Availability of data Is there enough data available to build the simulation, including calibration and validation of model parameters? And if not, can this data be obtained?

Microscopic models are in general computationally more demanding than macroscopic models, for two main reasons. First, the traffic state is calculated more often because of smaller time steps and within each time step there are more calculations—namely for every vehicle instead of for every group of vehicles or in every cell. Table 7.1 shows that in a microscopic model the state is computed up to several thousands times as often as in a macroscopic model. Note that this does not necessarily mean that it is also thousands times as slow: the time it takes to do one time step is not equal for all methods. Second, microscopic (and mesoscopic) models are often stochastic and simulation results vary each run. This is at least partly due to stochastic inflow at the inflow boundary. Therefore, many

Table 7.1 Comparison of typical number of calculations needed for an example simulation of 30 min of 10 km of road with 200 vehicles

	Micro	Macro			
		Fixed coordinates		Moving coordinates	
Grid cell size (Δx) in meters		50	250		
Number of cells		100	20		
Vehicle group size (Δn)				2	10
Number of vehicle groups				100	20
Time step size (Δt) in seconds	0.5	1.5	7.5	1.5	7.5
Number of time steps	3600	1200	240	1200	240
Number of state calculations	720,000	12,000	480	12,000	480

Furthermore, CFL numbers are set to 1, maximum speed is 120 km/hr and maximum characteristic speed in Lagrangian coordinates max $|\frac{\mathrm{d}V}{\mathrm{d}s}| = 1.33$ per second

simulations are needed before conclusions can be drawn on the results. Furthermore, stochastic models are not tractable and therefore filtering and optimal control is much more difficult, if at all possible. Microscopic models do remain important because it depends largely on the application whether fast numerical simulation is necessary. Macroscopic models will remain the first choice when computational speed is important, especially in combination with efficient numerical methods such as those based on the moving coordinate system. Table 7.1 does not show any difference between fixed and moving coordinates in number of state calculations. However, with moving coordinates, the calculations are often simpler, resulting in faster computations per time step.

Very little research has been done comparing the accuracy of numerical methods for traffic flow models as such. Most studies compare simulation results varying both the model and the numerical method. Some exceptions include Delis et al. (2014), van Wageningen-Kessels (2013) and Treiber and Kanagaraj (2015). Furthermore, it deserves to be noted that even though the Lagrangian (moving) coordinate system is very beneficial for macroscopic simulation of homogeneous road stretches, the numerical methods still needs further development to deal with inhomogeneities such as changes ramps and intersections (van Wageningen-Kessels et al. 2013). Finally, as has been discussed in Sect. 6.3, hybrid modelling combines the advantages of microscopic and macroscopic traffic flow modelling and can improve the computational efficiency by combining a car-following model with a macroscopic model in Lagrangian formulation.

7.3 Current Trends and Outlook

In the model tree several trends can be identified: (1) Certain branches converge towards a generalized model, (2) Existing models are extended and adapted to better reproduce key phenomena such as capacity drop, hysteresis, (3) Hybrid models combine microscopic and macroscopic models. (See Sect. 6.3)

7.3.1 Generalized Models

Generic formulations of certain types of models allow for an easier comparison, especially of qualitative properties. They can also be used to build efficient numerical methods for simulations:

The generic fundamental relation (Sect. 2.2.1) generalises all fundamental relations with certain desirable properties. The generic model includes a function ϕ and if that function satisfies certain criteria that can be checked relatively easily, then the fundamental diagram has the desirable properties.

The generic car-following model (Sect. 3.2.3) takes a similar approach. If a car following model fits into the generic model and if its acceleration function f satisfies certain criteria, then the model has certain desirable properties.

The generic multi-class kinematic wave model (Sect. 4.2) is used to compare this type of models for qualitative properties and to find the ranges of parameter settings under which the models behave as desired.

The generic second-order traffic flow model (Sect. 4.3.3) combines several higher order continuum models and the formulation is used to build an efficient numerical method for simulation purposes.

The generic gas-kinetic model (Sect. 6.2.1) is used to build a macroscopic gas-kinetic model that can then be applied for efficient numerical simulations.

The generic hybrid model (Sect. 6.3) provides a framework for hybrid models combining car-following and macroscopic models, again for efficient simulations.

7.3.2 Extensions and Adaptations of Existing Models

The earliest traffic flow models were simple and able to capture only few realistic phenomena. Recent models, can capture many complex, non-linear and dynamic phenomena. This is partly because the models have been extended to include, among others, more realistic vehicle and driver behaviour. Many extensions are inspired by a drive to better reproduce observed fundamental diagrams. Some of the most fruitful approaches are:

- Applying a fundamental relation with a specific shape, such as one which includes a capacity drop or multi-dimensional fundamental diagrams.
- Bounding acceleration (and possibly also deceleration) in microscopic models and in macroscopic models.
- Assigning a different type of behaviour to different vehicles (e.g. cars vs. trucks) and to drivers (e.g. timid vs. aggressive). This is a natural and relatively simple adaptation in microscopic models, but has also been applied to macro- and mesoscopic models.

- Including lane choice, lane changes and different behavior on each lane. This is commonly done in microscopic models, which often include advanced models for lane choice and lane change. (This has not been discussed in detail in this book.)
- Finally, stochasticity has been included to model variations in vehicle and driver behavior, including intra-vehicle/driver variations over time and space. This includes microscopic models and macroscopic models. (This has not been discussed in detail in this book.)

All these extensions and adaptations have also received critique, mostly because the resulting models lack parsimony: they may be more complex than necessary to explain the observed phenomena. A good example of this is given by Treiber et al. (2010). The authors show that the seemingly more advanced three phase model is not any better at reproducing certain phenomena than a simpler higher order model.

7.3.3 Outlook

Almost a decade ago, Wilson (2008) wrote 'we can expect over the next few years to definitely resolve the conflict between the various traffic modelling schools', continuing to argue that this could be done using novel, more detailed data. We have not reached this point yet, but the model tree can help in identifying future research and model development directions. We identify the following main directions:

Multi-class modelling Most branches include multi-class models. However, the development of multi-class models seems to lag behind for the branch of cellular automata models and for hybrid models.

Hybrid and multi-scale models Future research is not limited to extending each of the families and their branches further. More valuable results may be obtained by combining ideas from different branches. For example, hybrid models have been proposed but can be developed much further. They are able to combine the advantages of different types of models. It would be interesting to combine, for example, mesoscopic models with microscopic or macroscopic models. Furthermore, a new branch of hybrid models can combine mixed-class and multi-class models.

Generalized models Current generalized models include many models, but not all. Further generalizations can be developed and used to efficiently compare existing and new models.

Finally, computational methods can be improved further for faster and more accurate simulations. The Lagrangian formulation of macroscopic traffic flow models seems to be a good path to explore further. Moreover, comparison of existing and new numerical methods can give new insights and directions for further developments.

Problem Set

Some parts of the genealogical model tree seem to develop in less fruitful ways and may need 'pruning', other parts are expanding quickly.

7.1 Reflect on which parts of the tree you think can be pruned, and which parts can be 'fed' to encourage them to branch out further. Where are the gaps that can be filled and what would be the advantages of a model that fills such a gap.

7.2 Compare the simulations that you have done and reflect on the similarities and differences: which models and methods were easy or difficult to implement, which gave the best results. Which type of model and numerical method can be useful in applications that you are currently working with. How should they be adapted to become even more useful?

Further Reading

Aghabayk K, Sarvi M, Young W (2015) A state-of-the-art review of car-following models with particular considerations of heavy vehicles. Transp Rev 35(1):82–105

Barceló J (ed) (2010) Fundamentals of traffic simulation, international series in operations research & management science, vol 145. Springer, New York

Bellomo N, Dogbe C (2011) On the modeling of traffic and crowds: a survey of models, speculations, and perspectives. SIAM Rev 53:409–463

Brackstone M, McDonald M (1999) Car-following: a historical review. Transp Res F Traffic Psychol Behav 2(4):181–196

Darbha S, Rajagopal KR, Tyagi V (2008) A review of mathematical models for the flow of traffic and some recent results. Nonlinear Anal Theory Methods Appl 69(3):950–970

Papageorgiou M (1998) Some remarks on macroscopic traffic flow modelling. Transp Res A Policy Pract 32(5):323–329

van Wageningen-Kessels FLM, van Lint JWC, Vuik C, Hoogendoorn SP (2015) Genealogy of traffic flow models. EURO J Transp Logist 4:445–473

Chapter 8
Answers to Selected Problems

Answers to Selected Problems in Chap. 1

1.1 Apply (1.1), (1.2) and (1.3).

1.2 Apply the definition of instantaneous density (Definition 1.2), without letting $\Delta x \to 0$.

1.3 Apply the definition of local flow (Definition 1.1), without letting $\Delta t \to 0$.

1.4 The vehicles will distribute over both routes evenly (i.e. 50 on each route) and their travel time will be 20 min.

1.5 All vehicles will travel over the new route $A \to B \to C \to D$, which takes them 21 min. Note that if an individual traveller would decide to take the original route via B (i.e. $A \to B \to D$) or via C (i.e. $A \to C \to D$), that route would now take 25 min and has become unattractive.

Answers to Selected Problems in Chap. 2

2.1 The requirements are satisfied when parameters are positive. The third requirement can be checked by reformulating the fundamental relation in $v(\rho)$ form and then taking its derivative. The derivative should be nonpositive for almost all densities $\rho \in [0, \rho]$. For densities ρ^* at which the derivative does not exist (such as at critical density in the Daganzo and Smulders fundamental diagrams), the change should be nonpositive: $\lim \rho \uparrow \rho^* \geq \lim \rho \downarrow \rho^*$.

2.2 In the Daganzo fundamental diagram, the critical speed equals the maximum speed. The Smulders diagram has the critical density and critical speed as parameters of the model. For the other models, they can be computed by determining the

F. Kessels, *Traffic Flow Modelling*, EURO Advanced Tutorials
on Operational Research, https://doi.org/10.1007/978-3-319-78695-7_8

density $\rho \in (0, \rho_{\text{jam}})$ at which $Q'(\rho) = 0$. From this, the critical speed and capacity can be found.

2.3 The first 2 additional requirements are satisfied when parameters are positive. The concavity of the fundamental relations can be checked by determining the second derivative $Q''(\rho)$. Since the fundamental relations are all continuous, they are strictly concave if and only if for all densities $\rho \in [0, \rho_{\text{jam}}]$ for which the second derivative exists, it is negative: $Q''(\rho) < 0$. The fundamental relation is concave if and only if for all densities $\rho \in [0, \rho_{\text{jam}}]$ for which the second derivative exists, it is nonpositive: $Q''(\rho) \leq 0$. Note that the concavity may depend on the parameter values.

2.4 We refer the reader to the original paper (del Castillo 2012) for some plots of fundamental diagrams and a reflection on how they change with parameter settings. The bilinear fundamental diagram is recovered by the power function fundamental relation when $\theta \to \infty$ and by the exponential fundamental relation when $\omega \to \infty$.

2.5 Substitute $\hat{q} = q/q_0$, $\hat{\rho} = \rho/\rho_{\text{jam}}$ and define new parameters $a^* = \frac{a}{\rho_{\text{jam}}}$ and $b^* = \frac{b}{\rho_{\text{jam}}}$ to find:

$$Q(\rho) = q_0 \left[\frac{b^*}{\rho_{\text{jam}}} + (a^* - b^*)\rho - \phi^{-1} \left(\phi(a^*\rho) + \phi(b^*(\rho_{\text{jam}} - \rho)) - \phi(0) \right) \right] \tag{8.1}$$

2.6 The proof consists of proving that the function ϕ satisfies the conditions presented in the introduction of the problem.

2.7 Use (2.9) to calculate the parameters. Note that the parameter values only depend on the fraction of cars and trucks, and not on their actual densities.

2.8 See Fig. 8.1.

2.9 Speeds are equal for densities above critical density, i.e. in congestion. This is plausible when there are limited possibilities for overtaking in congestion. However, in light congestion (densities close to critical density), this might not be so realistic because then there are still opportunities for (faster) cars to overtake (slower) trucks.

2.10 The fundamental relations all have non-increasing speeds. Fundamental relations with capacity drop or hysteresis imply a non-unique fundamental relation: at a certain density (usually just above (outflow) capacity) the flow is not uniquely determined by the density but also depends on previous traffic states. None of the fundamental diagrams satisfies the strict concavity requirement. However, the three-dimensional fundamental relation by Chanut and Buisson (2003) is weakly concave in both ρ_{car} and ρ_{truck}.

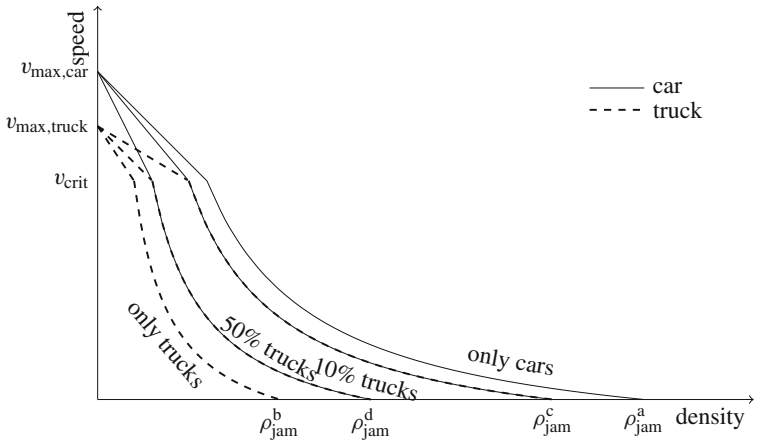

Fig. 8.1 Example heterogeneous fundamental diagram

Answers to Selected Problems in Chap. 3

3.1 For the speed to be in equilibrium we consider $v := v_n(t+\tau) = v_n(t) = v_{n-1}(t)$. Furthermore, to simplify notation we do not use n-indices and time indices and write:

$$v = a_{\min}\tau + \sqrt{a_{\min}^2\tau^2 - a_{\min}\left(2\big(s - s_{\text{jam}}\big) - v\tau - \frac{v^2}{a_{\min}}\right)} \tag{8.2}$$

The first part of the right-hand side is brought to the left, and both sides are squared:

$$(v - a_{\min}\tau)^2 = a_{\min}^2\tau^2 - a_{\min}\left(2\big(s - s_{\text{jam}}\big) - v\tau - \frac{v^2}{a_{\min}}\right) \tag{8.3}$$

Again reordering and noting that many terms drop out gives:

$$v = 2\frac{s - s_{\text{jam}}}{\tau} \tag{8.4}$$

The fundamental diagram is drawn in Fig. 8.2.

3.2 At high spacings, the free branch limits the speed to $V_{\max}$.

3.3 The fundamental diagram is drawn in Fig. 8.2.

3.4 Instructions on how to run this simulation are provided in the code.

3.6 The model is platoon stable for the default parameter values. This is proven by showing that the derivatives of the acceleration function (3.8) have the appropriate signs, as discussed in Sect. 3.2.3.

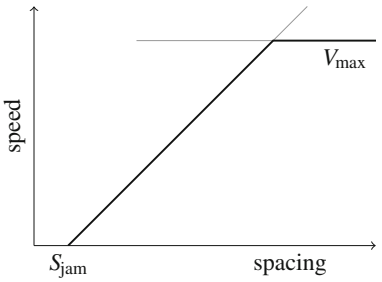

Fig. 8.2 Fundamental diagram of adapted Gipps' model

3.7 The sample code lets the user set the initial speed and corresponding equilibrium spacing on a ring road. After 30 s of simulation, there is a perturbation in the shape of a sudden maximum deceleration of vehicle number 1. As the resulting trajectories and speed plots in Fig. 8.3 show, with an initial equilibrium speed of 2 m/s, the flow shows string instability, while it is stable with and initial equilibrium speed of 26 m/s. In the first case, the instability moves both upstream and downstream.

Answers to Selected Problems in Chap. 4

4.1 See Fig. 8.4.

1. The maximum speed $v_{\max} = 30$ m/s.
2. Minus the congestion wave speed $-w = -\frac{\rho_{\text{crit}} v_{\max}}{\rho_{\text{jam}} - \rho_{\text{crit}}} = -7.5$ m/s
3. 0 (because there is no inflow)
4. The time it takes for the downstream front of the queue to spill back to the upstream front (which does not move), i.e. $\frac{200}{w} = 26.67$ s.

4.2 The method of characteristics is applied in the same way as in Problem 4.1: characteristics are drawn from the initial values and boundary values, their intersections lead to shocks, of which the velocities can be determined using the slope of the line between the corresponding points on the fundamental diagram. This leads to the solution as in Fig. 8.5.

4.4 See Fig. 8.6 for the simulation results.

4.6

$$y = v, \qquad \mathrm{J}(\mathbf{u}) = \begin{pmatrix} v & \rho \\ \frac{c^2}{\rho} & v \end{pmatrix}, \qquad \mathrm{f}(\mathbf{u}) = \begin{pmatrix} 0 \\ \frac{V-v}{t_r} \end{pmatrix} \tag{8.5}$$

The eigenvalues of the Jacobian are: $\lambda_1 = v - c$ and $\lambda_2 = v + c$.

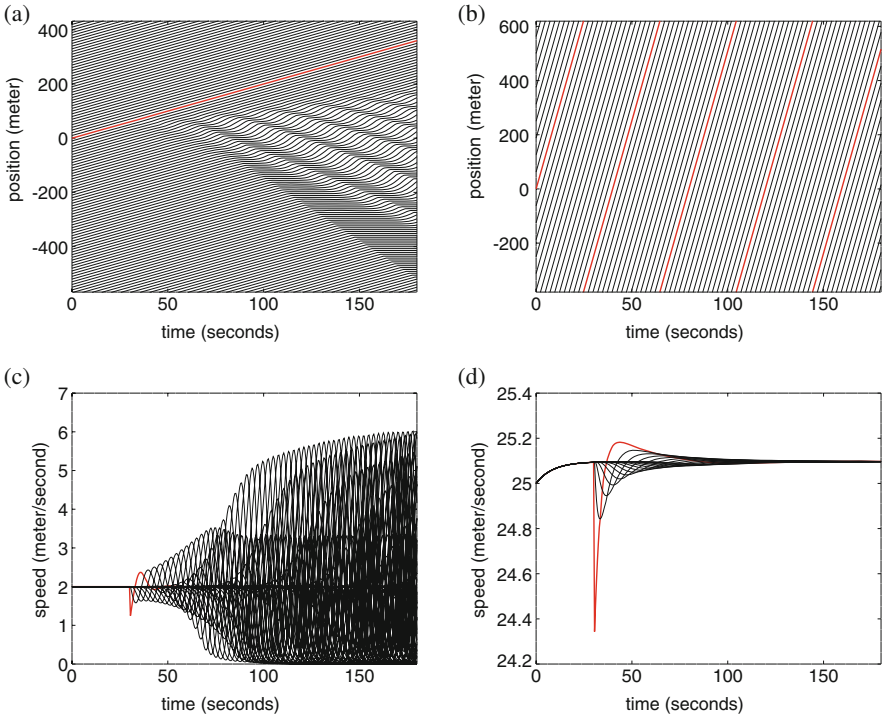

Fig. 8.3 Simulation results with IDM, testing for stability. The red line indicates the trajectory (top) or speed (bottom) of vehicle number 1. With a low initial equilibrium speed (left), the results show instabilities. In the trajectory plot, stop-and-go-waves seem to be created. After the perturbation at $t = 30$ s, the speeds start to oscillate. With a high initial equilibrium speed (right), the result shows stability. In the trajectory plot (top), the perturbation and its effect on the following vehicles is almost invisible. The speeds (bottom) show the perturbation and how it effects some of the leading vehicles, but also a quick recovery to equilibrium speed. (**a**) Trajectories, string unstable (initial equilibrium speed 2 m/s). (**b**) Trajectories, string stable (initial equilibrium speed 26 m/s). (**c**) Speeds, string unstable (initial equilibrium speed 2 m/s). (**d**) Speeds, string stable (initial equilibrium speed 26 m/s)

4.7

$$y = v, \qquad \mathrm{J}(\mathbf{u}) = \begin{pmatrix} v & \rho \\ 0 & v + \rho V'(\rho) \end{pmatrix}, \qquad \mathrm{f}(\mathbf{u}) = \begin{pmatrix} 0 \\ \mathbf{0} \end{pmatrix} \tag{8.6}$$

The eigenvalues of the Jacobian are: $\lambda_1 = v + \rho V'(\rho)$ and $\lambda_2 = v$.

4.8 In the Payne model, one of the eigenvalues is larger than the vehicle speed v for any nonzero value of c, and thus the corresponding characteristic is faster than the vehicles, i.e. the model is not anisotropic. (And if $c = 0$, then the Payne model reduces to the LWR model.)

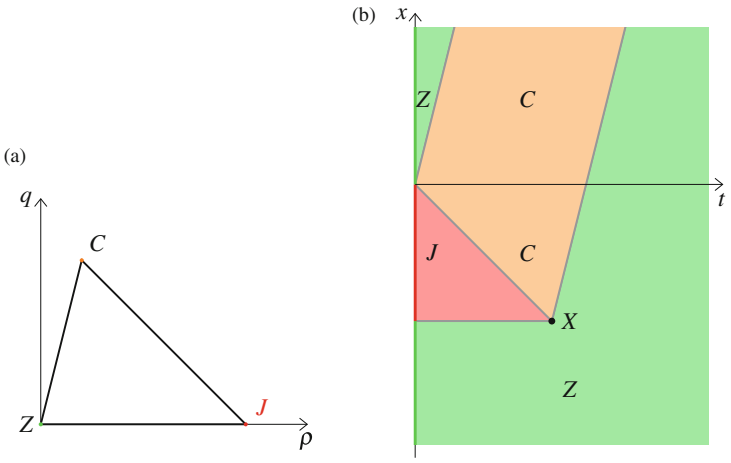

Fig. 8.4 Solving the initial value problem in Problem 4.1. (**a**) Fundamental diagram with traffic states. (**b**) Solution to initial value problem

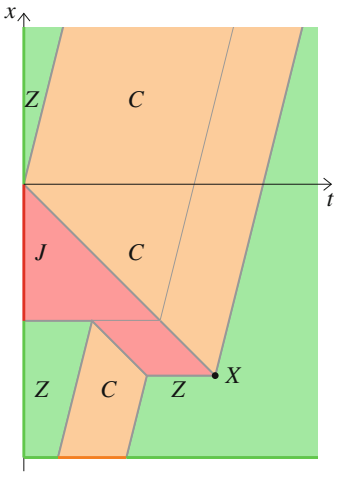

Fig. 8.5 Solution to the combined initial and boundary value problem in Problem 4.2

In the ARZ model, the second eigenvalue equals vehicles speed. Whether the first eigenvalue is not larger than the vehicle speed depends on the shape of the fundamental diagram. If it is nonincreasing (which is realistic, see also the discussion in Sect. 2.3), then $V'(\rho) < 0$ and thus the first eigenvalue λ_1 is not larger than the vehicle speed v. This implies that the characteristic is not faster than the vehicles and thus the model is anisotropic.

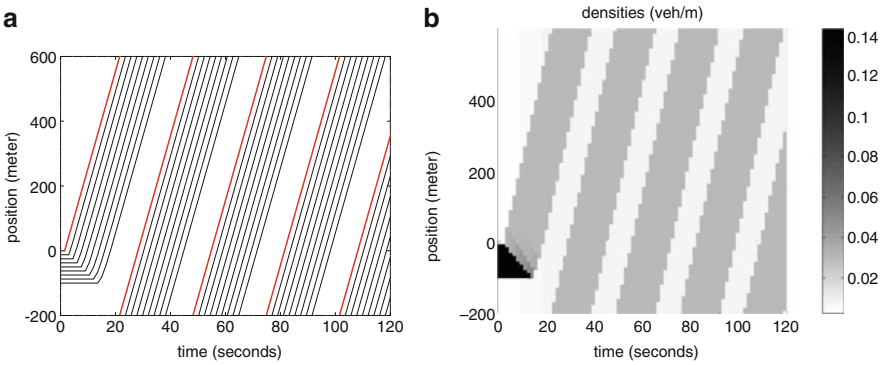

Fig. 8.6 Simulation results for the Problem 4.4. (**a**) Trajectories. (**b**) Densities

4.9

$$y = v + p(\rho), \qquad \mathbf{J}(\mathbf{u}) = \begin{pmatrix} v & \rho \\ 0 & v - \rho p'(\rho) \end{pmatrix}, \qquad \mathbf{f}(\mathbf{u}) = \mathbf{0} \tag{8.7}$$

The eigenvalues of the Jacobian are: $\lambda_1 = v - \rho p'(\rho)$ and $\lambda_2 = v$. With $p(\rho) = \rho^c$ as in the prototype model $\lambda_1 = v - c\rho^c$

4.14 The conservation equation in the Lagrangian coordinates is derived by substituting the definition of spacing (4.44) into the Eulerian conservation equation (4.1), applying the quotient rule and rewriting the result:

$$\frac{\partial}{\partial t}(1/s) + \frac{\partial}{\partial x}(v/s) = 0 \quad \Rightarrow \quad \frac{\partial s}{\partial t} - s\frac{\partial v}{\partial x} + v\frac{\partial s}{\partial x} = 0 \tag{8.8}$$

Subsequently substituting the Lagrangian time derivative (4.45) yields:

$$\frac{\mathrm{D}s}{\mathrm{D}t} - s\frac{\partial v}{\partial x} = 0 \tag{8.9}$$

Finally, the definition of spacing (4.44) is substituted to find the Lagrangian conservation equation:

$$\frac{\mathrm{D}s}{\mathrm{D}t} + \frac{\partial v}{\partial n} = 0 \tag{8.10}$$

4.15 For the derivation of a multi-class model in Lagrangian coordinates, we refer to van Wageningen-Kessels et al. (2010). To derive the GSOM in Lagrangian

formulation, rewrite Eq. (4.26b) as follows:

$$\frac{\partial}{\partial t}(\rho I) + \frac{\partial}{\partial x}(qI) = \rho\frac{\partial I}{\partial t} + I\frac{\partial \rho}{\partial t} + q\frac{\partial I}{\partial x} + I\frac{\partial q}{\partial x} = -\rho g(I) \tag{8.11}$$

Apply the conservation equation (4.26a) and $q = \rho v$ to find:

$$\rho\frac{\partial I}{\partial t} + q\frac{\partial I}{\partial x} = \rho\left(\frac{\partial I}{\partial t} + v\frac{\partial I}{\partial x}\right) = -\rho g(I) \tag{8.12}$$

Divide both sides by ρ and note that the term between brackets is the Lagrangian time derivative of the invariant:

$$\left(\frac{\partial I}{\partial t} + v\frac{\partial I}{\partial x}\right) = \frac{\mathrm{D}I}{\mathrm{D}t} = -g(I) \tag{8.13}$$

Answers to Selected Problems in Chap. 5

5.2 We first note that with a change in time step size, the code automatically adapts the grid cell size accordingly to keep the CFL number constant. With a larger time step size, the results are more 'block-like' (the grid becomes better visible). With a smaller time step size, the solution converges to the analytical solution. When the CFL number is reduced, the results may show more diffusion. However, when the CFL number increases to larger than one, the results may show numerical instabilities.

5.3 Adapting time step size and CFL number has the same effect as with the Godunov method (see solution to Problem 5.2).

5.7 The number of vehicles that we are trying to calculate equals the number of vehicles between (x_{j+1}, t^*) and (x_j, t^*) plus those between (x_j, t^*) and $(x_j, t+\Delta t)$. Noting that the density is constant gives the number of vehicles between (x_{j+1}, t^*) and (x_j, t^*) as:

$$N(x_j, t^*) - N(x_{j+1}, t^*) = \rho(x_j, t^*)L_{j+1/2} \tag{8.14}$$

Furthermore, the flow is also constant and thus the number of vehicles (x_j, t^*) and $(x_j, t+\Delta t)$ can be expressed as: $N(x_j, t+\Delta t) - N(x_j, t^*) = q(x_j, t^*)(t+\Delta t - t^*)$. We note that $t+\Delta t - t^* = L_{j+1/2}/w$ and applying the bilinear fundamental diagram gives:

$$N(x_j, t+\Delta t) - N(x_j, t^*) = w(\rho_{\text{jam}} - \rho(x_j, t^*))(t+\Delta t - t^*) = (\rho_{\text{jam}} - \rho(x_j, t^*))L_{j+1/2} \tag{8.15}$$

Taking the sum of the number of vehicles (i.e. (8.14) plus (8.15)) yields:

$$\begin{aligned} N(x_j, t + \Delta t) - N\left(x_{j+1}, t^*\right) &= N(x_j, t^*) - N(x_{j+1}, t^*) + N(x_j, t + \Delta t) - N(x_j, t^*) \\ &= \rho(x_j, t^*) L_{j+1/2} + (\rho_{\text{jam}} - \rho(x_j, t^*)) L_{j+1/2} \\ &= \rho_{\text{jam}} L_{j+1/2} \end{aligned} \tag{8.16}$$

Answers to Selected Problems in Chap. 6

6.1 Refer to equation (27) and (28) in Treiber et al. (1999). (27) can be reformulated as the Lagrangian conservation equation (4.38a). With $I = v$, the left-hand side of (28) equals the left-hand side of (4.38b), and thus $-g$ equals the right-hand side of (28).

Bibliography

Aghabayk K, Sarvi M, Young W (2015) A state-of-the-art review of car-following models with particular considerations of heavy vehicles. Transp Rev 35(1):82–105

Ansorge R (1990) What does the entropy condition mean in traffic flow theory? Transp Res B Methodol 24(2):133–143

Auberlet JM, Bhaskar A, Ciuffo B, Farah H, Hoogendoorn R, Leonhardt A (2014) Data collection techniques. In: Traffic simulation and data: validation methods and applications. CRC Press, Boca Raton

Aw A, Rascle M (2000) Resurrection of "second order models" of traffic flow? SIAM J Appl Math 60(3):916–938

Aw A, Klar A, Rascle M, Materne T (2002) Derivation of continuum traffic flow models from microscopic follow-the-leader models. SIAM J Appl Math 63(1):259–278

Bando M, Hasebe K, Nakayama A, Shibata A, Sugiyama Y (1995) Dynamical model of traffic congestion and numerical simulation. Phys Rev E Stat Nonlinear Soft Matter Phys 51:1035–1042

Bando M, Hasebe K, Nakanishi K, Nakayama A (1998) Analysis of optimal velocity model with explicit delay. Phys Rev E Stat Nonlinear Soft Matter Phys 58(5):5429–5435

Bellomo N, Brezzi F (2008) Traffic, crowds and swarms. Math Models Methods Appl Sci 18:1145–1148

Bellomo N, Dogbe C (2011) On the modeling of traffic and crowds: a survey of models, speculations, and perspectives. SIAM Rev 53:409–463

Bourrel E, Lesort JB (2003) Mixing microscopic and macroscopic representations of traffic flow hybrid model based on Lighthill-Whitham-Richards theory. Transp Res Rec J Transp Res Board 1852:193–200

Brackstone M, McDonald M (1999) Car-following: a historical review. Transp Res F Traffic Psychol Behav 2(4):181–196

Braess D (1968) Über ein paradoxon aus der verkehrsplanung. Unternehmensforschung 12:258–268, English translation available (Braess et al. 2005)

Braess D, Nagurney A, Wakolbinger T (2005) On a paradox of traffic planning. Transp Sci 39(4):446–450

Branston D (1976) Models of single lane time headway distributions. Transp Sci 10(2):125–148

Buckley DJ (1968) A semi-Poisson model of traffic flow. Transp Sci 2(2):107–133

Calvert S, Snelder M, Taale H, van Wageningen-Kessels FLM, Hoogendoorn SP (2015) Bounded acceleration capacity drop in a Lagrangian formulation of the kinematic wave model with vehicle characteristics and unconstrained overtaking. In: Proceedings of 2015 IEEE 18th international conference on intelligent transportation systems, Gran Canaria, Spain

F. Kessels, *Traffic Flow Modelling*, EURO Advanced Tutorials
on Operational Research, https://doi.org/10.1007/978-3-319-78695-7

Calvert SC, Taale H, Hoogendoorn SP (2016) Quantification of motorway capacity variation: influence of day type specific variation and capacity drop. J Adv Transp 50(4):570–588
Calvert SC, van Wageningen-Kessels FLM, Hoogendoorn SP (2018) Capacity drop through reaction times in heterogeneous traffic. J Traffic Transp Eng (English Edition) 5(2):96–104. https://doi.org/10.1016/j.jtte.2017.07.008
Casas J, Ferrer JL, Garcia D, Perarnau J, Torday A (2010) Traffic simulation with Aimsun. In: Fundamentals of traffic simulation. International series in operations research and management science, vol 145. Springer, New York, pp 173–232
Cassidy MJ, Bertini RL (1999) Some traffic features at freeway bottlenecks. Transp Res B Methodol 33(1):25–42
Chandler R, Herman R, Montroll E (1958) Traffic dynamics: studies in car following. Oper Res 6(2):165–184
Chanut S, Buisson C (2003) Macroscopic model and its numerical solution for two-flow mixed traffic with different speeds and lengths. Transp Res Rec J Transp Res Board 1852:209–219
Courant R, Friedrichs K, Lewy H (1967) On the partial difference equations of mathematical physics. IBM J Res Dev 11:215–234
Daganzo CF (1994) The cell transmission model: a dynamic representation of highway traffic consistent with the hydrodynamic theory. Transp Res B Methodol 28(4):269–287
Daganzo CF (1995) Requiem for second-order fluid approximations of traffic flow. Transp Res B Methodol 29(4):277–286
Daganzo CF (2002) A behavioral theory of multi-lane traffic flow. Part I: long homogeneous freeway sections. Transp Res. B Methodol 36(2):131–158
Daganzo CF (2006) On the variational theory of traffic flow: well-posedness, duality and applications. Netw Heterogen Media 1:601–619
Daganzo CF, Lin WH, del Castillo J (1997) A simple physical principle for the simulation of freeways with special lanes and priority vehicles. Transp Res B Methodol 31(2):103–125
Darbha S, Rajagopal KR, Tyagi V (2008) A review of mathematical models for the flow of traffic and some recent results. Nonlinear Anal Theory Methods Appl 69(3):950–970
del Castillo J (2012) Three new models for the flow-density relationship: derivation and testing for freeway and urban data. Transportmetrica 8(6):443–465
Delis A, Nikolos I, Papageorgiou M (2014) High-resolution numerical relaxation approximations to second-order macroscopic traffic flow models. Transp Res C Emerg Technol 44:318–349
Edie L (1961) Car-following and steady-state theory for noncongested traffic. Oper Res 9(1):66–76
Edie L (1965) Discussion on traffic stream measurements and definitions. In: The 2nd international symposium on the theory of traffic flow, 1963, pp 139–154
Elefteriadou L (2013) An introduction to traffic flow theory. Springer, New York
Fan S, Work DB (2015) A heterogeneous multiclass traffic flow model with creeping. SIAM J Appl Math 75(2):813–835
Gashaw SM, Goatin P, Harri J (2017) Modeling and analysis of mixed flow of cars and powered two wheelers. In: TRB 96th annual meeting compendium of papers, 17-05308
Gazis DC, Herman R, Rothery RW (1961) Nonlinear follow-the-leader models of traffic flow. Oper Res 9(4):545–567
Gentile G (2010) The general link transmission model for dynamic network loading and a comparison with the due algorithm. In: Immers LGH, Tampere CMJ, Viti F (eds) New developments in transport planning: advances in dynamic traffic assignment. Transport economics, management and policy series. Edward Elgar Publishing, Cheltenham
Gipps PG (1981) A behavioural car-following model for computer simulation. Transp Res B Methodol 15(2):105–111
Greenshields BD (1934) The photographic method of studying traffic behavior. In: Proceedings of the 13th annual meeting of the highway research board, pp 382–399
Greenshields BD (1935) A study of traffic capacity. In: Proceedings of the 14th annual meeting of the highway research board, pp 448–477
Hamdar SH, Treiber M, Mahmassani HS, Kesting A (2008) Modeling driver behavior as sequential risk-taking task. Transp Res Rec J Transp Res Board 2088:208–217

Helbing D (1997) Modeling multi-lane traffic flow with queuing effects. Phys A Stat Theor Phys 242(1-2):175–194
Helbing D (2001) Traffic and related self-driven many-particle systems. Rev Mod Phys 73:1067–1141
Helbing D (ed) (2008) Managing complexity: insights, concepts, applications. In: Understanding complex systems. Springer, Berlin
Helbing D (2009) Reply to comment on "On the controversy around Daganzo's requiem for and Aw-Rascle's resurrection of second-order traffic flow models" by H.M. Zhang. Eur Phys J B Condensed Matter Complex Syst 69:569–570
Helbing D, Schreckenberg M (1999) Cellular automata simulating experimental properties of traffic flow. Phys Rev E Stat Nonlinear Soft Matter Phys 59(3):2623
Helbing D, Treiber M (1999) Numerical simulation of macroscopic traffic equations. Comput Sci Eng 1(5):89–99
Himpe W, Corthout R, Tampère MC (2016) An efficient iterative link transmission model. Transp Res B Methodol 92(Part B):170–190, within-day Dynamics in Transportation Networks
Hoogendoorn SP (1999) Multiclass continuum modelling of multilane traffic flow. Ph.D. thesis, Delft University of Technology/TRAIL Research school, Delft
Hoogendoorn SP, Bovy PHL (2001a) Generic gas-kinetic traffic systems modeling with applications to vehicular traffic flow. Transp Res B Methodol 35(4):317–336
Hoogendoorn SP, Bovy PHL (2001b) State-of-the-art of vehicular traffic flow modeling. Proc Inst Mech Eng I J Syst Control Eng 215:283–303
Hoogendoorn SP, van Lint JWC, Knoop VL (2009) Dynamic first-order modeling of phase-transition probabilities. In: Appert-Rolland C, Chevoir F, Gondret P, Lassarre S, Lebacque JP, Schreckenberg M (eds) Traffic and granular flow 07. Springer, Berlin, pp 85–92
Jabari SE, Liu HX (2012) A stochastic model of traffic flow: theoretical foundations. Transp Res B Methodol 46(1):156–174
Jabari SE, Liu HX (2013) A stochastic model of traffic flow: Gaussian approximation and estimation. Transp Res B Methodol 47(0):15–41
Jin WL (2010) A kinematic wave theory of lane-changing traffic flow. Transp Res B Methodol 44:1001–1021
Joueiai M, Leclercq L, van Lint JWC, Hoogendoorn SP (2015) A multi-scale traffic flow model based on the mesoscopic LWR model. Transp Res Rec J Transp Res Board
Kerner BS (2009) Introduction to modern traffic flow theory and control: the long road to three-phase traffic theory. Springer, Berlin
Kerner BS, Rehborn H (1996) Experimental features and characteristics of traffic jams. Phys Rev E Stat Nonlinear Soft Matt Phys 53:1297–1300
Kerner BS, Klenov SL, Wolf DE (2002) Cellular automata approach to three-phase traffic theory. J Phys A Math Gen 35(47):9971–10013
Khelifi A, Haj-Salem H, Lebacque JP, Nabli L (2016) Lagrangian discretization of generic second order models: application to traffic control. Appl Math Inf Sci Int J 10(4):1243–1254
Knoop VL, Daamen W (eds) (2016) Traffic and granular flow '15. Springer, Delft
Knospe W, Santen L, Schadschneider A, Schreckenberg M (2004) Empirical test for cellular automaton models of traffic flow. Phys Rev E Stat Nonlinear Soft Matter Phys 70(1):016115
Kometani E, Sasaki T (1961) Dynamic behaviour of traffic with a nonlinear spacing-speed relationship. In: Herman R (ed) Theory of traffic flow 1959, proceedings. Elsevier, Amsterdam, pp 105–119
Krajzewicz D, Erdmann J, Behrisch M, Bieker L (2012) Recent development and applications of SUMO – Simulation of Urban MObility. Int J Adv Syst Meas 5(3–4):128–138
Laval JA (2011) Hysteresis in traffic flow revisited: an improved measurement method. Transp Res B Methodol 45(2):385–391
Laval JA, Daganzo CF (2006) Lane-changing in traffic streams. Transp Res B Methodol 40(3):251–264

Laval JA, Leclercq L (2010) A mechanism to describe the formation and propagation of stop-and-go waves in congested freeway traffic. Philos Trans R Soc A Math Phys Eng Sci 368(1928):4519–4541

Laval JA, Leclercq L (2013) The hamilton-Jacobi partial differential equation and the three representations of traffic flow. Transp Res B Methodol 52:17–30

Lebacque JP (1996) The Godunov scheme and what it means for first order traffic flow models. In: Lesort JB (ed) Transportation and traffic theory: proceedings of the 13th international symposium on transportation and traffic theory, 1996, Pergamon, pp 647–677

Lebacque JP (2003) Two-phase bounded-acceleration traffic flow model. Analytical solutions and applications. Transp Res Rec 1852:220–230

Lebacque JP, Mammar S, Haj Salem H (2007) Generic second order traffic flow modelling. In: Allsop RE, Bell MGH, Heydecker BG (eds) Transportation and traffic theory 2007. Elsevier, Oxford, pp 755–776

Leclercq L (2007) Hybrid approaches to the solutions of the "Lighthill-Whitham-Richards" models. Transp Res B Methodol 41(7):701–709

Leclercq L (2009) Le modèle LWR : théorie, confrontation expérimentale et applications au milieu urbain. Habilitation a diriger des recherches, présentée devant l'Institut National des Sciences Appliquées de Lyon et l'Université Claude Bernard Lyon I, in French

Leclercq L, Laval J, Chevallier E (2007) The Lagrangian coordinates and what it means for first order traffic flow models. In: Allsop RE, Bell MGH, Heydecker BG (eds) Transportation and traffic theory 2007. Elsevier, Oxford, pp 735–753

Lesort JB, Bourrel E, Henn V (2003) Various scales for traffic flow representation: some reflections. In: Hoogendoorn S, Luding S, Bovy P, Schreckenberg M, Wolf D (eds) Traffic and granular flow '03, Springer, Berlin, pp 125–139

Leutzbach W (1988) An introduction to the theory of traffic flow. Springer, Berlin

Li L, Chen X (2017) Vehicle headway modeling and its inferences in macroscopic/microscopic traffic flow theory: a survey. Transp Res C Emerg Technol 76:170–188

Lighthill MJ, Whitham GB (1955a) On kinematic waves I: flood movement in long rivers. Proc R Soc Lond A Math Phys Sci 229(1178):281–316

Lighthill MJ, Whitham GB (1955b) On kinematic waves II: a theory of traffic flow on long crowded roads. Proc R Soc Lond A Math Phys Sci 229(1178):317–345

Mahnke R, Kühne R (2007) Probabilistic description of traffic breakdown. In: Schadschneider A, Pöschel T, Kühne R, Schreckenberg M, Wolf DE (eds) Traffic and granular flow '05. Springer, Berlin, pp 527–536

Michaels RM (1965) Perceptual factors in car following. In: The 2nd international symposium on the theory of traffic flow, 1963, pp 44–59

Moutari S, Rascle M (2007) A hybrid Lagrangian model based on the Aw-Rascle traffic flow model. SIAM J Appl Math 68:413–436

Nagel K, Schreckenberg M (1992) A cellular automaton model for freeway traffic. J Phys I Fr 2(12):2221–2229

Nair R, Mahmassani HS, Miller-Hooks E (2011) A porous flow approach to modeling heterogeneous traffic in disordered systems. Transp Res B Methodol 45(9):1331–1345, Selected Papers from the 19th ISTTT

Newell GF (1961) Nonlinear effects in the dynamics of car following. Oper Res 9(2):209–229

Newell GF (1965) Instability in dense highway traffic, a review. In: The 2nd international symposium on the theory of traffic flow, 1963, pp 73–83

Newell GF (1993) A simplified theory of kinematic waves in highway traffic (part I-III). Transp Res B Methodol 27(4):281–313

Newell GF (2002) A simplified car-following theory: a lower order model. Transp Res B Methodol 36(3):195–205

Orosz G, Wilson RE, Stépán G (2010) Traffic jams: dynamics and control. Philos Trans R Soc A Math Phys Eng Sci 368:4455–4479

Papageorgiou M (1998) Some remarks on macroscopic traffic flow modelling. Transp Res A Policy Prac 32(5):323–329

Paveri-Fontana SL (1975) On Boltzmann-like treatments for traffic flow: a critical review of the basic model and an alternative proposal for dilute traffic analysis. Transp Res 9(4):225–235

Payne HJ (1971) Models of freeway traffic and control. In: Simulation council proceedings, mathematical models of public systems, pp 51–61

Pipes LA (1953) An operational analysis of traffic dynamics. J Appl Phys 24(3):274–281

Prigogine I (1961) A Boltzmann-like approach to the statistical theory of traffic flow. In: Herman R (ed) Theory of traffic flow 1959, proceedings. Elsevier, Amsterdam, pp 158–164

Prigogine I, Andrews FC (1960) A Boltzmann-like approach for traffic flow. Oper Res 8(6):789–797

Rahman M, Chowdhury M, Xie Y, He Y (2013) Review of microscopic lane-changing models and future research opportunities. IEEE Trans Intell Transp Syst 14(3):1942–1956

Richards PI (1956) Shock waves on the highway. Oper Res 4(1):42–51

Saifuzzaman M, Zheng Z (2014) Incorporating human-factors in car-following models: a review of recent developments and research needs. Transp Res C Emerg Technol 48:379–403

Schnetzler B, Louis X (2013) Anisotropic second-order models and associated fundamental diagrams. Transp Res C Emerg Technol 27:131–139, selected papers from the Seventh Triennial Symposium on Transportation Analysis (TRISTAN VII)

Smulders S (1990) Control of freeway traffic flow by variable speed signs. Transp Res B Methodol 24(2):111–132

Srivastava A, Geroliminis N (2013) Empirical observations of capacity drop in freeway merges with ramp control and integration in a first-order model. Transp Res C Emerg Technol 30:161–177

Sun Y, Work D (2017) Scaling the Kalman filter for large-scale traffic estimation. IEEE Trans Control Netw Syst

Tampère CMJ, van Arem B, Hoogendoorn SP (2003) Gas-kinetic traffic flow modeling including continuous driver behavior models. Transp Res Rec J Transp Res Board 1852:231–238

Tampère CMJ, Hoogendoorn SP, van Arem B (2005) A behavioural approach to instability, stop and go waves, wide jams and capacity drop. In: Mahmassani HS (ed) Transportation and traffic theory. Flow, dynamics and human interaction. 16th international symposium on transportation and traffic theory. Elsevier, Amsterdam, pp 205–228

Transportation Engineering Group at the George Washington University (2017) Conference on traffic and granular flow

Treiber M, Kanagaraj V (2015) Comparing numerical integration schemes for time-continuous car-following models. Phys A Stat Mech Appl 419:183–195

Treiber M, Kesting A (2013) Traffic flow dynamics: data, models and simulation. Springer, Berlin

Treiber M, Hennecke A, Helbing D (1999) Derivation, properties, and simulation of a gas-kinetic-based, nonlocal traffic model. Phys Rev E Stat Nonlinear Soft Matter Phys 59(1):239–253

Treiber M, Hennecke A, Helbing D (2000) Congested traffic states in empirical observations and microscopic simulations. Phys Rev E Stat Nonlinear Soft Matter Phys 62(2):1805–1824

Treiber M, Kesting A, Helbing D (2006) Delays, inaccuracies and anticipation in microscopic traffic models. Phys A Stat Mech Appl 360(1):71–88

Treiber M, Kesting A, Helbing D (2010) Three-phase traffic theory and two-phase models with a fundamental diagram in the light of empirical stylized facts. Transp Res B Methodol 44(8–9):983–1000

Treiterer J, Myers JA (1974) The hysteresis phenomenon in traffic flow. In: Buckley D (ed) Proceedings of the 6th international symposium on transportation and traffic theory, 1974. Elsevier, Amsterdam, pp 13–38

Tyagi V, Darbha S, Rajagopal KR (2008) A dynamical systems approach based on averaging to model the macroscopic flow of freeway traffic. Nonlinear Anal Hybrid Syst 2(2):590–612. In: Proceedings of the international conference on hybrid systems and applications, Lafayette, LA, USA, May 2006: Part II

van Lint JWC, Djukic T (2012) Applications of Kalman filtering in traffic management and control. In: Tutorials in operations research. INFORMS, Catonsville

van Lint JWC, Hoogendoorn SP, Schreuder M (2008) Fastlane: a new multi-class first order traffic flow model. Transp Res Rec J Transp Res Board 2088:177–187
van Wageningen-Kessels FLM (2013) Multi class continuum traffic flow models: analysis and simulation methods. Ph.D. thesis, Delft University of Technology/TRAIL Research school, Delft
van Wageningen-Kessels FLM (2016) Framework to assess multi-class continuum traffic flow models. Transp Res Rec J Transp Res Board 2553:150–160
van Wageningen-Kessels FLM, van Lint JWC, Hoogendoorn SP, Vuik C (2009) Implicit time stepping schemes applied to the kinematic wave model in Lagrangian coordinates. In: Traffic and Granular Flow '09, Shanghai, China
van Wageningen-Kessels FLM, van Lint JWC, Hoogendoorn SP, Vuik C (2010) Lagrangian formulation of a multi-class kinematic wave model. Transp Res Rec J Transp Res Board 2188:29–36
van Wageningen-Kessels FLM, Schreiter T, van Lint JWC, Hoogendoorn SP (2011) Modelling traffic flow phenomena. In: 2nd international conference on models and technologies for ITS, Leuven, Belgium
van Wageningen-Kessels FLM, Yuan Y, Hoogendoorn SP, van Lint JWC, Vuik C (2013) Discontinuities in the Lagrangian formulation of the kinematic wave models. Transp Res C Emerg Technol 34:148–161
van Wageningen-Kessels FLM, van Lint JWC, Vuik C, Hoogendoorn SP (2014) New generic multi-classkinematic wave traffic flow model: model development and analysis of its properties. Transp Res Rec J Transp Res Board Traffic Flow Theory Charact 2(2422):50–60
van Wageningen-Kessels FLM, van Lint JWC, Vuik C, Hoogendoorn SP (2015) Genealogy of traffic flow models. EURO J Transp Logist 4:445–473
Ward JA, Wilson RE (2011) Criteria for convective versus absolute string instability in car-following models. Proc R Soc A Math Phys Eng Sci 467:2185–2208
Wardrop JG (1952) Some theoretical aspects of road traffic research. ICE Proc Eng Div 1(3):325–362
Wiedemann R (1974) Simulation des Strassenverkehrsflusses. Technical Report, Institute for Traffic Engineering, University of Karlsruhe
Wilson RE (2008) Mechanisms for spatio-temporal pattern formation in highway traffic models. Philos Trans R Soc A Math Phys Eng Sci 366(1872):2017–2032
Wilson RE, Ward JA (2011) Car-following models: fifty years of linear stability analysis: a mathematical perspective. Transp Plan Technol 34(1):3–18
Wong GCK, Wong SC (2002) A multi-class traffic flow model: an extension of LWR model with heterogeneous drivers. Transp Res A Policy Pract 36(9):827–841
Yperman I (2007) The link transmission model for dynamic network loading. Ph.D. thesis, Katholieke Universiteit Leuven
Yu L, ke Shi Z, Li T (2014) A new car-following model with two delays. Phys Lett A 378(4):348–357
Yuan K, Knoop VL, Hoogendoorn SP (2017) A kinematic wave model in Lagrangian coordinates incorporating capacity drop: application to homogeneous road stretches and discontinuities. Phys A Stat Mech Appl 465:472–485
Zhang HM (1999) A mathematical theory of traffic hysteresis. Transp Res B Methodol 33(1):1–23
Zhang HM (2001) New perspectives on continuum traffic flow models. Netw Spat Econ 1:9–33
Zhang HM (2002) A non-equilibrium traffic model devoid of gas-like behaviour. Transp Res B Methodol 36(3):275–290
Zhang HM (2003) Anisotropic property revisited—does it hold in multi-lane traffic? Transp Res B Methodol 37(6):561–577